UNIVERSITY OF CALIFORNIA

Los Angeles

Evolutionary Dynamics of Pathogen Emergence at Multiple Scales

A dissertation submitted in partial satisfaction
of the requirements for the degree
Doctor of Philosophy in Biology

by

Miran Hwan Park

2017

ABSTRACT OF THE DISSERTATION

Evolutionary Dynamics
of Pathogen Emergence
at Multiple Scales

by

Miran Hwan Park
Doctor of Philosophy in Biology
University of California, Los Angeles, 2017
Professor James O. Lloyd-Smith, Chair

The evolution and emergence of pathogens is subject to a wide array of ecological and evolutionary forces acting at multiple mechanistic scales. Theoretical work regarding pathogen emergence has largely neglected the influence of selection acting at multiple scales, and methodologies for analyzing cross-scale data are scarce. Chapter one presents a novel cross-scale model of evolutionary emergence, considering selection the effect of selection at within-host and between-host scales on the evolutionary emergence of novel pathogens. The stochastic population genetic model demonstrates the complexities that arise when considering pathogen emergence at multiple scales: positive correlations between fitness can unexpectedly hasten emergence, conflicts across scales can lead to evolutionary dead ends, and evolution of the pathogen can be disproportionately influenced by neighboring genotypes in the fitness landscape. Chapter two builds upon the foundation of the stochastic modeling framework introduced in chapter one, and explores the application to drug resistance. This analysis shows that varying selection regimes, arising from prophylactic drug use and intermittent treatment compliance, interact with the fitness of the resistant genotype to create trade-offs between epidemic control and drug resistance outcomes. Chapter three addresses the empirical domain of cross-scale analysis, and presents a framework for jointly estimating within-host and between-host fitness using a Bayesian data augmentation approach. Data at the within-host and between-host scales from influenza A transmission

experiments in ferrets are used as a real-world case study to explore how fitness values at the two scales are correlated, and to determine how these parameter estimates can aid in predicting influenza transmissibility in humans. Despite small sample sizes, this approach was validated using simulated data, demonstrating a promising methodology for analyzing pathogen data at multiple scales. The body of work presented here introduces novel frameworks for theoretical development, presents new methodologies for analyzing pathogen data, and highlights the importance of considering multiple scales of selection acting on pathogen evolution and emergence.

The dissertation of Miran Hwan Park is approved.

Priyanga A. Amarasekare

Ren Sun

James O. Lloyd-Smith, Committee Chair

University of California, Los Angeles

2017

To Jamie—

from whom I've learned so much:

thank you for the privilege of being your first student.

And to my family and friends—

for your support, kindness, and belief in me

throughout the years.

TABLE OF CONTENTS

LIST OF FIGURES

LIST OF TABLES

ACKNOWLEDGMENTS

Chapter one is a version of Park, M., Loverdo, C., Schreiber, S.J., Lloyd-Smith, J.O. Multiple scales of selection influence the evolutionary emergence of novel pathogens. Phil. Trans. R. Soc. B. 2013. 368(1614):20120333 DOI: 10.1098/rstb.2012.0333.

In Chapter One, S. J. Schreiber and C. Loverdo contributed to development and analysis of model, and editorial feedback on text.

In Chapter Three, J. A. Belser and T. Maines provided data sources and input on interpretation of data.

Chapter Two and Chapter Three are in preparation for publication.

P.I. James O. Lloyd-Smith contributed to developmental and analysis of models, and editorial feedback on all three chapters.

This material is based upon work supported by the National Science Foundation Graduate Research Fellowship under Grant No. DGE-1144087.

The project described was supported by Grant Number T32GM008185 from the National Institute of General Medical Sciences. The content is solely the responsibility of the authors and does not necessarily represent the official views of the National Institute of General Medical Sciences or te Nation Institute of Health.

VITA

2006–2010	B.S. (Biophysics - Individual Major), University of California, Davis.
2010–2014	Edwin W. Pauley Fellow, University of California, Los Angeles.
2010–2017	Research Assistant, Biology, University of California, Los Angeles.
2011–2014	Teaching Assistant, Biology, University of California, Los Angeles.
2011–2012	Systems and Integrative Biology Trainee, NIH/University of California, Los Angeles.
2012–2015	NSF Graduate Research Fellow, NSF.
2014–2015	Undergraduate research mentor, University of California, Los Angeles.
2014–2015	UCLA EEB R/Python Users Group - Founder and Administrator, University of California, Los Angeles.
2015	Chair's Fellow, University of California, Los Angeles.

PUBLICATIONS

Park, M., Belser, J.A., Lloyd-Smith, J.O. Joint estimation of within-host and transmission fitness of a virus from experimental data: influenza in ferrets as a case study. 2017. *(in prep)*

Park, M., Lloyd-Smith, J.O. Effects of prophylaxis and intermittent selection on the emergence of drug resistance. 2017. *(in prep)*

Schreiber, S.J., Ke, R., Loverdo, C., Park, M., Ahsan, P., Lloyd-Smith, J.O. Cross scale dynamics and the evolution of infectious diseases. bioRxiv. 2015. 066688. DOI: 10.1101/066688

Buhnerkempe, M., Gostic, K., Park, M., Lloyd-Smith, J.O. Mapping influenza transmission in the ferret model to transmission in humans. eLife. 2015. 4:e07969. DOI: 10.7554/eLife.07969

Park, M., Loverdo, C., Schreiber, S.J., Lloyd-Smith, J.O. Multiple scales of selection influence the evolutionary emergence of novel pathogens. Phil. Trans. R. Soc. B. 2013. 368(1614):20120333. DOI: 10.1098/rstb.2012.0333

Loverdo, C., Park, M., Schreiber, S.J., Lloyd-Smith, J.O. Influence of viral replication mechanisms on within-host evolutionary dynamics. Evolution. 2012. 66(11):3462-3471. DOI: 10.1111/j.1558-5646.2012.01687.x

Schraiber, J.G., Kaczymarcyk, A.N., Kwok, R., Park, M., Silverstein, R., Rutaganira, F.U., Aggarwal, T., Schwemmer, M.A., Hom, C.L., Grosberg, R.K., Schreiber, S.J. Constraints on the use of lifeshortening Wolbachia to control dengue fever. J. Theor. Biol. 2011. 297:26-32, DOI: 10.1016/j.jtbi.2011.12.006

CHAPTER 1

Multiple scales of selection influence the evolutionary emergence of novel pathogens

Miran Park, Claude Loverdo, Sebastian J. Schreiber, James O. Lloyd-Smith

1.1 Abstract

When pathogens encounter a novel environment, such as a new host species or treatment with an antimicrobial drug, their fitness may be reduced so that adaptation is necessary to avoid extinction. Evolutionary emergence is the process by which new pathogen strains arise in response to such selective pressures. Theoretical studies over the last decade have clarified some determinants of emergence risk, but have neglected the influence of fitness on evolutionary rates and have not accounted for the multiple scales at which pathogens must compete successfully. We present a cross-scale theory for evolutionary emergence, which embeds a mechanistic model of within-host selection into a stochastic model for emergence at the population scale. We explore how fitness landscapes at within-host and between-host scales can interact to influence the probability that a pathogen lineage will emerge successfully. Results show that positive correlations between fitnesses across scales can greatly facilitate emergence, while cross-scale conflicts in selection can lead to evolutionary dead ends. The local genotype space of the initial strain of a pathogen can have disproportionate influence on emergence probability. Our cross-scale model represents a step toward integrating laboratory experiments with field surveillance data to create a rational framework to assess emergence risk.

1.2 Introduction

Emerging infectious diseases impose major health and economic burdens worldwide, and arise through a range of ecological and evolutionary mechanisms [41, 30, 35]. A recurring theme in many emergence events is that a pathogen lineage is exposed to a novel environment (e.g. a new host species or an antimicrobial drug) in which its fitness is reduced. When the initial pathogen genotype has fitness below the replacement level, the pathogen lineage will go extinct unless it adapts quickly enough to improve its fitness and successfully invade this new environment (e.g. new host species) or escape a lethal selection pressure (e.g. drug or vaccine) [27]. Adaptation can occur at several evolutionary stages and through different mechanisms, and key mutations may occur in the reservoir or the novel environment [48]. Here we focus on evolution in the novel environment, and we call this process evolutionary emergence. There is growing evidence that such adaptation has played an important role in host jumps of viruses such as influenza and SARS-CoV [47, 48]. Studying the evolutionary dynamics of this process, and linking theory to current empirical efforts that characterize the basic determinants of viral fitness, is an important frontier in understanding conditions that favour pathogen emergence. Developing theoretical tools allows us to assess possible emergence threats and what ecological and evolutionary mechanisms facilitate emergence. The acute need for such progress is evident from the recent controversy surrounding the reports that just a few mutations are sufficient to enable airborne transmission of highly pathogenic H5N1 avian influenza virus among mammals [26, 24, 15].

Empirical research on pathogen evolution is defining the dimensions of the problem of evolutionary emergence. Notable steps have been taken toward mapping the fitness landscapes associated with pathogen emergence events, by measuring the fitness (or a proxy for fitness) of pathogen genotypes and effects of pertinent mutations [49]. Two studies have mapped the fitness landscapes associated with development of drug resistance in *E. coli* and *Plasmodium falciparum* genes, by phenotyping all intermediate genotypes bearing some subset of the resistance mutations [59, 37]. Another recent study has extended this comprehen-

sive approach to a viral host jump, studying capsid protein mutations in canine parvovirus [57]. A related strategy, taken by the H5N1 influenza studies cited above [26, 24] and across the literature for other emerging viruses such as SARS-CoV [48], is to characterize several traits associated with fitness for a more limited set of genotypes that comprise a putative pathway to emergence. A powerful complementary approach has tracked viral evolution *in vivo* by measuring changes in genotype frequencies in the course of experimental infection and transmission studies [26, 24, 25, 43, 44]. Ultimately, the aim is to connect these various experimental approaches to genotype frequencies detected in field surveillance, either before [53] or after [10] an emergence event occurs.

A conspicuous pattern arising from empirical studies is that measures of pathogen fitness (or fitness components) can be taken at different biological scales. For instance, recent studies of H5N1 influenza report cell receptor binding, viral titers in different tissues, *in vivo* replication kinetics, airborne transmission efficiency, and time to host death for a range of viral genotypes [26, 24]. These diverse empirical measures of fitness support the need to distinguish within-host fitness, describing the pathogen's ability to grow within infected individuals, from between-host fitness, or transmissibility. Given a set of pathogen genotypes, we must define separate fitness landscapes corresponding to within-host and between-host fitness, i.e. each genotype has a fitness at both scales. This aligns with current research in other domains of infectious disease dynamics [26, 24, 44], and opens the possibility of conflicts, correlations, or other interactions among selective forces acting at multiple scales, which can profoundly influence evolutionary outcomes [60, 33, 45].

The fitnesses of particular pathogen genotypes at within-host and between-host scales are not always positively correlated. Higher pathogen loads often lead to higher rates of transmission [18, 51, 5], in which case there may be positive correlation between fitnesses at the two scales. However, as explored in the extensive literature on virulence evolution, various costs can cause total transmissibility to decline if the pathogen load gets too high [19, 50]. Different pathogen life histories and tissue tropisms may also influence the relation-

ship between fitnesses across scales. For bloodborne pathogens we would expect a positive correlation between pathogen load and infectiousness; indeed this is observed for HIV-1 set-point viral load, although a concomitant effect on the duration of infection causes total transmissibility to peak at intermediate viral load [18]. Thus the correlation between within-host fitness (as reflected by viral load) and between-host fitness can be positive or negative. Similarly, pathogens that infect numerous tissue types, or that involve intermediate hosts or environmental stages in transmission, can exhibit complex relationships between fitnesses at the two scales. A well-known and relevant example is the tissue tropism of influenza virus, where higher binding affinity for different conformations of sialic acid on epithelial cells leads viruses to target the upper or lower respiratory tract. A viral mutation that increases affinity for the α-2,3 conformation might increase within-host replication while decreasing transmissibility by moving the infection deeper into the lung [52]. Such tissue tropism is thought to be a crucial determinant of host adaptation for influenza [26, 24], so it is possible that cross-scale conflicts in selection play an important role in evolutionary emergence. We now know that circulating strains of H5N1 avian influenza are within a few mutations of genotypes that transmit much more efficiently among mammals [26, 53, 34]. Many mammals (human and otherwise) have been infected with H5N1 influenza – why haven't these transmissible genotypes arisen, given that they certainly would confer a fitness benefit to the virus in mammal populations? One possible explanation is that these transmissible genotypes (or intermediate genotypes en route to them) are less fit at the within-host scale so they might not rise to high enough frequencies within hosts to realize their transmission advantage.

Translating our growing empirical knowledge of pathogen phenotypes into an improved understanding of emergence risks will require analytical methods to integrate the key mechanisms across scales. Theoretical study of pathogen emergence has previously focused on evolutionary invasion at the host population scale: an introduced pathogen exhibits weak transmission in the novel host environment, and must mutate to higher transmissibility before the transmission chain dies out. Stochastic models such as multi-type branching processes have been used to compute the probability of emergence for simple genotype spaces

and corresponding (between-host) fitness landscapes [6, 27]. These studies have yielded important insights, showing that even when initial transmissibility is too low to start an epidemic, higher values of transmissibility (bringing the pathogen closer to the threshold for sustained spread) lead to greatly increased probability of evolutionary emergence [6]. Subsequent work has explored the influence of epidemiological complexities [62, 7, 1], but key elements of the evolutionary dynamics have not yet been addressed. Crucially, the model parameters describing evolutionary change of the pathogen have been assumed not to depend on the fitnesses of the genotypes involved. Within-host fitness, and the consequent action of within-host selection, has not been included. André & Day [4] contributed the valuable extension of considering selective sweeps during the course of an individual's infection, but similarly to previous work the rate of fixation of new mutants was assumed not to depend on the strength of selection within hosts. These omissions separate the current theory from the empirical evidence, which largely focuses on within-host fitness [48], and overlook the fact that selection acts most immediately within a host, as pathogen genotypes compete with each other for target cells or other resources or to escape the immune system [3, 28, 42].

We present a theoretical framework to study how the evolutionary emergence of pathogens is influenced by selection at within-host and between-host scales. Our aim is to create a tractable cross-scale model from which analytical insights and biological intuition can be derived. We represent the between-host scale using multi-type branching processes as in previous models [6, 4]. However, instead of assuming equal rates of mutation between all pairs of genotypes, we introduce a sub-model for within-host selection based on population genetic theory. In particular, we follow the approach used in recent analyses of mutational trajectories in empirical fitness landscapes [59, 37, 12] and apply the strong selection, weak mutation (SSWM) limit to derive a compact representation of adaptive evolution [21]. Using this framework, we analyze how fitness landscapes at within-host and between-host scales can interact to influence the probability that a pathogen lineage will emerge. Here we focus on the mechanisms involved in host jumps of pathogens, because our model describes invasion of a pathogen into a large susceptible population; later we discuss how this model could

be applied to other emergence situations such as developing resistance to an antimicrobial drug. At the within-host scale, selection acts on relative fitnesses of adjacent genotypes, with strong selection leading to rapid fixation of new beneficial mutants. At the between-host scale, we consider a stochastic transmission framework that depends on the absolute fitness of neighboring genotypes, where individuals are infected with a particular genotype. We explore two scenarios of simple genotype spaces, illustrating basic principles of multi-scale selection in this context, and exploring the potential for emergence to be prevented by evolutionary conflicts across scales. We hope that this cross-scale mechanistic model begins to bridge the gap between the growing body of empirical data from laboratory experiments and pathogen sequencing studies, and large-scale public health questions about emergence risk. We conclude by discussing necessary extensions and possible links to empirical studies.

1.3 A cross-scale model of evolutionary emergence

1.3.1 Defining the system

Studying the evolutionary dynamics of pathogen populations at multiple scales can lead to substantial complexity, so it is necessary to make simplifying assumptions. Following earlier work [6, 4], we assume that each infected host has a single pathogen genotype at any point in time, and we characterize the host individual by this type. Parameters are marked with a subscript or superscript i corresponding to the pathogen genotype in question. We analyze evolutionary dynamics on a defined genotype space, which consists of a set of pathogen genotypes and the pathways of mutation that connect them. A mutation is broadly defined as a change at a specific locus in the genome giving rise to a new genotype; this can include point mutations, insertions, deletions, or other mechanisms of genetic change. Each pathogen genotype has two measures of fitness associated with it, corresponding to the within-host and between-host scales; these define two fitness landscapes over the genotype space. At the between-host scale, the fitness of the pathogen corresponds to its ability to transmit through the population. At the within-host scale, the fitness of the pathogen describes how well it

replicates within a host. For our analyses, we create case studies of fitness landscapes and explore how they interact to drive pathogen evolution.

The between-host fitness of genotype i is given by the reproductive number, $R_0^{(i)}$, which is the average number of secondary infections caused by a type-i host in a completely susceptible population. For our evolutionary emergence problem, we consider a pathogen that is initially maladapted to the novel environment, i.e. genotype 1 has $R_0^{(1)} < 1$. Such a pathogen causes short chains of transmission but goes extinct with certainty if it does not evolve. Through mutation and selection, which we treat as within-host processes, new genotypes can arise and fix in some host individuals. Eventually the pathogen lineage may reach an 'emergence genotype' with $R_0^{(i)} > 1$, which has a non-zero chance of successfully invading the new host population.

For our numerical work we consider simple scenarios for which the initial and intermediate genotypes always have $R_0^{(i)} < 1$ and there is only one emergence genotype. We calculate the probability that the emergence genotype arises and successfully invades the host population, $P(emergence)$, using techniques described below. Calculating $P(emergence)$ allows us to compare interactions between different fitness landscapes, lending an understanding of general trends that arise as selection acts across scales.

1.3.2 Between-host transmission dynamics

Building on existing literature in evolutionary emergence [4], we use a continuous-time multitype branching process to model the stochastic dynamics of transmission, recovery, and genotype change at the population scale. The model tracks the population dynamics of infected individuals, which are classified according to the pathogen genotype of their infection. We assume a well-mixed homogeneous population in which the number of susceptibles is large enough that it is not significantly depleted by the limited number of cases that occur

before pathogen emergence.

Each infected host of type i infects other host individuals at a constant rate b_i, giving rise to an additional infected host of the same type, and ceases to be infectious (through recovery or death) at a rate d_i. The reproductive number for type i is $R_0^{(i)} = b_i/d_i$. Within-host evolutionary processes cause the dominant genotype to change from type i to type j at a rate $m_{i,j}$ during the course of an individual's infection, where $m_{i,j} = 0$ for a genotype j that is more than one mutational step away from genotype i. During a small time interval of length Δt, these events occur with approximate probabilities $b_i\Delta t$, $d_i\Delta t$, and $m_{i,j}\Delta t$, respectively.

1.3.3 Within-host evolutionary dynamics

Previous models of evolutionary emergence assume that substitution rates do not depend on the fitnesses of the genotypes involved. Here, we replace this assumption with a mechanistic model for within-host evolution, which we embed within the branching process framework used for population-scale dynamics. To represent the key population genetic mechanisms in a compact manner, we use the strong selection, weak mutation (SSWM) paradigm [21].

In the SSWM limit, strong selection means that only beneficial mutations are considered, and mutation rates are sufficiently low that simultaneous mutation events can be neglected. The simplicity of the SSWM limit arises because beneficial mutations go to fixation much faster than new mutations arise, so at any point in time the population is essentially fixed for some genotype. This fixed genotype can only be displaced by pathogen genotypes with higher within-host fitness.

The SSWM assumption allows changes in the infectious genotype within the host to be modelled as a continuous time Markov chain [21]. We begin by defining the absolute within-host fitness of a particular genotype i as w_i. The relationship between the absolute

within-host fitness of genotype i and that of a different genotype j is $w_j = (1+s_{i,j})w_i$, where $s_{i,j}$ is the selection coefficient of the genotype j invading a system with genotype i at its equilibrium. If the current genotype within the host is type i and a substitution occurs, the probability that type j fixes next is given by $s_{i,j}/\sum_{k\in M_i} s_{i,k}$, where M_i is the set of genotypes that are a single mutational step away from genotype i. The waiting time before the next jump occurs is dependent on the size of the virus population, N, and the mutation rate, μ, and is exponentially distributed with mean proportional to $1/(N\mu \sum_{k\in M_i} s_{i,k})$ [21]. Therefore in the SSWM limit we can express the substitution rate for each genotype j:

$$m_{i,j} \propto N\mu s_{i,j}. \tag{1.1}$$

The population size N and mutation rate are assumed to be constant; in the Appendix we present a derivation of equation (1.1) from a model of within-host viral dynamics which leads to an alternative interpretation of these quantities when SSWM is applied to viruses. From this derivation we are able to make intuitive connections between our model and traditional ideas in population genetics, broadly supporting the use of the SSWM framework for within-host evolution. Calculating $m_{i,j}$ from equation (1.1) requires a constant of proportionality; for our numerical calculations, we set this constant to 0.4 following the original assumption by Gillespie (who interpreted it as a measure of the strength of selection) [21]. While this choice is arbitrary, it does not affect the qualitative results, as it affects all substitution rates equally and the timescales of these processes are otherwise arbitrary.

The SSWM model for within-host evolution means that a higher relative fitness of a neighboring genotype leads to a faster rate of substitution, so in general each step through genotype space has a different speed at which it occurs. The biological basis for this effect derives from the probability of fixation of a new genotype when it first arises within a host. A greater fitness advantage for the new genotype leads to a higher likelihood that it will fix after it arises. Consequently, even if all neighboring genotypes arise at the same rate, the rate of substitution is faster when the relative fitness difference is large.

1.3.4 Calculating the probability of emergence

The branching process model gives us a framework to calculate the probability of emergence $P(emergence)$. For our models, there are two ways to compute the emergence probabilities from the embedded discrete-time branching process: numerically using standard methods [23] or using the exact solutions we derive in the Appendix. While both approaches yield the same results, we only present results based on the exact solutions. To gain intuition into the determinants of emergence, we also present a simple approximation for the probability of emergence in the limit of low initial between-host fitness (low $R_0^{(1)}$) and low mutation rates.

We first consider a simple, sequentially connected chain of genotypes, where for each genotype, there exists only one "neighboring" genotype that is more fit. If the Lth genotype is the emergence genotype with $R_0^{(L)} > 1$, then we can derive an approximation for the probability of emergence, combining elements of arguments from Iwasa et al. [27] and André & Day [4], and using branching process theory:

$$P(emergence)_{\text{seq.}} \approx \left(\frac{1}{1-R_0^{(1)}}\right)\left(\frac{m_{1,2}}{m_{1,2}+d_1}\right)\cdots\left(\frac{1}{1-R_0^{(L-1)}}\right)\left(\frac{m_{L-1,L}}{m_{L-1,L}+d_{L-1}}\right)\left(1-\frac{1}{R_0^{(L)}}\right). \qquad (1.2)$$

This expression breaks down into three biologically meaningful factors. Each factor of $\frac{1}{1-R_0^{(i)}}$ is the expected number of infections in a subcritical chain of transmission initiated by a type-i individual in the absence of evolution. The factors $\frac{m_{i,j}}{m_{i,j}+d_i}$ give the probability of the fixed genotype changing from type i to type j before recovery or death of a host infected with type i. The final factor, $1-\frac{1}{R_0^{(L)}}$, is the probability that the emergence genotype will successfully invade the host population if it arises in a single host individual.

We can extend this approximation to the more general case of an arbitrary genotype space. To estimate the probability of emergence starting with one infected individual of

type 1, let $L-1$ be the minimal number of mutational steps from the initial genotype to an emergence genotype. The probability of emergence will be proportional to μ^{L-1} as longer paths to emergence add terms of order μ^L or higher (though note that factors of μ are implicit in $m_{i,j}$). Let $\mathcal{P}$ be the set of mutational pathways of length L, each spanning genotype i_1 to an emergence genotype i_L. Then the probability of emergence can be approximated as:

$$P(emergence) \approx \sum_{(i_1,\ldots,i_L)\epsilon\mathcal{P}} \left(1 - \frac{1}{R_0^{(i_L)}}\right) \prod_{k=1}^{L-1} \frac{1}{1 - R_0^{(i_k)}} \frac{m_{i_k,i_{k+1}}}{(m_{i_k,i_{k+1}} + d_{i_k})}. \tag{1.3}$$

Each term within the summation corresponds to a particular mutational pathway, and matches the approximation shown in equation (1.2). The low mutation rate assumption allows us to neglect outcomes where more than one virus lineage reaches emergence. In the analyses presented below, we illustrate that the approximation works well through most of the parameter range considered.

1.4 Effects of cross-scale selection on pathogen emergence

We analyze two scenarios to explore the possible influence of multiple scales of selection on evolutionary emergence. In the first scenario we consider a simple genotype space, and a basic set of qualitatively distinct fitness landscapes, to understand the fundamentals of how fitness landscapes at the two scales interact to produce evolutionary outcomes. In the second scenario we extend these fitness landscapes to consider multiple competing pathways of pathogen evolution, creating the potential for conflict across scales.

1.4.1 Scenario 1: Exploring interactions between scales of selection in a simple genotype space

We consider a simple genotype space, with three genotypes sequentially connected in a chain and explore how selection at different scales impacts disease emergence (Figure 1). To

distinguish fitness landscapes in our scenarios from the general theoretical results presented above, we refer to these particular genotypes by a capital letter and numerical subscript i, e.g. genotype A_1.

At the between-host scale we consider three fitness landscapes (Figure 1(a)). We explore scenarios where the initial and emergence genotypes have fixed fitnesses, and explore the landscapes arising from differing fitnesses of the intermediate genotype. In the "jackpot" landscape, between-host fitness does not change until the pathogen reaches the emergence genotype (and thus hits the jackpot) ($R_0^{(1)} = R_0^{(2)} < R_0^{(3)}$). In the "uphill" landscape, the fitness increases with each step through genotype space ($R_0^{(1)} < R_0^{(2)} < R_0^{(3)}$). We arbitrarily choose fitnesses that increase linearly for this example. In the "valley" landscape, the fitness of the intermediate genotype is lower than the fitness of the initial genotype, so the pathogen must traverse a valley of lower fitness to reach emergence ($R_0^{(1)} > R_0^{(2)} \ll R_0^{(3)}$) (Figure 1(a)). For simplicity, in all of our examples, we assume rates of recovery or death (d_i) are equal across genotypes. Variation in the recovery or death rates d_i lead to qualitatively similar results, though the probabilities of emergence increase more rapidly with $R_0^{(1)} = R_0^{(2)}$ because the rising reproductive numbers correspond to longer infectious periods $1/d_i$, allowing more time for substitution events to occur [4].

At the within-host scale, only pathways with increasing fitness are relevant under the SSWM framework, so we consider three cases that span the qualitative range of possible fitness landscapes, given that we fix the fitnesses of the initial and emergence genotypes (Figure 1(b)). We define the "equal-rate" landscape as the case that has equal gains in relative fitness when moving from the initial to the intermediate genotype, and from the intermediate to the emergence genotype. Under the SSWM model for within-host evolution, this yields equal substitution rates for the two mutational steps ($m_{1,2} = m_{2,3}$). We note that the equal-rate landscape under SSWM corresponds to previous models that have assumed equal substitution rates and no back-mutations. The "fast-slow" landscape has a greater fitness gain from the initial to the intermediate genotype than from the intermediate to the

terminal genotype; thus the substitution rate for the first substitution is faster than the second ($m_{1,2} > m_{2,3}$). The "slow-fast" landscape is the opposite case, with the substitution rate for the first substitution slower than the second ($m_{1,2} < m_{2,3}$). We assume a symmetry of fitnesses between the fast-slow and slow-fast landscapes, for ease of comparison: $m_{1,2}$ in the fast-slow case is equal to $m_{2,3}$ in the slow-fast case and vice-versa. To depict the within-host fitness landscapes, we plot the logarithm of the absolute fitnesses w_i. This emphasizes the multiplicative relationships that define relative fitnesses which drive the SSWM framework. For example, the equal-rate landscape is linear in log-scaled absolute fitness (Figure 1(b)).

The approximation (equation (1.2)) shows that the probability of emergence is maximized when $m_{1,2} = m_{2,3}$. This is because, when the fitnesses of the initial and emergence genotypes are fixed, the product of substitution rates is maximized when the rates are equal (and hence when the relative fitnesses for each genotype transition are equal). This in turn maximizes the overall probability of emergence, since faster substitution means less chance that the competing recovery rates d_i will prevail. This outcome can also be explained through Jensen's inequality [29], because the logarithm of the product of terms $\frac{m_{i,j}}{m_{i,j}+d_i}$ in equation (1.2) is concave down as a function of $m_{i,j}$. Thus we expect anything other than the equal-rate case to have lower probability of emergence, because variation in the $m_{i,j}$'s decreases the value of this product. We test this prediction, and illustrate the interplay between fitness landscapes at different scales, by considering how the probability of emergence for a jackpot between-host landscape is affected by different within-host fitness landscapes (Figure 2(a)). The equal-rate scenario has the highest probability of emergence, as we predicted; we also see that the approximation (equation (1.2)) is quantitatively accurate through most of the parameter range considered (Figure 2(b)). The fast-slow and slow-fast cases have virtually identical probabilities of emergence, given the jackpot between-host landscape and our assumption of symmetry between the fast-slow and the slow-fast landscapes.

We can explore the different qualitative interactions across scales by varying the intermediate values for both within-host and between-host fitness landscapes, fixing the initial and

emergence fitnesses at both scales. Figure 3(a) shows how the probability of emergence varies across a range of possible intermediate values, spanning from valley to uphill landscapes for the between-host scale, and from slow-fast to fast-slow landscapes at the within-host scale. The probability of emergence increases going from a valley to uphill between-host landscape (i.e. along the horizontal axis), as expected intuitively and known from earlier studies [6, 4, 27]. Considering different within-host landscapes, we see that the probability of emergence is maximal close to the equal-rate case, as predicted from the approximation, but deviations from this pattern arise from interactions between the fitness landscapes at each scale. For clarity, we focus on the three within-host landscapes shown in Figure 1(b), and track how the probability of emergence varies as the between-host fitness of the intermediate state increases (Figure e(b); shown as slices of the plot in Figure 3(a)). When the intermediate between-host fitness is greater than the initial fitness ($R_0^{(2)} > R_0^{(1)}$), it is more advantageous for the pathogen to mutate immediately and gain the between-host fitness advantage so the fast-slow scenario is more favorable for emergence. When the intermediate fitness is below the initial fitness ($R_0^{(2)} < R_0^{(1)}$), it is more advantageous for the pathogen to spend less time in the intermediate state, so the slow-fast scenario is more favorable for emergence (Figure 3(b)). Based on these arguments, we would expect the curves for the slow-fast and fast-slow cases to cross at $R_0^{(2)} = 0.5$, the fitness of the initial genotype. However, the crossing point is shifted slightly in favor of the fast-slow scenario, reflecting an additional evolutionary benefit to spending more time in the A_2 genotype. All else equal, it is beneficial to spend more time in the A_2 genotype than the A_1 genotype, because all new cases infected by an A_2-infected individual are born into the A_2 genotype (and have a chance of mutating directly to the A_3 genotype) and thus have a head-start towards emergence. (This effect also causes the slight inequality between emergence probabilities for the slow-fast and fast-slow landscapes in figure Figure 2(b)). This scenario illustrates how selection can interact across scales in non-obvious ways, as the geometry of the within-host fitness landscape can shift between-host outcomes and change the expected probabilities of emergence.

1.4.2 Scenario 2: Alternative pathways illustrate the potential for conflict across scales

To explore the potential for conflicts in selection pressure across scales to influence pathogen emergence, we extend our analysis to a more complex scenario where two neighboring mutations are available to the initial genotype B_0: one that leads to a pathway of decreasing between-host fitness and eventual extinction (B_1', B_2'), and one that leads to a pathway of increasing between-host fitness and possible emergence (B_1, B_2). We assume that these pathways have linearly decreasing or linearly increasing between-host fitness values, respectively (Figure 4(a)). As a first exploration of interactions across scales, we consider simple within-host scenarios by fixing the extinction pathway (B_1', B_2') to have a particular equal-rate landscape and exploring the space of possible equal-rate landscapes for the emergence pathway (B_1, B_2) (Figure 4(b)). This creates a potential conflict at the two scales for some pathways (i.e. when the within-host landscape for the emergence pathway (B_1, B_2) is relatively flat) as within-host selection favours the pathway that leads to extinction at the between-host scale. We summarize this effect with the Pearson's correlation coefficient between the fitness values at the within-host scale (w_i) and the fitness values at the between-host scale ($R_0^{(i)}$) for each genotype. When within-host fitness is negatively correlated with between-host fitness (i.e. when (B_1, B_2) is flat), the probability of emergence is low. The emergence probability drops drastically as the negative correlation becomes stronger, as the lineage almost always evolves into the extinction pathway; in effect, the lineage is lured into an evolutionary dead end. When within-host fitness is positively correlated with between-host fitness, then the probability of emergence is higher as the lineage almost always evolves along the emergence pathway (Figure 4(c)).

To explore the generality of these insights, we examine a much broader set of scenarios by assigning random values to the within-host fitnesses of all genotypes (B_1', B_2', B_1, B_2) (Figure 5(a,b)). The positive association between the probability of emergence and the correlation of fitnesses across scales is maintained (Figure 5(c)). There is significant scatter in

the relationship, because the correlation is influenced by the fitnesses of genotypes B_2 and B_2', which may have minimal influence on the probability of emergence depending on the fitnesses of B_1 and B_1'. Thus, having a high correlation between the two fitnesses at the two scales does not necessarily mean the lineage will be drawn towards the emergence pathway by within-host selection. Additionally, because correlation describes the linear dependence between the fitnesses at both scales, it becomes a less appropriate measure given the nonlinearity of the within-host fitness values. To clarify this relationship, we plot the probability of emergence versus the probability that the first mutational step is to genotype B_1 and therefore the emergence pathway (Figure 5(d)). This shows a strong positive relationship with less scatter, indicating that the probability of emergence is influenced powerfully by which evolutionary pathway is taken by the pathogen population, and hence by the within-host fitnesses of the mutational neighbors of the introduced strain. The residual scatter comes from randomly-generated landscapes for genotypes B_1 and B_2 that correspond to the fast-slow scenario. A high within-host fitness w_1 leads to a high probability of stepping toward emergence, but then the fitness w_2 is only marginally higher, so the substitution rate $m_{1,2}$ is slow and there is a high likelihood that the lineage never reaches emergence. The strong influence of the first mutational step partially results from the absence of back-mutations (a consequence of strong selection), which means if the first mutational step is towards the extinction pathway (which may be favorable at the within-host scale despite its cost at the between-host scale) the pathogen is unable to reach emergence.

1.5 Discussion

We have presented a cross-scale model of evolutionary emergence of pathogens, drawing on population genetic theory to embed a mechanistic model for within-host selection into a branching process model for population-scale emergence. Our results show that within-host fitness plays an important role in evolutionary emergence and that interactions between selection pressures at the within-host and between-host scales can have a substantial effect

on the probability of emergence. A growing number of studies are mapping the structure of within-host fitness landscapes for pathogens [14, 17, 8], making it clear that within-host selection plays a non-trivial role in real-world emergence scenarios. At the same time, empirical research has started to measure fitness at multiple scales [26, 24] and track cross-scale evolution [43, 44, 46] for pathogens linked to emergence events. Improving our understanding of pathogen emergence in novel environments requires integration of evolutionary and ecological phenomena across scales [48]. Our model provides a framework to begin this integration, offering the potential of coupling phenotypic data from experimental studies to pathogen genotypes detected in field surveillance.

The most important results of our analysis are the qualitative insights about the relative risk of different emergence pathways. Our simulations illustrate two key points about the interactions between selection at the within-host and between-host scales when multiple evolutionary trajectories are available. First, and most broadly, positive correlations between the fitnesses across scales increase the likelihood of emergence. Because within-host selection drives movement through genotype space, this conclusion is consistent with theory showing that positive correlations between fitness and dispersal patterns increase the establishment likelihood of invasive species [55]. This also echoes themes from prior theoretical studies of the influence of cross-scale selection on the evolution of virulence, which have emphasized the importance of conflicts in selection and the consequences for optimal virulence and coexistence of strains with different strategies [20, 11, 40]. Second, the local neighborhood of the initial genotype in the within-host fitness landscape has a dominant effect on emergence probabilities, because the first mutational step determines what evolutionary trajectories are accessible, reflecting empirical results in bacteriophage experiments [9]. The importance of the local neighborhood of the initial genotype is especially pertinent when selection is strong, so that the probability of back-mutation is negligible. Both of these effects are masked when emergence dynamics are studied at a single scale.

Our analysis shows that selection acts differently at the within-host and between-host

scales in the evolutionary emergence scenarios we are considering. At the within-host scale, under assumptions of SSWM, evolutionary change is driven by the relative fitness of neighboring genotypes (compared to the current fixed genotype), and the effects of selection are manifested chiefly in the duration that a given genotype is fixed. At the between-host scale, the absolute fitness of the current genotype ($R_0^{(i)}$) is the crucial measure, as it determines whether the transmission chain continues or goes extinct. These differences stem from basic population dynamic properties of the emergence problem, which apply to many emerging infections, such as weakly-transmitting zoonoses [35]. Because $R_0^{(i)} < 1$ for unadapted genotypes, the between-host process is in an invasion regime, and competition for susceptible hosts is negligible. We have assumed that all genotypes are viable at the within-host scale in order to focus our attention on population-scale emergence, and because the emerging pathogens of greatest concern are those that are already able to infect the novel host. However, it is important to recognize that the pathogen can also undergo evolutionary invasion or escape within the host, and that these can be cross-scale problems involving within-cell processes [36, 27, 42, 46].

We have used the SSWM framework to incorporate mechanistic evolutionary principles at the within-host scale. The SSWM model has been a favored approach to analyzing evolutionary trajectories in empirically derived fitness landscapes [59, 37, 12]. Some aspects of the SSWM framework are very well suited to modelling pathogen emergence, such as the stochastic nature of mutation and fixation and the strong selection pressures experienced by pathogens in novel environments [59, 46]. However, other aspects of the SSWM model are poor approximations to many pathogen emergence problems. For instance, the assumption of weak mutation (and consequently, a single genotype within each host) does not match the high mutation rates of RNA viruses and the tremendous diversity that can result [61, 54]. Quasispecies theory may provide a more accurate portrayal of pathogens with high mutation rates, where selection acts on a "cloud" of mutants rather than any individual genotype [13, 39]. The assumption of constant population size inherent to SSWM is also a strong simplification, because pathogen loads can vary markedly throughout an infection (and between

infections). An important future aim is to integrate the within-host population dynamics of the pathogen, which will influence the relative strength of selection versus drift. A particularly important application is to study evolutionary change during transmission bottlenecks, which can be extremely narrow [32, 58] so drift can act strongly. André & Day [4] presented an elegant model showing how this effect can interact with within-host substitutions to influence evolutionary emergence, but further work is needed to model both evolutionary processes in the context of explicit within-host genetic diversity. These strong assumptions of the SSWM model should be borne in mind when interpreting our results, as well as those in earlier studies applying the SSWM framework to pathogen emergence problems. Indeed, we have shown that previous models assuming equal substitution rates for all genotypes, and no back-mutations, are equivalent to the SSWM model for within-host evolution with a equal-rate fitness landscape. Therefore the caveats outlined above apply equally to these earlier studies, with the added caution that the equal-rate landscape tends to give an upper bound for probabilities of emergence.

The SSWM framework has previously been applied to extracellular parasites and bacteria, as well as viruses [59, 37, 12]. Because viruses have a distinctive life history involving reproduction within host cells, we have explored the applicability of the SSWM framework to viruses by deriving the substitution rate under SSWM assumptions from a basic model of within-host viral dynamics (see Appendix). This derivation reveals additional assumptions that are implicit in using SSWM to represent viral evolution. Namely, we assumed that all within-host fitness differences among genotypes arise from replication rates (not cell infection or within-host clearance), that viruses reproduce by budding at a constant rate, and that mutations in offspring virions of a given host cell occur independently [36]. Our result also gives new perspectives into the population size component of the SSWM substitution rate. First, the derivation shows that the relevant population size is the equilibrium abundance of infected target cells, not viral particles. Second, this population size will vary as a function of within-host viral fitness, and will not remain constant for all genotypes as assumed under the classical SSWM formulation. Further investigation of how within-host dynamics lead

to shifts in viral genotypes is an important avenue to developing improved cross-scale models.

Recent empirical studies have increasingly reported measures of viral fitness or tracked viral evolutionary dynamics across biological scales. These show how our work could be applied, and also guide priorities for on-going theory development. As a first example, we consider the recent studies describing mutations that enable H5N1 influenza to transmit among mammals [26, 24]. This work shows a predominantly positive correlation between fitness measures across scales, indicating that some mammal-transmissible genotypes may be favoured at the within-host scale [26]. This amplifies concerns that these genotypes could emerge in naturally circulating virus populations, though we emphasize that there is no evidence that the higher-fitness genotypes would have $R_0 > 1$ in humans, since experiments were performed in ferrets under laboratory conditions. It is also possible that other nearby genotypes (as yet uncharacterized) may have higher within-host fitness, leading to evolutionary dead ends as illustrated in figures 4 and 5. Nevertheless, our study contributes new insights to the assessment of risk from these H5N1 influenza genotypes by providing a theoretical framework in which to qualitatively assess and compare the risk of emergence of particular genotypes that could arise through mutation, given fitness measures at within-host and between-host scales. The model also presents a complementary approach to other modeling analyses that have focused on the within-host dynamics of emergence [53]. Conversely, consideration of these influenza studies reveals complexities in current data that our model does not address. Future work will need to relate temporal changes in viral titre to within-host fitness (and hence selection), and consider the potentially crucial influence of different tissue compartments within a host [52].

Similar opportunities are evident when we consider recent studies of viruses that have emerged across species boundaries, such as canine parvovirus [31, 57, 2] and severe acute respiratory syndrome coronavirus (SARS-CoV) [63, 56]. Extensive laboratory work on SARS-CoV, motivated by genotypes detected in field samples, has identified adaptive mutations that improve cell receptor binding in humans; these were found in viruses transmitted be-

tween humans, but not in civet isolates [56]. Tracking the spread of such mutations in the early stages of human-to-human transmission would provide a unique opportunity to reconstruct an evolutionary emergence event, if the data can be linked [63]. Beyond-consensus sequencing studies have mapped out changes in genotype frequencies within hosts and through transmission chains, giving a window into cross-scale dynamics [43, 44] and showing preliminary evidence of how viral diversity is influenced by transmission bottlenecks. Such data sets will allow us to test the validity of cross-scale evolutionary models, and refine our understanding of pertinent mechanisms. A recent study of HIV-1 highlights the unexpected insights than can arise from considering sequence data across scales. Investigating the phenomenon that HIV-1 exhibits faster substitution rates within hosts than between hosts, it concludes that the probable mechanism is that viruses closely related to the infecting strain are preferentially transmitted following storage in long-lived CD4+ T cells [38]. Such a finding demonstrates the potential importance of considering specific (and sometimes idiosyncratic) biological factors when addressing questions about particular host-pathogen systems, and shows the power of cross-scale data to advance our understanding of pathogen evolution.

Accurate quantitative prediction of emergence probabilities is probably a distant goal, but mechanistic models help us better understand the relative risk of different pathogen genotypes, and assess which pathogens may be closer to emergence. As a simple example, if two viral strains are each shown to be two mutations from an emergence genotype with $R_0 > 1$, but the within-host fitness landscape is smoothly uphill for one trajectory and rugged for the other, then the strain with a smooth evolutionary path is the greater risk. Our theoretical results show us how relationships between fitnesses at multiple scales influence emergence, providing an integrative lens through which to view accumulating data on emerging pathogens. These data are arising from a broad array of approaches, from empirical mapping of fitness landscapes to deep-sequencing studies of evolutionary dynamics, and from *in vitro* and *in vivo* experiments to global field surveillance. All of these approaches can yield insight on evolutionary dynamics of pathogens at within-host or between-host scales. We applaud the recent trend toward characterizing transmissibility and inter-host evolu-

tion, since this has been a crucial data gap [48]; however, our results show that within-host fitness must be measured in parallel to arrive at a holistic picture of emergence risk. As the complexity and abundance of empirical work on emerging pathogens (or pathogens that threaten to emerge) continue to grow, the need for theoretical frameworks to analyze the resulting data and draw integrative conclusions will be even greater. The model introduced here represents a foundation for such an integrative cross-scale theory.

1.6 Appendix

1.6.1 Deriving the SSWM transition probabilities from a model of viral dynamics

For a population of viruses with a single strain or genotype, let V denote the density of the virus, U denote the density of uninfected target cells, and I denote the density of infected target cells. The uninfected target cell population has a net growth rate $f(U)$. In the absence of infection, assume that dU/dt has a unique positive, stable equilibrium at U^*, i.e. $f(U^*) = 0$ and $f'(U^*) < 0$ (the virus-free equilibrium). Free viral particles encounter and infect uninfected target cells at a rate aU. Infected cells produce new viral particles via budding at a rate β and infected cells die at a rate δ. Viral particles are cleared from the host at a rate c. With the exception of $f(U)$, all rates are per capita. Provided the viral population is sufficiently large we can describe the viral and host cell dynamics by a mean field equation:

$$\begin{aligned} \frac{dU}{dt} &= f(U) - aUV \\ \frac{dI}{dt} &= aUV - \delta I \\ \frac{dV}{dt} &= \beta I - cV - aUV. \end{aligned} \tag{1.4}$$

When the virus initially infects the host at low numbers, we approximate the establishment probability within the host by assuming that $U = U^*$ is constant and I, and V are determined by a continuous time branching process with transitions:

$$\begin{aligned}
&(I, V) \to (I + 1, V - 1) \text{ with rate } aUV \\
&(I, V) \to (I, V + 1) \text{ with rate } \beta I \\
&(I, V) \to (I, V - 1) \text{ with rate } cV.
\end{aligned} \tag{1.5}$$

Then a single viral particle infects a cell with probability:

$$q = \frac{aU^*}{c + aU^*} \tag{1.6}$$

and does not infect a cell (i.e. is cleared by the host) with probability $1 - q$. In the event that a viral particle infects a cell, it gives rise to a number of offspring viruses that is geometrically distributed with mean $n = \beta/\delta$. Thus the reproductive number for a virus, which is the expected number of viruses produced after one full cycle of cell infection, is qn. The generating function for the complete offspring distribution is given by [36]:

$$g(x) = 1 - q + \frac{q}{1 + n(1 - x)}. \tag{1.7}$$

From basic branching process theory, the ultimate probability of extinction for the viral lineage is given by the non-zero solution to $g(e) = e$. We can then solve for the probability of establishment for a single viral particle, which is $q - 1/n$ [36].

If the viral population establishes, under appropriate assumptions, the quasi-stationary distribution is concentrated on the attractor of the system [16]. For simplicity, let us assume that this attractor is an equilibrium. We denote this equilibrium with established virus by the † superscript. The probability that a virus infects a cell is denoted $q^\dagger$ and is found by substituting $U^\dagger$ for U^* in equation (1.6). Because the system is at equilibrium, $q^\dagger n = 1$,

giving:

$$\frac{aU^\dagger}{c+aU^\dagger}n = 1. \tag{1.8}$$

From this we can solve for $U^\dagger$ and for the nontrivial equilibrium of equation (1.4):

$$\begin{aligned} U^\dagger &= \frac{c}{a(n-1)} \\ I^\dagger &= \frac{f(U^\dagger)}{\delta} \\ V^\dagger &= \frac{f(U^\dagger)}{aU^\dagger}. \end{aligned} \tag{1.9}$$

Now consider two competing viral genotypes, genotype 1 and genotype 2. Assume there is no superinfection, i.e. each cell has only one fixed viral genotype, and that infection, clearance, and infected cell death rates for the two viral types are the same (i.e. $a_1 = a_2 = a$, $c_1 = c_2 = c$, and $\delta_1 = \delta_2 = \delta$). Then the viral dynamics are given by:

$$\begin{aligned} \frac{dU}{dt} &= f(U) - aU(V_1 + V_2) \\ \frac{dI_i}{dt} &= aUV_i - \delta I_i \\ \frac{dV_i}{dt} &= \beta_i I_i - cV_i - aUV_i. \end{aligned} \tag{1.10}$$

Define the equilibrium abundance of uninfected cells when only viral type i is present as:

$$U_i^\dagger = \frac{c}{a(n_i - 1)} \tag{1.11}$$

where $n_i = \beta_i/\delta$. With this deterministic model linearization of the boundary equilibrium suggests that the viral population with the lower $U_i^\dagger$ invades and displaces the other viral type. This aligns with classical theory of ecological competition for a single limiting resource. Without loss of generality, assume that $U_1^\dagger > U_2^\dagger$, which occurs when $n_2 > n_1$. Note that, because $a_1 = a_2$ and $c_1 = c_2$, the cell infection probabilities $q_1 = q_2 = q$ for a given uninfected

cell density U. Therefore the n_i are proportional to the reproductive numbers for each viral type, and the condition $n_2 > n_1$ means that type 2 has higher fitness.

If viral type 1 has already established in the host and is at equilibrium abundance $U_1^\dagger$, we can approximate the invasion dynamics of the other genotype with a continuous time branching process with transitions:

$$\begin{aligned}
&(I_2, V_2) \to (I_2 + 1, V_2 - 1) \text{ with rate } aU_1^\dagger V_2 \\
&(I_2, V_2) \to (I_2, V_2 + 1) \text{ with rate } \beta_2 I_2 \\
&(I_2, V_2) \to (I_2, V_2 - 1) \text{ with rate } cV_2.
\end{aligned} \tag{1.12}$$

Following from the probability of establishment of viral type 2 being $q_2 - \frac{1}{n_2}$ and using equation (1.8), the probability of establishment of viral type 2 is:

$$\frac{aU_1^\dagger}{c + aU_1^\dagger} - \frac{1}{n_2} = \frac{1}{n_1} - \frac{1}{n_2} \tag{1.13}$$

where $\frac{aU_1^\dagger}{c+aU_1^\dagger}$ corresponds to q for viral type 2 invading over viral type 1 at equilibrium. This probability is always positive given our assumption of $U_1^\dagger > U_2^\dagger$.

When viral type 1 is at equilibrium, mutant viruses are produced at a rate $\nu\beta_1 I_1^\dagger$ where ν is the probability that a given offspring virion will bear a mutation at the locus that converts type 1 to type 2. Altogether this gives the rate of substitution (in which viral genotype 2 displaces viral genotype 1) as:

$$m_{1,2} = \nu\beta_1 I_1^\dagger (\frac{1}{n_1} - \frac{1}{n_2}) \tag{1.14}$$

We equate the establishment probability $(\frac{1}{n_1} - \frac{1}{n_2})$ with the selection coefficient $s_{1,2}$ from the main text. This choice is consistent with Haldane's proof that a beneficial allele with selection coefficient s sweeps to fixation with a probability directly proportional to s [22], and is equivalent with Gillespie's definition of s in the weak selection limit used in his original SSWM derivation. We can then compare quantities from the derivation above with

the classical SSWM formulation showin in the main text: $\nu\beta_1$ in our result is equivalent to the mutation rate μ, and $I_1^\dagger$ in our result is equivalent to the population size N. Thus the expression $\nu\beta_1 I_1^\dagger(\frac{1}{n_1} - \frac{1}{n_2})$ derived here corresponds closely to the $m_{i,j}$ expression in the main text (equation (1.1)).

We have shown conditions under which the viral dynamics model reduces to a form closely analogous to the SSWM formulation for substitution rates. Yet this derivation cannot be interpreted as an exact derivation of the SSWM model, as there are some subtle inconsistencies. The measure of population size, $I_1^\dagger$ corresponds to the infected host cell population, not the total number of viral particles. Significantly, the quantity $I_1^\dagger$ is a function of within-host viral fitness, leading to the potential for viral fitness to impact substitution rates through the rate at which new mutants are generated. This demographic impact of higher fitness is neglected in the classical SSWM formulation. Overall, though, the derivation shows that a close analogue of the SSWM framework can be derived from a simple model of viral dynamics, subject to similar assumptions about the strength of selection and mutation processes. Further work to explore how within-host pathogen dynamics can link to simple models of genotype substitution would be valuable, given the widespread usage of SSWM in the empirical literature.

1.6.2 Exact solution for the probability of emergence in a sequentially connected landscape

To write down an exact solution for the extinction probabilities, we consider the "embedded" discrete-time branching process where one unit of time corresponds to an update of the continuous time branching process. The extinction probabilities for the embedded process and the original continuous time process are equivalent. The i-th component of the generating map $G : [0,1]^k \to [0,1]^k$ for the embedded branching process is given by a power series

$$G_i(z_1, \ldots, z_k) = \sum_{n_1,\ldots,n_k} p_i(n_1, \ldots, n_k) z_1^{n_1} z_2^{n_2} \ldots z_k^{n_k}$$

where $p_i(n_1, \ldots, n_k)$ is the probability that an individual of type i has n_1 offspring of type 1, n_2 offspring of type 2, etc.

For our model, an update of an individual host infected with genotype i leads to death with probability $\frac{d_i}{b_i+d_i+\sum_{j\in M_i} m_{i,j}}$, leads to a birth with probability $\frac{b_i}{b_i+d_i+\sum_{j\in M_i} m_{i,j}}$, or leads to a substitution event in which genotype i is replaced by genotype j with probability $\frac{m_{i,j}}{b_i+d_i+\sum_{j\in M_i} m_{i,j}}$ for each genotype j in M_i. Hence, the i-th component of the generating map is

$$G_i(z_1, \ldots, z_k) = \frac{1}{b_i + d_i + \sum_{j\in M_i} m_{i,j}} \left(b_i z_i^2 + d_i + \sum_{j\in M_i} m_{i,j} z_j \right).$$

Let e_i be the extinction probability of the process given the initial condition of one individual infected with genotype i. Provided that the branching process is supercritical (i.e. there is a positive probability of emergence), the vector of extinction probabilities $e = (e_1, \ldots, e_k)$ is the unique solution to $G(e) = e$ in $[0, 1)^k$.

For the landscapes considered in the text, we can solve for e explicitly in an inductive fashion. Consider the case of a sequential landscape for which $M_1 = \{2\}$, $M_2 = \{3\}$, $\ldots M_{k-1} = \{k\}$, and $M_k = \emptyset$. For $1 \leq i < k$, let $m_i = m_{i,i+1}$. As in the text, we assume that $b_k/d_k > 1$ i.e. type k is an emergence genotype. To solve for the extinction probabilities, we proceed inductively from genotype k back to genotype 1. The extinction probability e_k is the unique solution $e_k = z_k$ to

$$\frac{b_k z_k^2 + d_k}{b_k + d_k} = z_k \text{ for } z_k \in (0, 1)$$

which is given by

$$e_k = \frac{d_k}{b_k}.$$

Proceeding inductively, suppose that we have solved for e_{i+1}. The i-th component of the generating map G_i only depends on z_i and z_{i+1}. Slightly abusing notation, e_i is the unique

solution $e_i = z_i$ to $G_i(z_i, e_{i+1}) = z_i$ with $z_i \in (0,1)$. Equivalently, e_i is the unique solution to

$$\frac{b_i z_i^2 + d_i + m_i e_{i+1}}{b_i + d_i + m_i} = z_i \text{ for } z_i \in (0,1)$$

which is given by

$$e_i = \frac{-\sqrt{-4\, b_i m_i e_{i+1} + m_i^2 + 2(d_i + b_i)m_i + d_i^2 - 2b_i d_i + b_i^2} + m_i + d_i + b_i}{2b_i}.$$

A similar induction method can be used to find the exact solutions to the landscapes with two linear paths emanating from genotype i. More generally, it is possible to write down an exact solution for landscapes whenever the underlying directed graph has no directed cycles. This result will be presented in a future study.

Figure 1

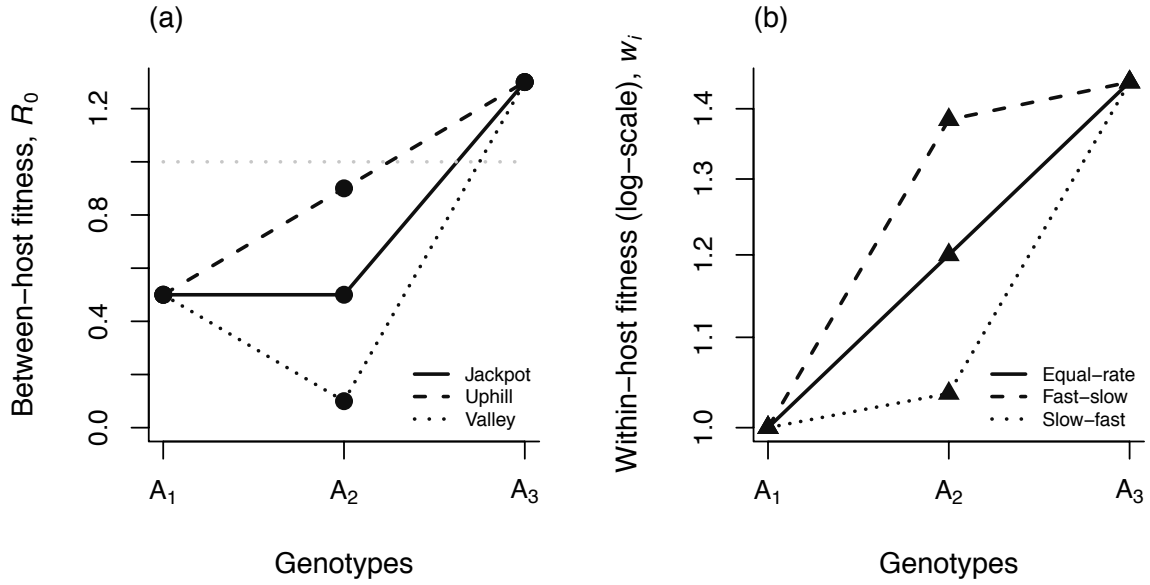

Figure 1.1: *Fitness landscapes at between-host and within-host scales.* Example landscapes are shown for a simple genotype space, with three genotypes connected sequentially. For this illustrative example, we consider landscapes where the fitnesses of initial (A_1) and emergence (A_3) genotypes are fixed, and only the fitness of the intermediate genotype (A_2) varies. (a) At the between-host scale the intermediate genotype may be more fit (yielding an "uphill" landscape), of equal fitness ("jackpot"), or less fit ("valley") than the initial genotype but only the emergence genotype A_3 has $R_0 > 1$. (b) At the within-host scale, under the SSWM model, the gain in relative fitness determines the rate of substitution between neighboring genotypes. The "equal-rate" landscape arises when relative fitness gains are equal for each step, the "fast-slow" landscape when the first step yields greater fitness gain than the second, and the "slow-fast" landscape in the reverse case. Note that we plot the logarithm of the absolute within-host fitnesses w_i, as noted in the text, because $w_j = (1 + s_{i,j})w_i$. We have normalized the fitnesses such that $w_1 = 1$. ($R_0^{(i)}$(uphill) $= [0.5, 0.9, 1.3], R_0^{(i)}$(jackpot) $= [0.5, 0.5, 1.3], R_0^{(i)}$(valley) $= [0.5, 0.1, 1.3], w_i$(equal-rate) $= [1, 1.2, 1.44], w_i$(fast-slow) $= [1, 1.38, 1.44], w_i$(slow-fast) $= [1, 1.04, 1.44]$

Figure 2

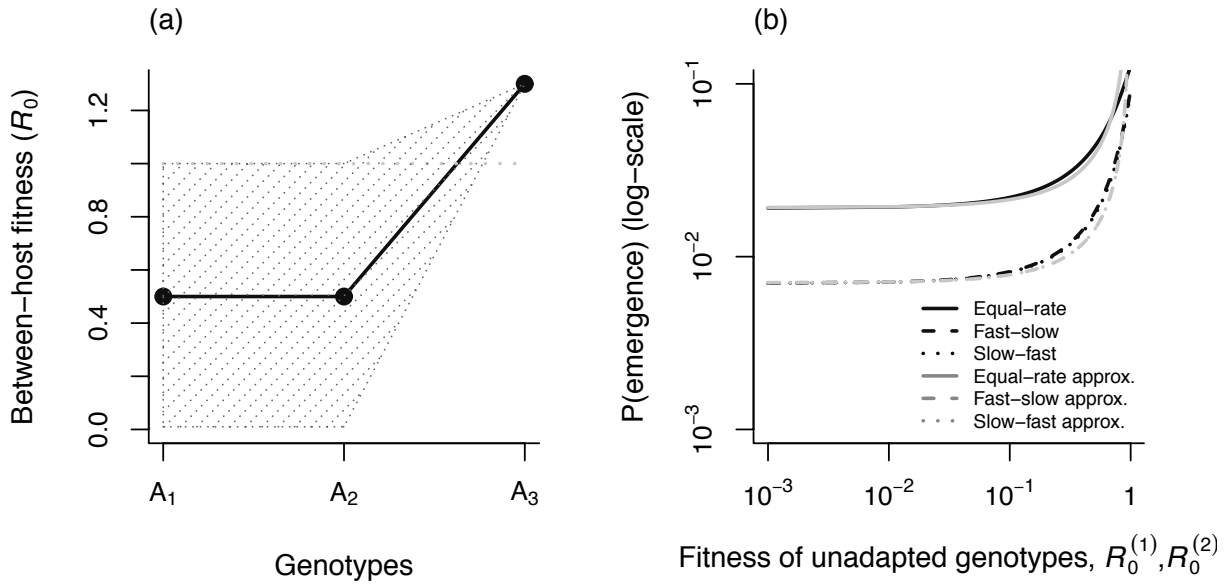

Figure 1.2: *Example of the interaction between selection at different scales.* (a) We consider a set of jackpot landscapes at the between-host scale, with a range of fitness values for the initial (A_1) and intermediate (A_2) genotypes (indicated by the shaded region). (b) The probability of emergence as a function of the between-host fitness of the A_1 and A_2 genotypes, showing the interaction with the three within-host landscapes. The equal-rate landscape gives the highest probability of emergence because it gives the fastest substitutions overall. Results for fast-slow and slow-fast landscapes overlap almost exactly. Black lines show exact solutions; grey lines show the approximation from equation (1.2), which fits well until $R_0^{(1)}$ and $R_0^{(2)}$ approach 1. ($d_1 = d_2 = d_3 = 1; b_3 = 1.3, b_1$ and b_2 adjusted to yield desired $R_0^{(i)}$ values; $N = 10^6, \mu = 10^{-6}$, constant of proportionality $= 0.4$).

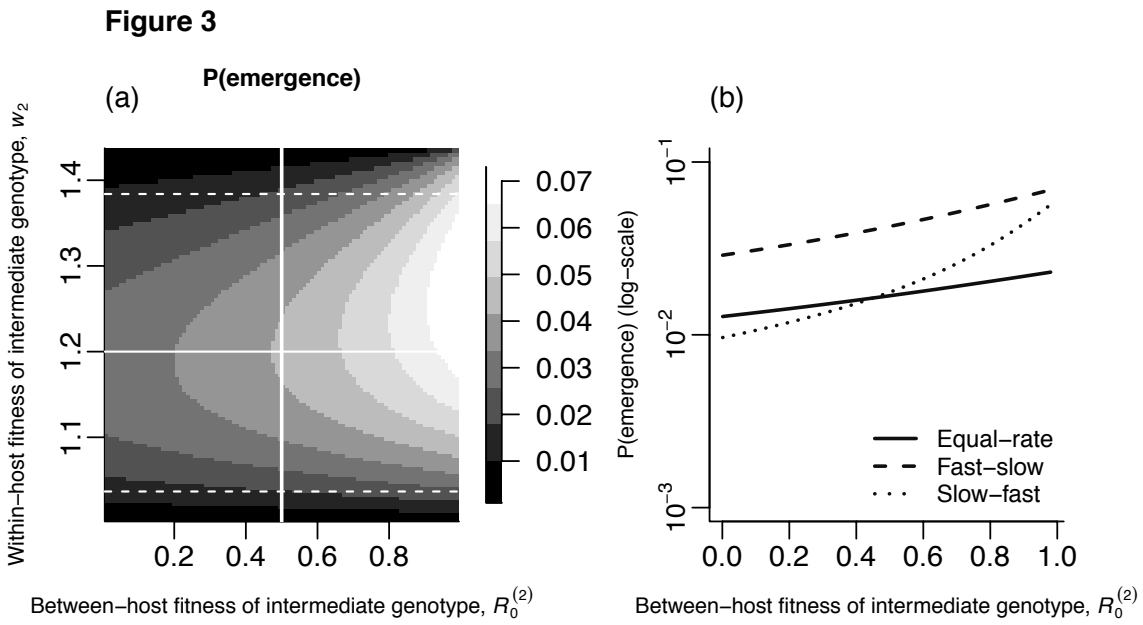

Figure 1.3: *Cross-scale interactions for all combinations of landscapes in a three-genotype chain.* (a) Heat-map showing the probability of emergence as the intermediate genotype is varied in fitness at both the within-host and between-host scales. Fitnesses of the initial and emergence genotypes are fixed, as in figure 1. The vertical solid line marks the between-host jackpot scenario and the horizontal solid line marks the within-host equal-rate scenario. The dotted and dashed lines represent the slow-fast (bottom) and fast-slow (top) from figure 1*b*, respectively. (b) Probability of emergence as a function of the between-host fitness of the intermediate genotype, $R_0^{(2)}$, for three within-host landscapes, corresponding to the horizontal lines in (a). The grey vertical shows where $R_0^{(2)} = 0.5$, i.e. the same value as $R_0^{(1)}$.

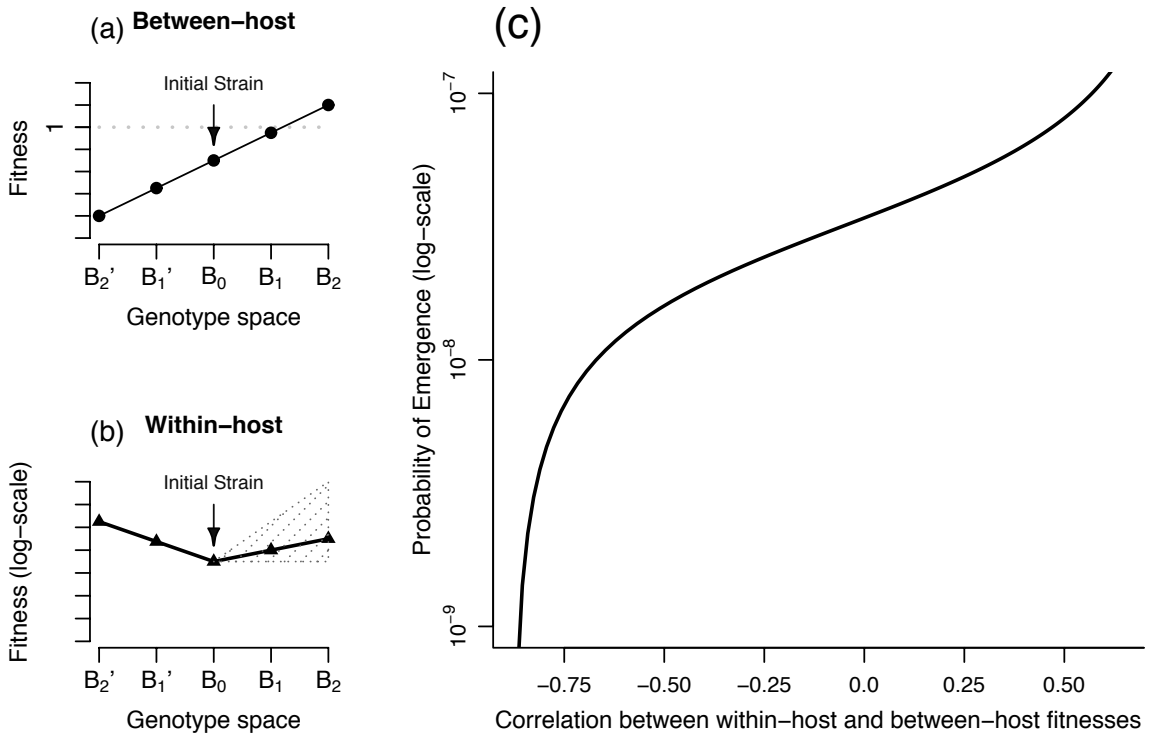

Figure 1.4: *Alternative pathways can lead to conflict between scales.* We assume the initial case is infected with genotype B_0, and two evolutionary pathways are available to the pathogen population. (a) At the between-host scale, fitness increases along the B_1, B_2 pathway, leading to possible emergence; fitness decreases along the B_1', B_2' pathway, leading to certain extinction. (b) At the within-host scale we assume equal-rate landscapes on both pathways, but vary the slope of the B_1, B_2 pathway (as indicated by the shaded area). Depending on the slope of the B_1, B_2 pathway at the within-host scale, substitution rates toward B_1 and B_2 can be higher or lower than toward B_1' and B_2'. (c) The correlation between fitnesses at within-host and between-host scales is a strong determinant of the probability of emergence. Positive correlations favor emergence, while negative correlations (which corresponds to lower slopes of the within-host B_1, B_2 landscape) cause the pathogen lineage to be drawn toward lower between-host fitness and extinction. We use Pearson's correlation coefficient to measure the linear dependence between the fitnesses at the two scales. ($R_0[B_2', B_1', B_0, B_1, B_2] = [0.2, 0.45, 0.7, 0.95, 1.2], d_i[B_2', B_1', B_0, B_1, B_2] = [0.1, 0.1, 0.1, 0.1, 0.1, 0.1], w_i[B_2', B_1', B_0, B_1, B_2]$ were drawn uniformly from the ranges $[1.44, 1.2, 1, 1.01 - 2.24, 1.02 - 2.25]$, within-host parameters N and μ as in previous figures).

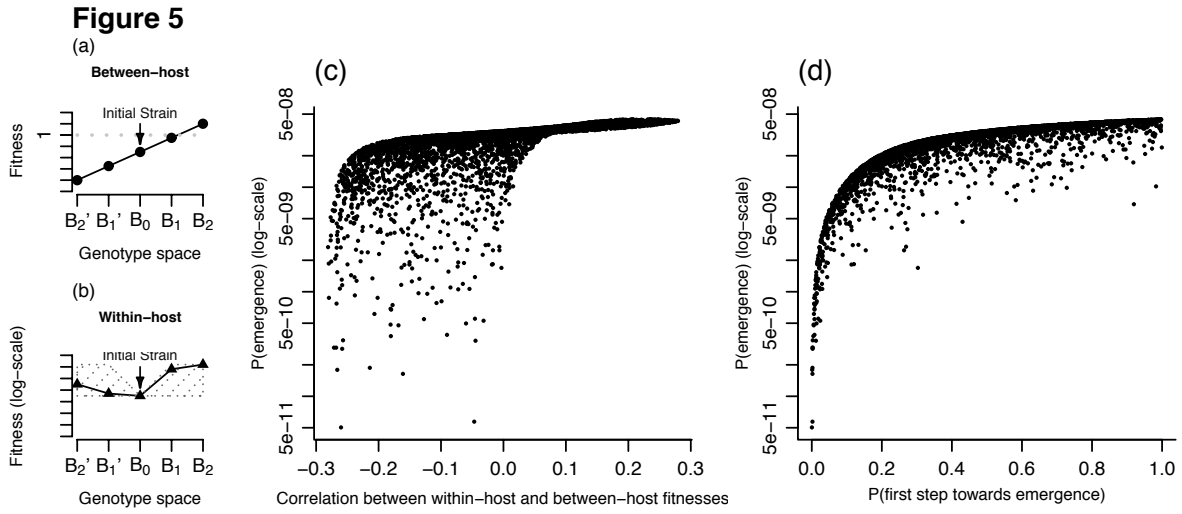

Figure 1.5: *Exploration of alternative pathways for general within-host landscapes.* This figure generalizes figure 4, such that (a) the between-host landscape is identical, but (b) the within-host landscapes sample a much broader set of possibilities. Within-host fitness of genotypes B_2', B_1', B_0, B_1, and B_2 were selected randomly, such that $w_i[B_2', B_1', B_0, B_1, B_2]$ were drawn uniformly from the ranges $[1.02 - 2.25, 1.01 - 2.24, 1, 1.01 - 2.24, 1.02 - 2.25]$. (c) The probability of emergence shows a positive association with the correlation between fitnesses across scales, though with considerable scatter. (d) The probability of emergence is more strongly associated with the probability that the first substitution event is toward genotype B_1 (i.e. toward possible emergence). Points for plots in (c) and (d) show the results of 5000 simulated within-host landscapes. (All parameters as in figure 4).

1.7 References

Bibliography

[1] H. Alexander and T. Day. Risk factors for the evolutionary emergence of pathogens. *Journal of The Royal Society Interface*, 7(51):1455–1474, 2010.

[2] A. B. Allison, C. E. Harbison, I. Pagan, K. M. Stucker, J. T. Kaelber, J. D. Brown, M. G. Ruder, M. K. Keel, E. J. Dubovi, E. C. Holmes, et al. Role of multiple hosts in the cross-species transmission and emergence of a pandemic parvovirus. *Journal of Virology*, 86(2):865–872, 2012.

[3] M. Amaku, M. N. Burattini, F. A. B. Coutinho, and E. Massad. Modeling the dynamics of viral evolution considering competition within individual hosts and at population level: the effects of treatment. *Bulletin of Mathematical Biology*, 72(5):1294–1314, 2010.

[4] J.-B. André and T. Day. The effect of disease life history on the evolutionary emergence of novel pathogens. *Proceedings of the Royal Society of London B: Biological Sciences*, 272(1575):1949–1956, 2005.

[5] R. Antia, B. R. Levin, and R. M. May. Within-host population dynamics and the evolution and maintenance of microparasite virulence. *The American Naturalist*, 144(3):457–472, 1994.

[6] R. Antia, R. Regoes, J. Koella, and C. Bergstrom. The role of evolution in the emergence of infectious diseases. *Nature*, 426(6967):658, 2003.

[7] N. Arinaminpathy and A. McLean. Evolution and emergence of novel human infections. *Proceedings of the Royal Society of London B: Biological Sciences*, page rspb20091059, 2009.

[8] C. L. Burch and L. Chao. Evolution by small steps and rugged landscapes in the rna virus ϕ6. *Genetics*, 151(3):921–927, 1999.

[9] C. L. Burch and C. Lin. Evolvability of an rna virus is determined by its mutational neighbourhood. *Nature*, 406(6796):625, 2000.

[10] C. S. M. E. Consortium et al. Molecular evolution of the SARS coronavirus during the course of the SARS epidemic in china. *Science*, 303(5664):1666–1669, 2004.

[11] D. Coombs, M. A. Gilchrist, and C. L. Ball. Evaluating the importance of within- and between-host selection pressures on the evolution of chronic pathogens. *Theoretical Population Biology*, 72(4):576–591, 2007.

[12] J. da Silva, M. Coetzer, R. Nedellec, C. Pastore, and D. E. Mosier. Fitness epistasis and constraints on adaptation in a human immunodeficiency virus type 1 protein region. *Genetics*, 185(1):293–303, 2010.

[13] M. Eigen. Viral quasispecies. *Scientific American*, 269(1):42–49, 1993.

[14] S. F. Elena and R. Sanjuán. Virus evolution: insights from an experimental approach. *Annu. Rev. Ecol. Evol. Syst.*, 38:27–52, 2007.

[15] A. S. Fauci and F. S. Collins. Benefits and risks of influenza research: lessons learned. *Science*, 336(6088):1522–1523, 2012.

[16] M. Faure, S. J. Schreiber, et al. Quasi-stationary distributions for randomly perturbed dynamical systems. *The Annals of Applied Probability*, 24(2):553–598, 2014.

[17] G. Fernàndez, B. Clotet, and M. A. Martínez. Fitness landscape of human immunodeficiency virus type 1 protease quasispecies. *Journal of Virology*, 81(5):2485–2496, 2007.

[18] C. Fraser, T. D. Hollingsworth, R. Chapman, F. de Wolf, and W. P. Hanage. Variation in hiv-1 set-point viral load: epidemiological analysis and an evolutionary hypothesis. *Proceedings of the National Academy of Sciences*, 104(44):17441–17446, 2007.

[19] V. V. Ganusov and R. Antia. Trade-offs and the evolution of virulence of microparasites: do details matter? *Theoretical Population Biology*, 64(2):211–220, 2003.

[20] M. A. Gilchrist and D. Coombs. Evolution of virulence: interdependence, constraints, and selection using nested models. *Theoretical Population Biology*, 69(2):145–153, 2006.

[21] J. H. Gillespie. Molecular evolution over the mutational landscape. *Evolution*, 38(5):1116–1129, 1984.

[22] J. B. S. Haldane. A mathematical theory of natural and artificial selection, part v: selection and mutation. In *Mathematical Proceedings of the Cambridge Philosophical Society*, volume 237, pages 838–844. Cambridge University Press, 1927.

[23] T. E. Harris. *The theory of branching processes*. Berlin:Springer, 1963.

[24] S. Herfst, E. J. Schrauwen, M. Linster, S. Chutinimitkul, E. de Wit, V. J. Munster, E. M. Sorrell, T. M. Bestebroer, D. F. Burke, D. J. Smith, et al. Airborne transmission of influenza A/H5N1 virus between ferrets. *Science*, 336(6088):1534–1541, 2012.

[25] K. Hoelzer, P. R. Murcia, G. J. Baillie, J. L. Wood, S. M. Metzger, N. Osterrieder, E. J. Dubovi, E. C. Holmes, and C. R. Parrish. Intrahost evolutionary dynamics of canine influenza virus in naive and partially immune dogs. *Journal of Virology*, 84(10):5329–5335, 2010.

[26] M. Imai, T. Watanabe, M. Hatta, S. C. Das, M. Ozawa, K. Shinya, G. Zhong, A. Hanson, H. Katsura, S. Watanabe, et al. Experimental adaptation of an influenza H5 haemagglutinin (HA) confers respiratory droplet transmission to a reassortant H5 HA/H1N1 virus in ferrets. *Nature*, 486(7403):420, 2012.

[27] Y. Iwasa, F. Michor, and M. A. Nowak. Evolutionary dynamics of invasion and escape. *Journal of Theoretical Biology*, 226(2):205–214, 2004.

[28] Y. Iwasa, F. Michor, and M. A. Nowak. Virus evolution within patients increases pathogenicity. *Journal of Theoretical Biology*, 232(1):17–26, 2005.

[29] J. L. W. V. Jensen. Sur les fonctions convexes et les inégalités entre les valeurs moyennes. *Acta Mathematica*, 30(1):175–193, 1906.

[30] K. E. Jones, N. G. Patel, M. A. Levy, A. Storeygard, D. Balk, J. L. Gittleman, and P. Daszak. Global trends in emerging infectious diseases. *Nature*, 451(7181):990–993, 2008.

[31] J. T. Kaelber, A. Demogines, C. E. Harbison, A. B. Allison, L. B. Goodman, A. N. Ortega, S. L. Sawyer, and C. R. Parrish. Evolutionary reconstructions of the transferrin receptor of caniforms supports canine parvovirus being a re-emerged and not a novel pathogen in dogs. *PLoS Pathogens*, 8(5):e1002666, 2012.

[32] B. F. Keele, E. E. Giorgi, J. F. Salazar-Gonzalez, J. M. Decker, K. T. Pham, M. G. Salazar, C. Sun, T. Grayson, S. Wang, H. Li, et al. Identification and characterization of transmitted and early founder virus envelopes in primary hiv-1 infection. *Proceedings of the National Academy of Sciences*, 105(21):7552–7557, 2008.

[33] L. Keller. *Levels of selection in evolution*. Princeton University Press, 1999.

[34] T. Kuiken, E. C. Holmes, J. McCauley, G. F. Rimmelzwaan, C. S. Williams, and B. T. Grenfell. Host species barriers to influenza virus infections. *Science*, 312(5772):394–397, 2006.

[35] J. O. Lloyd-Smith, D. George, K. M. Pepin, V. E. Pitzer, J. R. Pulliam, A. P. Dobson, P. J. Hudson, and B. T. Grenfell. Epidemic dynamics at the human-animal interface. *Science*, 326(5958):1362–1367, 2009.

[36] C. Loverdo, M. Park, S. J. Schreiber, and J. O. Lloyd-Smith. Influence of viral replication mechanisms on within-host evolutionary dynamics. *Evolution*, 66(11):3462–3471, 2012.

[37] E. R. Lozovsky, T. Chookajorn, K. M. Brown, M. Imwong, P. J. Shaw, S. Kamchonwongpaisan, D. E. Neafsey, D. M. Weinreich, and D. L. Hartl. Stepwise acquisition of pyrimethamine resistance in the malaria parasite. *Proceedings of the National Academy of Sciences*, 106(29):12025–12030, 2009.

[38] K. A. Lythgoe and C. Fraser. New insights into the evolutionary rate of hiv-1 at the within-host and epidemiological levels. In *Proc. R. Soc. B*, page rspb20120595. The Royal Society, 2012.

[39] A. Más, C. López-Galíndez, I. Cacho, J. Gómez, and M. A. Martínez. Unfinished stories on viral quasispecies and darwinian views of evolution. *Journal of Molecular Biology*, 397(4):865–877, 2010.

[40] N. Mideo, S. Alizon, and T. Day. Linking within-and between-host dynamics in the evolutionary epidemiology of infectious diseases. *Trends in Ecology & Evolution*, 23(9):511–517, 2008.

[41] D. M. Morens, G. K. Folkers, and A. S. Fauci. The challenge of emerging and re-emerging infectious diseases. *Nature*, 430(6996):242, 2004.

[42] J. I. Mullins, M. Rolland, and T. M. Allen. Viral evolution and escape during primary human immunodeficiency virus-1 infection: implications for vaccine design. *Current Opinion in HIV and AIDS*, 3(1):60–66, 2008.

[43] P. R. Murcia, G. J. Baillie, J. Daly, D. Elton, C. Jervis, J. A. Mumford, R. Newton, C. R. Parrish, K. Hoelzer, G. Dougan, et al. Intra-and interhost evolutionary dynamics of equine influenza virus. *Journal of Virology*, 84(14):6943–6954, 2010.

[44] P. R. Murcia, J. Hughes, P. Battista, L. Lloyd, G. J. Baillie, R. H. Ramirez-Gonzalez, D. Ormond, K. Oliver, D. Elton, J. A. Mumford, et al. Evolution of an eurasian avian-like influenza virus in naive and vaccinated pigs. *PLoS Pathogens*, 8(5):e1002730, 2012.

[45] S. Okasha. *Evolution and the levels of selection*. Oxford University Press, 2006.

[46] A. W. Park, J. M. Daly, N. S. Lewis, D. J. Smith, J. L. Wood, and B. T. Grenfell. Quantifying the impact of immune escape on transmission dynamics of influenza. *Science*, 326(5953):726–728, 2009.

[47] C. R. Parrish, E. C. Holmes, D. M. Morens, E.-C. Park, D. S. Burke, C. H. Calisher, C. A. Laughlin, L. J. Saif, and P. Daszak. Cross-species virus transmission and

the emergence of new epidemic diseases. *Microbiology and Molecular Biology Reviews*, 72(3):457–470, 2008.

[48] K. M. Pepin, S. Lass, J. R. Pulliam, A. F. Read, and J. O. Lloyd-Smith. Identifying genetic markers of adaptation for surveillance of viral host jumps. *Nature Reviews Microbiology*, 8(11):802, 2010.

[49] F. J. Poelwijk, D. J. Kiviet, D. M. Weinreich, and S. J. Tans. Empirical fitness landscapes reveal accessible evolutionary paths. *Nature*, 445(7126):383, 2007.

[50] T. C. Porco, J. O. Lloyd-Smith, K. L. Gross, and A. P. Galvani. The effect of treatment on pathogen virulence. *Journal of Theoretical Biology*, 233(1):91–102, 2005.

[51] T. C. Quinn, M. J. Wawer, N. Sewankambo, D. Serwadda, C. Li, F. Wabwire-Mangen, M. O. Meehan, T. Lutalo, and R. H. Gray. Viral load and heterosexual transmission of human immunodeficiency virus type 1. *New England Journal of Medicine*, 342(13):921–929, 2000.

[52] L. A. Reperant, T. Kuiken, B. T. Grenfell, A. D. Osterhaus, and A. P. Dobson. Linking influenza virus tissue tropism to population-level reproductive fitness. *PLoS ONE*, 7(8):e43115, 2012.

[53] C. A. Russell, J. M. Fonville, A. E. Brown, D. F. Burke, D. L. Smith, S. L. James, S. Herfst, S. Van Boheemen, M. Linster, E. J. Schrauwen, et al. The potential for respiratory droplet–transmissible A/H5N1 influenza virus to evolve in a mammalian host. *Science*, 336(6088):1541–1547, 2012.

[54] R. Sanjuan, M. R. Nebot, N. Chirico, L. M. Mansky, and R. Belshaw. Viral mutation rates. *Journal of Virology*, 84(19):9733–9748, 2010.

[55] S. J. Schreiber and J. O. Lloyd-Smith. Invasion dynamics in spatially heterogeneous environments. *The American Naturalist*, 174(4):490–505, 2009.

[56] T. Sheahan, B. Rockx, E. Donaldson, D. Corti, and R. Baric. Pathways of cross-species transmission of synthetically reconstructed zoonotic severe acute respiratory syndrome coronavirus. *Journal of Virology*, 82(17):8721–8732, 2008.

[57] K. M. Stucker, I. Pagan, J. O. Cifuente, J. T. Kaelber, T. D. Lillie, S. Hafenstein, E. C. Holmes, and C. R. Parrish. The role of evolutionary intermediates in the host adaptation of canine parvovirus. *Journal of Virology*, 86(3):1514–1521, 2012.

[58] G. P. Wang, S. A. Sherrill-Mix, K.-M. Chang, C. Quince, and F. D. Bushman. Hepatitis c virus transmission bottlenecks analyzed by deep sequencing. *Journal of Virology*, 84(12):6218–6228, 2010.

[59] D. M. Weinreich, N. F. Delaney, M. A. DePristo, and D. L. Hartl. Darwinian evolution can follow only very few mutational paths to fitter proteins. *Science*, 312(5770):111–114, 2006.

[60] G. C. Williams. *Natural selection: domains, levels, and challenges*. Oxford University Press, 1992.

[61] C. Wright, M. Morelli, G. Thébaud, N. Knowles, P. Herzyk, D. Paton, D. Haydon, and D. King. Beyond the consensus: dissecting within-host viral population diversity of foot-and-mouth disease virus by using next-generation genome sequencing. *Journal of Virology*, 85(5):2266, 2011.

[62] A. Yates, R. Antia, and R. R. Regoes. How do pathogen evolution and host heterogeneity interact in disease emergence? *Proceedings of the Royal Society of London B: Biological Sciences*, 273(1605):3075–3083, 2006.

[63] G.-p. Zhao. SARS molecular epidemiology: a chinese fairy tale of controlling an emerging zoonotic disease in the genomics era. *Philosophical Transactions of the Royal Society of London B: Biological Sciences*, 362(1482):1063–1081, 2007.

CHAPTER 2

Effects of prophylaxis and intermittent selection on the emergence of drug resistance

Miran Park, James O. Lloyd-Smith

2.1 Abstract

Drug resistance is an increasing concern in the treatment and control of pathogen outbreaks. Individual behavior regarding antimicrobial treatments can create intermittent selection environments that change rapidly relative to pathogen life-history parameters. Prophylactic treatment can also create a host environment where evolutionary selection for resistance is present from the moment of first exposure to the pathogen. Previous theoretical studies have described how different treatment regimens and administration of prophylaxis give rise to different resistance outcomes. However, these studies have favored different optimal treatment strategies: some have recommended widespread drug treatment to reduce transmission and suppress epidemic growth, with aggressive treatment to suppress the emergence of resistance; others have argued that aggressive treatment increases the selective pressure for resistance to unacceptable levels. Often, there is a high fitness cost assumed for resistance mutations which may additionally limit the scope of qualitative outcomes. Here, we explore both short-term and long-term outcomes of drug resistance using stochastic models of pathogen emergence to better understand the influence of treatment and pathogen fitness on the emergence of drug resistance in the early phase of an epidemic. We find that treatment always (and prophylaxis often) reduces both the probability of establishment of the

epidemic and the intensity of the epidemic, but increasing treatment may worsen resistance outcomes, especially combined with prophylaxis and a small fitness cost for resistance. Our analysis shows that the effects of prophylaxis and treatment depend strongly on the fitness of the resistant genotype and efficacy of the prophylaxis, and advances our understanding of tradeoffs between efforts to control epidemic versus resistance outcomes. In light of our results, we propose further theoretical and experimental analysis regarding the emergence of resistance, prophylaxis and treatment protocols, and studies on pathogen fitness.

2.2 Introduction

Antimicrobial resistance is an increasing concern for many infectious diseases, and the scope of the resistance problem is expanding with respect to pathogens, drugs, and geographic areas affected [40, 15]. Although drug resistance is a major concern for many pathogens, other priorities in epidemic control, such as using treatment to reduce transmission and control epidemic growth, may sometimes conflict with optimal outcomes in terms of resistance emergence. Individual behavior related to treatment usage, such as personal stockpiling of drugs and poor treatment adherence, can influence the selective pressures acting on resistance and rapidly change the evolutionary landscape experienced by the pathogen [37, 49]. Pathogens can evolve quickly, and if individuals go on and off treatment on a short timescale relative to the infection duration (e.g. going on and off treatment on a daily basis versus a two-week infection duration), this rapidly changing treatment environment creates fluctuating selection pressures for the pathogen. Prophylaxis (i.e. taking an antimicrobial before contracting a disease in order to prevent transmission) has also been shown to select for resistance in certain cases, such as in pre-exposure prophylaxis for HIV [31], oseltamivir resistance for influenza [4, 14, 39], and doxycycline prophylaxis for malaria [34]. Also, while the early phase of an epidemic has been shown to be important to resistance outcomes [12, 57], most studies have focused on the long-term evolutionary dynamics of drug resistance in a deterministic setting [57, 51]. The few studies that have examined the earlier, transient

phase of dynamics have shown that stochasticity can be important to resistance outcomes; for example, stochastic variability in epidemic size can make treatment more favorable if it prevents an outbreak [56, 57]. Understanding the mechanistic underpinnings of the factors driving resistance and epidemic outcomes in the inherently stochastic environment of epidemic establishment and growth is a crucial part of understanding the underlying factors influencing emergence of resistance as a whole.

Human behavior can lead to great variation in how individuals interact with antimicrobial drugs [7]. Increased media reports about pandemics and emerging infectious disease events have garnered concern regarding preparation and control policies, including regarding resistance [36]. Previously, influenza epidemics and media reports have likely led to an increase in filled prescriptions of oseltamivir, the most commonly prescribed influenza antiviral, for personal stockpiling [41, 16]. Personal stockpiling of antimicrobials can lead to insufficient doses or inadequate courses of therapy as individuals may take the treatment more randomly or at-will, without the supervision of a medical provider [37]. Individuals prescribed antibiotics inappropriately (e.g. for a viral infection for which antibiotics would have no effect) are at risk of developing persistent drug resistance as commensal bacteria acquire resistance under the selection pressure of the antibiotic, creating a potential source of resistant genotypes as gene transfer can occur with pathogenic species during subsequent infection [9]. Similarly, prolonged and inadequate prophylaxis can lead to the generation of resistance [23]. Given this evidence, it is important to consider how individual behavior and time spent on treatment can affect the evolutionary pressures selecting for resistance, as population-wide treatment measures may not have their intended effect on epidemic control.

Theoretical models have been analyzed to study how structured populations, fitness cost of resistance, and timing of treatment and prophylaxis can affect the emergence of drug resistance. It has been shown that there are trade-offs between controlling epidemic severity and the emergence and proliferation of resistance [57, 51]. A number of studies, many of which have assumed a high fitness cost to resistance, have found trade-offs between con-

trolling epidemic severity and the proliferation of resistance [11, 21, 22, 13, 56, 45, 52], and perspectives differ about optimal timing of treatment and prophylaxis. Some studies have shown that controlling epidemic size is generally preferable as it leads to a decreased number of transmission events occurring overall, giving less opportunity for the pathogen to develop resistance because of reduced numbers of infections [1, 13, 22]. However, other analyses have shown that although treatment and prophylaxis may significantly reduce epidemic transmission events, this can result in the greatest number of resistant infections due to increased selection on the pathogen for resistance [1, 21, 32, 35, 52]. Both perspectives show that the treatment regimen during initial stages of the epidemic is crucial, and that efforts to strongly suppress the epidemic can be beneficial but may not outweigh the added risk of high resistance if the pathogen is able to establish an epidemic in the population. However, existing work has not considered how these outcomes and expectations may be altered given the interaction of differing levels of treatment and prophylaxis with different fitness of the resistant genotypes.

The fitness of drug-resistant genotypes can vary widely across pathogens and antimicrobial drugs. Fitness costs are often expected for resistant mutations but empirical studies have revealed some exceptions [44, 27, 33]). Transmission fitness has been shown to be compromised by the evolution of resistance to atovaquone in malaria, and multiple drug-resistance mutations have been shown to be completely unable to transmit from mouse to mouse via mosquito [20]. In contrast, the H274Y mutation conferring oseltamivir resistance in influenza has been shown to have little to no fitness cost for transmission in ferrets [27], and possibly in human data, which may be due to compensatory mutations or genetic hitchhiking on an escape mutation [6]. Describing the evolutionary fitness of a pathogen is complicated by the fact that pathogens exhibit fitness at multiple scales [43, 19, 42]. At the within-host scale, fitness is measured by a pathogen's ability to grow within an infected individual, while at the between-host scale, fitness is measured by a pathogen's transmissibility. Within-host fitnesses may not correspond to between-host fitnesses, as in the example mentioned for H274Y, where the resistant genotype is outcompeted within-host by the sensitive genotype

but without any effective difference at the between-host (transmission) scale [27]. A difference of fitness across scales is implicit in any situation where drug-resistant strains, which are selected at the within-host scale when drug is present, have poor transmission, as with the example of atovaquone-resistance in malaria. Higher resistant genotype fitnesses will be favored by selection, but it is unclear how evolutionary outcomes will interact with treatment, prophylaxis, and the selection acting at multiple scales.

We still lack a complete understanding of how treatment and prophylaxis can affect early-stage evolutionary and epidemiological dynamics, and how these dynamics may affect longer-term resistance outcomes. Additionally, while individual behaviors determine the evolutionary selection environment for the pathogen (which may change rapidly as individuals go on and off treatment), most previous studies have modeled treatment at the population level without considering these effects. Here we present a model that represents the early dynamics of an epidemic while incorporating these important factors (individual behavior, prophylaxis, selection at multiple scales) to better understand the mechanisms that drive emergence of drug resistance during the emergence and establishment of an epidemic. Following established literature on pathogen emergence [3, 43], we use a stochastic multitype branching process model to represent the stochasticity of emergence of an epidemic and the behavior of individuals as they switch on and off drug treatment. We also present longer-term stochastic expectations of the model after the epidemic has established, in order to study the overall growth rate of the epidemic and the prevalence of resistant genotypes in the population. Using this model we address questions about the influences of treatment and prophylaxis on the emergence of resistance, and we present an explanation for discrepancies among past studies by showing how different regions of parameter space lead to different qualitative outcomes.

2.3 Model structure

We use a continuous-time, multitype branching process model to represent the stochastic dynamics of transmission, recovery, and pathogen genotype change (at individual and population scales) during the initial stages of an epidemic. We make the assumption of a well-mixed population that is homogenous with respect to all traits other than antimicrobial drug use, in which the number of susceptibles is initially large enough that it is not significantly depleted by the initial phase of the epidemic considered here. We use a simple one-allele model for resistance (no compensatory or permissive mutations, or partially resistant genotypes) as a basic model, reflecting empirical examples such as point mutations in influenza conferring drug resistance [4], but the model can be expanded readily to incorporate multiple genotypes.

Each infected host is characterized by a single pathogen genotype (drug-sensitive or drug-resistant) and treatment status at any point in time. These types consist of sensitive/untreated (s_u), sensitive/treated (s_t), resistant/untreated (r_u), and resistant/treated (r_t) (Figure 1). For readability, in the text following, we will refer to these genotype and treatment combinations as types $i = 1$, 2, 3, and 4, respectively. At the population scale, the reproductive number, R_0, is the number of new infections an infection will create over its duration, and is an important determinant of epidemic potential. If R_0 is less than 1, then the epidemic will die out, whereas if R_0 is greater than 1, the epidemic can establish with nonzero probability. We assume that without drug, the sensitive genotype has a reproductive number greater than 1, and that the treatment is effective such that in a treated population the sensitive genotype has a reproductive number less than 1. Parameters are marked with a subscript or superscript i corresponding to the four numbered pathogen genotypes. Each infected individual of type i infects other individuals at a constant rate b_i (modified by prophylaxis and the protective efficacy of prophylaxis), and in a successful transmission will give rise to a new infected individual of the same genotype but of either treatment status. Infected hosts of type i cease to be infectious, through recovery or death, at per capita rate

d_i. In order to consider the effects of differing genotype fitnesses, we define the reproductive number of each type. We herein define each type's fitness (corresponding specifically to a between-host transmission fitness measure) as the ability to transmit through a homogenous population of hosts of that type: $R_0(i) = b_i/d_i$ for type i. We note that this quantity refers to an individual of type i's ability to reproduce when existing as that type, however infections of type i may also be created by other types, as shown in Figure 1 and detailed below in the mechanistic structure of the model. The fitnesses for the sensitive/untreated (type 1) and sensitive/treated (type 2) types are fixed, at supercritical and subcritical values, respectively, while we vary the resistant/untreated (type 3) and resistant/treated (type 4) fitnesses to reflect how differing fitnesses of resistant genotypes influence resistance emergence. However, we assume that the resistant/untreated and resistant/treated types have equal fitness, i.e. we assume that the resistance phenotype nullifies any effect of treatment, and that the between-host transmission cost of resistance is not influenced by whether the host is on treatment.

We incorporate fitness at the within-host scale implicitly through the parameter μ, which represents both the rate at which the resistance mutation occurs and the probability that it goes to fixation in the host, since each host is assumed to have a single dominant genotype of pathogen. In past work, drawing upon the strong selection, weak mutation model from population genetics [18], we have shown that this model formulation can represent within-host fitness, subject to the assumptions that only beneficial mutations have a non-zero chance of fixation [43]. We need two parameters for this process (Figure 1): $\mu_{s\to r}$, representing a change from the sensitive to resistant genotype (only selected while under treatment), and $\mu_{r\to s}$, representing a change from the resistant to sensitive genotype (only selected while not under treatment). We choose $\mu_{s\to r} > \mu_{r\to s}$, reasoning that within-host selection for the resistant genotype over the sensitive genotype when an individual is undergoing treatment will be stronger than selection for the sensitive genotype over resistant genotype when the individual is not undergoing treatment, i.e. the benefit of resistance under treatment outweighs the cost of resistance when not under treatment.

Treatment is represented through the parameters ρ and σ, which represent per capita rates of switching on and off treatment, respectively. For simplification we represent the σ parameter as a scaled factor of ρ, such that $\sigma = k\rho$ (Figure 1). We assume that changes in treatment status and changes in genotype of infection occur independently, and that a genotype change event and a treatment switching event cannot occur simultaneously, e.g. the sensitive/untreated type cannot change directly to the resistant/treated type. We assume that a proportion p of the population is on prophylaxis at any point in time, and that mixing patterns are independent of prophylaxis; thus we divide up all potential transmission events occurring from each type, with the fraction p going to individuals on prophylaxis, and $(1-p)$ to individuals not on prophylaxis (Figure 1). We also accommodate the protective efficacy of prophylaxis using the parameter c (which we herein call the "protective efficacy" referring specifically to that of prophylaxis); this parameter only applies for transmission occurring from the sensitive genotype, as we assume that prophylaxis is not protective when the pathogen is resistant to treatment. When c is 1, prophylaxis is completely effective and all transmission of the susceptible genotype to individuals on prophylaxis is halted. Similarly, when c is 0, prophylaxis has no protective efficacy and transmission rates are not affected by whether the target individuals are taking prophylaxis.

2.4 Model analysis

We analyze this stochastic model to obtain the probability of emergence, $P(emergence)$, which denotes the probability that the epidemic breaks out in the population (which can include any mixture of types). We calculate $P(emergence)$ numerically using standard methods for the multi-type branching process model, here we use a functional iteration of the generating functions to first calculate the probability of extinction, $P(extinction)$, and then calculate the probability of emergence as $P(emergence) = 1 - P(extinction)$ [24, 30]. The generating functions used in these calculations are as follows:

$$
\begin{aligned}
g(s_u) &= \frac{1}{b_1(1-p) + b_1(1-c)p + \rho + d_1} b_1(1-p)s_u^2 + b_1(1-c)ps_u s_t + \rho s_t + d_1 \\
g(s_t) &= \frac{1}{b_2 p + b_2(1-p) + \sigma + d_2 + \mu_{s\to r}} b_2(1-c)ps_t^2 + b_2(1-p)s_u s_t + \sigma s_u + d_2 + \mu_{s\to r} r_t \\
g(r_u) &= \frac{1}{b_3(1-p) + b_3(1-c)p + \rho + d_3 + \mu_{r\to s}} b_3(1-p)r_u^2 + b_3(1-c)pr_u r_t + \rho r_t + d_3 + \mu_{r\to s} s_u \\
g(r_t) &= \frac{1}{b_4(1-c)p + b_4(1-p) + \sigma + d_4} b_4(1-c)pr_t^2 + b_4(1-p)r_u r_t + \sigma r_u + d_4
\end{aligned}
\tag{2.1}
$$

Each equation describes the dynamics of each type in our system, and each term in the equation reflects the probability of different outcomes in a competing rates formulation. The first denominator term represents the overall rate of any event occurring, with each term containing the rate of that process occurring and the quantity of index variables reflecting the types created or transitioned from that state, e.g. the term containing $b_1(1-p)s_u^2$ in $g(s_u)$ describes the infection and creation of another individual of type s_u which requires a successful infection b_1 and for the transmission to be an individual on not on prophylaxis $(1-p)$ resulting in two s_u individuals total (hence the exponent of 2), divided by the overall rate (first denominator term).

The extinction probability when the epidemic is initialized with one individual of type s_u is the first value of the smallest nonnegative root of $g(\vec{x}) = x$ (where $\vec{x}$ is the vector of host types in the model, i.e. $\vec{x} == \{s_1, s_2, r_1, r_2\}$). We can calculate this root by functional iteration of this recurrence relation, starting the process at a value of $\{0, 0, 0, 0\}$ and iterating the equation to convergence of the extinction probability. It is possible to calculate the extinction probability for any initial distribution and abundance of individuals given these relationships by substituting the initial distribution into the equations described and calculating by a similar process [48]

We can obtain the fundamental matrix N for the transitions of genotype and treatment state of an individual during infection using the relationship:

$$N = (I - Q)^{-1} \tag{2.2}$$

[29] where I is an identity matrix of the same dimensions as N, and Q is the infinitesimal generator of the Markov chain, where each element q_{ij} is a rate reflecting the transition probability from type i to type j:

$$Q = \begin{pmatrix} 1 - d_1 - \rho & \rho & 0 & 0 \\ \sigma & 1 - d_2 - \sigma & 0 & \mu_{s \to r} \\ \mu_{r \to s} & 0 & 1 - d_3 - \rho & \rho \\ 0 & 0 & \sigma & 1 - d_4 - \sigma \end{pmatrix}. \tag{2.3}$$

This matrix includes the individual state transitions (i.e. changes in treatment status, mutations in genotype) but excludes transmission rates.

The fundamental matrix then tells us the expected time an infected individual will spend in each type, given the type they were in when they became infected (i.e. row 1 indicates starting the system with an individual of s_u (sensitive/untreated), with the columns corresponding to the time spent in each of the other respective types) [53].

For results relating to after the epidemic has established, following previous work we obtain the next-generation matrix, given by $K = FV^{-1}$ [53, 38], where F is a matrix describing the rate of new infections in each type i from each type j, and V is the matrix describing

the rate of transitions out of state − the transitions into a state, with transitions out of the type occurring on the diagonal and all other transitions into a type occurring on off-diagonal according to their indices. Here F and V are as follows:

$$F = \begin{pmatrix} b_1(1-p) & b_2(1-p) & 0 & 0 \\ b_1(1-c)p & b_2(1-c)p & 0 & 0 \\ 0 & 0 & b_3(1-p) & b_4(1-p) \\ 0 & 0 & b_3(1-c)p & b_4(1-c)p \end{pmatrix} \tag{2.4}$$

and

$$V = \begin{pmatrix} d_1+\rho & -\sigma & -\mu_{r\to s} & 0 \\ -\rho & d_2+\sigma+\mu_{s\to r} & 0 & 0 \\ 0 & 0 & d_3+\rho+\mu_{r\to s} & -\sigma \\ 0 & -\mu_{s\to r} & -\rho & d_4+\sigma \end{pmatrix}. \tag{2.5}$$

Note that V^{-1} is equivalent to the transpose of the fundamental matrix derived above [53, 38].

R_0 of the epidemic incorporating all types is found by calculating the largest eigenvalue (spectral radius) of K. (When we refer to R_0 without superscript in the text following, we are referring to this quantity regarding the system as a whole.)

In order to calculate an instantaneous prevalence of each type after the epidemic has established, we calculate the quasi-stationary distribution of the system. By finding the normalized left-eigenvector associated with the dominant eigenvalue of the next-generation matrix, we are able to find the proportion of new infections occurring in each type conditioned on emergence in the system [10]. We then normalize the fundamental matrix by rows, creating a matrix $N*$ for which the element $N*_{i,j}$ is the proportion of time spent in type j by an individual who begins their infection as type i. We can multiply the eigenvector

$\vec{u}$ by each column of the normalized fundamental matrix and sum these values to get an instantaneous prevalence $\vec{a}$ of each type after the epidemic has established:

$$\vec{a} = \vec{u} \cdot N^*. \tag{2.6}$$

This allows us to analyze the instantaneous prevalence of resistance of each type given different parameter values and combinations akin to potential real-world scenarios.

Throughout our work, we have used these analytic results to compute desired quantities, and confirmed their accuracy by simulation (Supplemental Figure 1).

2.5 Results

2.5.1 Model parameterization

We chose illustrative parameter values comparable to values used in previous studies of this topic [13, 21, 32, 35, 52]. Our main analyses explore a range of values for the fitness of resistant genotypes, and a range of values for the proportion of time spent on treatment, for scenarios with and without prophylaxis (Table 1). In later analyses we explore the sensitivity of our findings to these parameters values. For simplicity, when varying the amount of time spent on treatment we fix ρ (going on treatment) and vary σ (going off treatment). Fitness for the sensitive/untreated and sensitive/treated types are fixed at $R_0^{(1)} = 1.5$ and $R_0^{(2)} = 0.5$ respectively, as the sensitive wild-type pathogen is assumed to be fit enough to sustain an epidemic when no treatment is administered, and the treatment is assumed to be effective in reducing the burden of susceptible strains, but not effective enough to clear infection entirely.

2.5.2 Effect of treatment and prophylaxis on epidemic outcomes

In Figure 2, we outline the dependence of R_0, $P(emergence)$, and the long-term prevalence of the resistant genotype on the impact of control measures (treatment, prophylaxis) and fitness of the resistant genotype. Each curve corresponds to a different value of the resistant genotype fitnesses (which are equal in untreated and treated hosts, i.e. $R_0^{(3)} = R_0^{(4)}$) ranging from 0.3 to 1.7 to encompass a fitness range from lower than the sensitive/treated to higher than the sensitive/untreated types.

Without prophylaxis, more time on treatment (increasing x-axis) generally leads to a lower R_0, except when the resistant genotype is more fit than the wild-type (Figure 2(a)). More treatment always reduces $P(emergence)$ (Figure 2(b)), but there is a trade-off where increasing time spent on treatment increases the resistant genotype prevalence if the epidemic does become established (Figure 2(c)). The combination of these patterns leads to a subtlety in the behavior of the system R_0: when the resistant strain is slightly less fit than the sensitive/untreated strain, R_0 has a minimum at intermediate treatment levels, when the sensitive strain is suffering the fitness reduction from effective treatment, then increases towards the fitness of the resistant genotypes as the prevalence of resistance rises with more treatment (Figure 2(a,c)).

We then considered a scenario with a moderate level of prophylactic use of antimicrobials (specifically, 30% of people use prophylaxis, and it is 70% effective at blocking infection by the sensitive strain). With prophylaxis, results are similar for R_0 (Figure 2(d)), with slightly more extreme values, where there is a broader range of resistant fitness values for which the curve is strictly increasing due to the additional reduction in fitness from prophylaxis. Note that values on the x-axis are a ratio of the ρ and σ parameters and do not account that some cases are started in the treated state. Absolute values of $P(emergence)$ with prophylaxis (Figure 2(e)) are lower than those without prophylaxis (Figure 2(b)), however, these values increase slightly as time spent on treatment increases. This is consistent with previous re-

sults which have generally found a benefit to prophylaxis for curbing resistance emergence via containing the outbreak [21]. The prevalence of resistance also generally rises with time on treatment, as before, with a small dip for the resistant genotype values with the highest fitness as treatment is initially increased. This dip occurs because time spent in the resistant/untreated type decreases rapidly as treatment is increased, and then resistant/treated prevalence increases as time spent on treatment is increased due to the evolutionary advantage of higher resistant fitness (results not shown). Based on these results, a moderate level of prophylaxis appears to be generally valuable for suppressing $P(emergence)$ and therefore the probability of an epidemic, without too much effect on other outcomes of interest. However, we have identified interesting non-monotonic relationships between time spent on treatment and epidemic outcomes when prophylaxis is present, implying more careful consideration is needed for both prophylaxis and treatment measures. We will explore these relationships further in order to understand what is causing this more complex behavior and its implications on epidemic outcomes.

2.5.3 Trade-offs in epidemic control versus prevalence of resistance

To explore the relationships between probability of emergence, R_0, resistant genotype prevalence, and prophylaxis we plot these quantities against each other in Figure 3. We see again that, for a given fitness of the resistant genotype, the probability of emergence is lower with prophylaxis than without (dashed vs. solid lines respectively). More fit resistant genotypes lead to both higher probability of emergence and higher population-level R_0 values and thus, unsurprisingly, are of greater concern (Figure 3(a)). As time spent on treatment is increased (following each trajectory starting at the circle marker and ending at the triangle marker), generally, both $P(emergence)$ and R_0 initially decrease. As treatment time increases, however, a trade-off emerges between $P(emergence)$ and R_0. Generally the probability of emergence continues to decrease with increasing time spent on treatment, but eventually R_0 increases, implying that although there is less probability of an epidemic establishing, once the epidemic establishes it will be more severe. This effect becomes more

marked as the fitness of the resistant mutant increases. As time on treatment is increased even further, the trajectory can slope back upwards, implying increased risk with respect to both the probability of the epidemic establishing and the intensity of the epidemic. This is especially evident for trajectories with prophylaxis (dashed lines). Although prophylaxis lowers $P(emergence)$ and R_0 for a given fitness of the resistant genotype, increasing amounts of treatment after infection often lead to worse control outcomes with regard to severity of the epidemic, and can also potentially increase the probability of emergence. With more extreme values of higher resistant fitness the increases in epidemic severity and probability of emergence can also occur without prophylaxis, however for infection and recovery rates this requires the resistant genotype(s) to be significantly more fit than the sensitive genotype(s), which is an unlikely scenario.

In Figure 3(b), we illustrate the strong trade-off between probability of emergence and prevalence of the resistant genotype. Greater time spent on treatment generally decreases the probability of emergence, but there is virtually always an increase in the resistant genotype prevalence if the outbreak were to establish, especially when there is no prophylaxis. With prophylaxis and higher resistant genotype fitness it is shown that higher treatment increases both probability of emergence and resistant genotype prevalence.

2.5.4 Characterizing the effects of prophylaxis and resistant genotype fitness on resistance prevalence

Given the importance of prophylaxis for resistant genotype prevalence and epidemic outcomes, we explore the different qualitative outcomes comparing prophylaxis and no prophylaxis for multiple scenarios of resistant genotype fitness and treatment intensity (Figure 4). This heat map shows the increase of resistant genotype prevalence when prophylaxis is added to a system, with all other parameter values fixed at values spanning the full range examined previously. For some of the explored range of parameter values there aren't no-

table differences when adding prophylaxis to the system, however, there is a broad regime of parameter combinations where the resistant genotype prevalence is significantly increased.

Generally, when the resistant genotype fitness is high, increasing the time spent on treatment decreases the difference in the prevalence of resistance when adding prophylaxis. Notably, the most extreme differences arise when the resistant genotype has comparable fitness to the wild-type, and when time spent in treatment is near zero. This can be understood because the prevalence of such highly fit resistant strains will be high in the presence of any antimicrobial selection, so the marginal impact of prophylaxis is greates when other treatment rates are low (Figure 2(c,f)). When the resistant genotype fitness is lower (but still high enough to generate significant numbers in an outbreak), adding prophylaxis can still increase the resistant genotype prevalence substantively, despite its lowered fitness. If the prevalence of the resistant genotype is an important control outcome, it is worthwhile to consider that there may exist combinations of parameter trade-offs that can suppress or favor resistance, especially in the context of prophylaxis.

To further elucidate the interaction between the resistant genotype prevalence and severity of the outbreak and epidemic potential, we simulated 1000 outbreaks per set of parameters and recorded their sizes and resistant genotype prevalences (Figure 5). Simulation was conducted as a stochastic branching process model using the Gillespie forward simulation algorithm [17]. Outbreak size was captured as the number of total cases in existence at a set time after iteration (150 time steps), and outbreaks were considered established if epidemic size reached over 100 cases. Here we assumed that 30% of the population used prophylaxis ($p = 0.3$) throughout, and we explore different values of c, the proportion by which prophylaxis reduces risk of infection with the sensitive strain, to understand how protective efficacy can affect epidemic outcomes. Here we compare values of $c = 0.3$ and $c = 0.7$, to represent approximate values corresponding to notable examples of established prophylactic regimens [25, 50] and to demonstrate different qualitative outcomes.

Figure 5 elaborates upon the trade-offs we have discussed, to explore varying efficacies of prophylaxis. For lower fitness of the resistant genotype (black and blue points), effective prophylaxis helps curb epidemic emergence overall and outbreak size, indicated by the lack of successful outbreaks (in number) and lowered outbreak size. Additionally, the prevalence of the resistant genotype is generally low due to its poor fitness. Notably, however, when prophylaxis is more effective (black points), there is a tendency toward outbreaks with significantly higher resistant genotype prevalence – though these are few and small in size, so ultimately a minor health risk. For higher fitness of the resistant genotype (red and purple points), we see larger epidemics (note the log-scale on the x-axis) which have a large proportion of resistant infections. In this case, more effective prophylaxis (red points) leads to significantly higher prevalence of the resistant genotype, though outbreak sizes tend to be smaller than for less effective prophylaxis (purple points), and the number of successful emergence events is fairly comparable for the two scenarios, showing a limited influence of c on this parameter set. This illustrates that the trade-offs identified in our analysis extend to weighing outbreak size versus resistance prevalence, and to varying efficacies of prophylaxis.

2.6 Discussion

Here we have presented a model to explore how patterns in antimicrobial treatment usage shape the early-stage evolutionary dynamics during an epidemic that drive resistance outcomes. The complexity of interactions and range of outcomes identified in our study enable us to reconcile previous findings which appeared, at face value, to give conflicting results. Our results also show how parameter values in different spaces spaces may lead to qualitatively different control recommendations. Specifically, our analysis revealed trade-offs between time spent on treatment and prophylaxis in terms of epidemic outcomes, including resistant genotype prevalence. When resistant genotypes have low fitness, treatment has little influence, whereas when the resistant genotype is more fit, prophylaxis can increase resistant genotype prevalence. Overall, in the parameter regimes explored, both prophylaxis

and treatment tend to be beneficial to epidemic control with respect to preventing the epidemic from becoming established, and controlling it if it establishes. However, caution is needed if the resistant genotype has transmission fitness approaching that of the wild-type; here increased treatment or prophylaxis can spur higher prevalence of resistant genotypes in conjunction with significant outbreak sizes, potentially incurring larger, less controllable, resistant-dominant epidemics. One take-home message from our work is that the fitness of the resistant genotype is an essential determinant of the outcome, and if possible should be empirically characterized in order to better understand the implications of control strategies. Another is that greater protective efficacy of prophylaxis can select more strongly for resistance, leading to unexpectedly worse epidemic outcomes. Overall, our findings show that resistant genotype fitness – which has not been a focus of previous analyses of this problem – is a key influence on epidemic outcomes, and that control measures such as treatment intensity and prophylaxis must be considered in the appropriate evolutionary context when weighing the risk of emergence and establishment of resistance.

The broad range of qualitative outcomes we have found, for different regions of parameter space, provide a way to reconcile conflicting findings in the published literature, since previous studies can be mapped onto various sub-spaces of the model described here. Ferguson et al 2003 [13] assumed that, for their particular example in influenza, there is little risk of resistance even with high levels of treatment, but their example has a very low estimated fitness of the resistant genotype (10% that of the sensitive genotype) and thus aligns with trajectories on the left half of Figure 3b. Moghadas 2008 [35] found that as treatment increases, there is generally a decrease in epidemic size until resistance emerges and causes increased numbers of infections; this study considered a resistant genotype fitness comparable to that of the sensitive pathogen, consistent with the higher-valued trajectories without prophylaxis in our results. Alexander et al 2007 [1] and Handel et al 2009 [21] both showed that it is optimal to control an epidemic quickly (especially with effective prophylaxis) to prevent emergence of resistance, which corresponds in our model to the left-half of figure 3a, but otherwise it is better to use intermediate levels of control to reduce the risk of selecting for resistance

emergence (where control can be either treatment or prophylaxis). Our model shows that it is also necessary to account for the fitness of the resistant genotype (as demonstrated in Figure 3) and the amount of prophylaxis (discussed below) to understand where and how these trade-offs can arise with varying amounts of treatment. Unlike Handel et al 2009 [21], we find that if the epidemic establishes, moderate amounts of treatment can decrease overall R_0 but will always increase the prevalence of the resistant genotype in long-term epidemic outcomes. Additionally, in the presence of prophylaxis, any amount of treatment can even increase R_0 when resistant genotype fitnesses are higher, adding further unexpected complexity to judgements about prophylaxis as a control strategy. These differences in results likely arise at least partially from different implementation of treatment within the models, as we assume constant per capita rates of treatment, and Handel et al 2009 [21] considers a population-wide control measure after a certain number of infected cases has been established.

In order to explore this high-dimensional problem we have made several simplifying assumptions. Pharmacokinetics and pharmacodynamics play an important role in the effects of antimicrobial treatments, as the concentration of drug within a host will affect the strength of selection acting on the resistant genotype of a pathogen [28, 46]. As a preliminary investigation, we built a model with intermediate treatment states in between our untreated and treated states, using with intermediate parameter values to represent a treatment state when drug concentrations are waning after a patient?s last dose. Our core results did not differ qualitatively, as the intermediate treatment state acts effectively as a delay in transition dynamics, though we emphasize that a full investigation is needed to more realistically capture varying treatment levels as individuals go on and off drug treatment. We have also made simplifying assumptions about individual treatment behaviors. We used constant per capita rates of going on and off treatment, but people may be more likely to stay in a given treatment status once they have transitioned into it. This could be incorporated easily into our analysis by implementing different rates of staying on or off treatment when already on or off treatment, but data on individual dosing patterns are limited. Related to this, trans-

mission may also be non-random with respect to treatment status, for instance in hospital settings where there may be concentrated groups of individuals with higher contact, treatment, and prophylaxis rates which could lead to an increased risk for resistance. Some of these factors have been explored in previous work [54], but would benefit from a mechanistic and stochastic depiction of prophylaxis and treatment, which we have shown this can be influential in the emergence of resistance.

We have assumed that the duration of infection is not affected by treatment, however treatment is likely to shorten the duration of infection in some scenarios. Although we have focused on fixed durations of infection for simplicity, our time units are relative, and therefore the model could be applied to acute or chronic infections by adjusting the relative ratios of time on treatment and duration of infection. It has been argued theoretically that relatively longer infections provide greater opportunity for evolutionary adaptation of pathogens [2], however others have shown that selective disadvantage within-host (which can occur for resistant mutations [27]) may impede emergence in chronic infections, providing an interesting avenue to pursue further development of the model [47]. The competing timescales of infection duration and other life-history traits in comparison to treatment rates could also be coupled with empirical data for individual behavior regarding treatment adherence in more chronic infections such as HIV [26].

Another important frontier is to account for broader sets of pathogen genotypes. We can speculate about how the relative fitnesses of more genotypes, in the context of different treatment environments, will affect the emergence of drug resistance. As an example, permissive [5] and compensatory [8] mutations have been shown to play a role in allowing or sustaining drug resistance mutations. Our model could be extended to examine these factors and explore how strongly the fitness of such mutations, potentially at multiple scales, can help or hinder the emergence of resistance. Fitness landscapes and the interaction of phenotypes present at multiple scales are still largely unexplored, however new sources of data are revealing that these aspects can factor influentially on evolutionary trajectories [55, 42]. We

have largely subsumed within-host fitness aspects to a single mutation and fixation parameter with some qualifying assumptions, however it has been shown that correlations between within-host and between-host fitnesses can facilitate selection and emergence [43]. This is an important aspect to explore as we have shown the between-host transmission fitness of the resistant genotype to be a crucial part in understanding epidemic outcomes and emergence of resistance, and it is important to see how these results may change with more realistic within-host fitness dynamics. Future developments on this work could incorporate important factors regarding within-host evolution, such as the innate immune system, and demonstrate how within-host and between-host evolutionary dynamics could interact to affect epidemic and evolutionary outcomes.

The findings presented here show qualitative trends of emergence, epidemic intensity, and resistance that have not been previously demonstrated. Although the work presented does not aim to make quantitative predictions regarding treatment and control, it lends a further understanding how these control measures can influence emergence, and how several mechanistic aspects of treatment and prophylaxis can affect epidemic outcomes in a broad range of parameter space. Additionally, it provides a context for the measurement of resistant genotype fitnesses and how these might interplay with the epidemic control measures described, and demonstrated that this is a key challenge to improving our understanding of resistance emergence. The model introduced here helps to resolve previous studies that gave apparently conflicting results, and provides a basis for further exploration of how prophylaxis and treatment can influence the emergence of resistance in an evolutionary context.

Variable description	**Variable name**	**Value(s) used**
infection rate	b_i	[0.15, 0.05, 0.03 - 0.17, 0.03 - 0.17]
death or recovery rate	d_i	[0.1, 0.1, 0.1, 0.1]
rate of treatment	ρ	1
rate of going off treatment	σ	[0.01 - 20.0]
mutation from sensitive to resistant	$\mu_{s\to r}$	0.04
mutation from resistant to sensitive	$\mu_{r\to s}$	0.02
proportion of prophylactic transmission	p	0, 0.3
protective efficacy	c	0.3, 0.7

Table 2.1: *Parameter values used for studying a qualitative range of epidemic outcomes.* Note here that all parameters are positively valued, though the possible range of values for p and c are between 0 and 1.

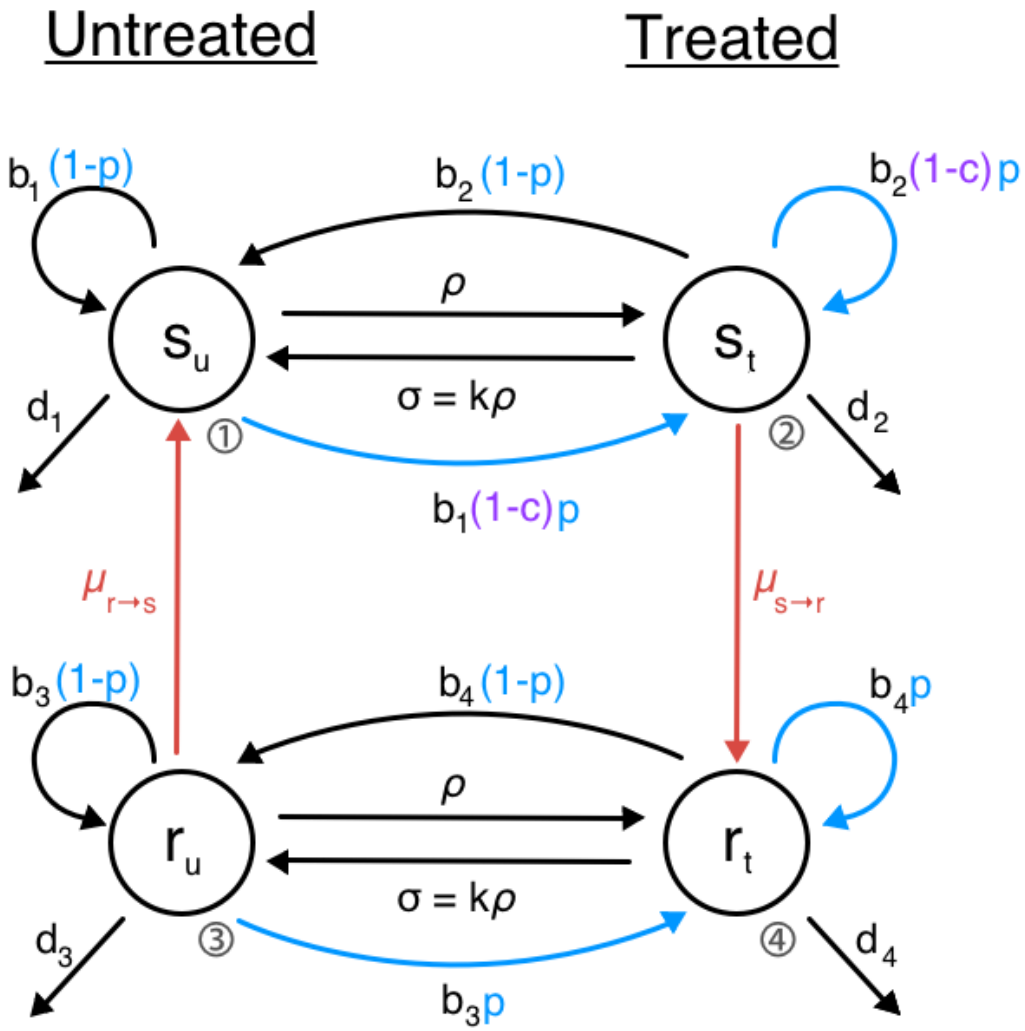

Figure 2.1: *Schematic of the model.* s_i indicate sensitive genotypes, r_i indicate resistant genotypes; subscript u indicates the untreated state, subscript t indicates the treated state. Numerical shorthand used in the text also indicated, where $[s_u, s_t, r_u, r_t] = [i = 1, i = 2, i = 3, i = 4]$. p is the proportion of transmission to individuals on prophylaxis, c is the protective efficacy of prophylaxis where $c = 1$ indicates prophylaxis is completely protective against transmission. (There is no c term for transmission to individuals on prophylaxis for resistant genotypes as we assume that resistant genotypes are not affected by prophylaxis). Arrows represent infection (b_i), death or recovery (d_i), treatment status changes (ρ, σ which represent going on and off of treatment, respectively) and genotype change through mutation and effective fixation ($\mu_{s\to r}$, $\mu_{r\to s}$, for mutations from sensitive to resistant, and resistant to sensitive types, respectively). Blue arrows and terms represent dynamics of prophylaxis while red arrows represent dynamics of mutations in genotype.

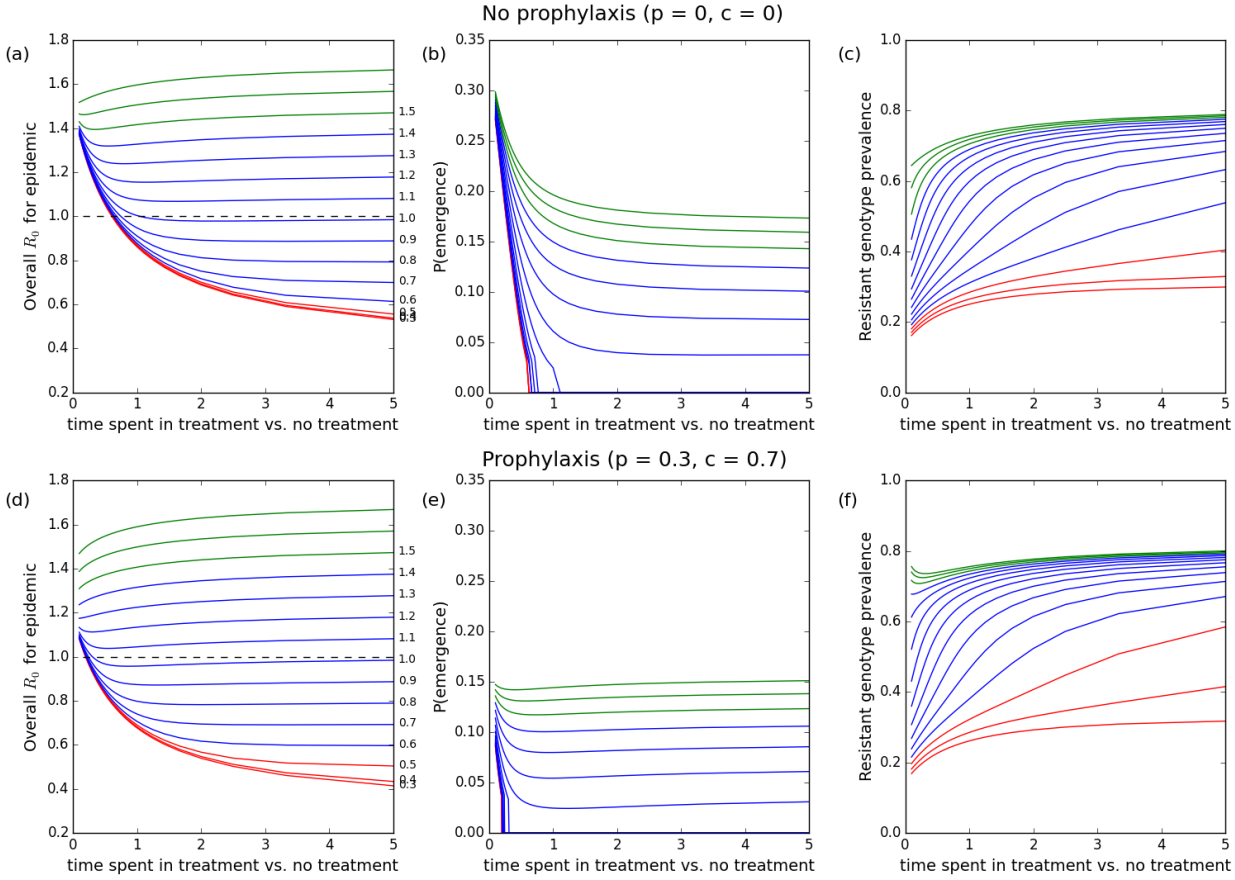

Figure 2.2: *Effects of time spent on treatment on epidemic outcomes, for scenarios without and with prophylaxis.* Curves represent different between-host fitnesses of the resistant genotype, with red values indicating lower fitness than the sensitive/treated type, green values indicating higher fitness than the sensitive/untreated type, and blue representing intermediate values (see values on right hand axis of (a) and (d). The x-axis is the ratio of time spent on treatment to time spent untreated ($\rho : \sigma$ ratio). The y-axis in the leftmost column represents the overall epidemic R_0, the y-axis of the middle column represents $P(emergence)$ when the epidemic is started with a single individual of the s_u type, and the y-axis of the rightmost column represents the resistant genotype prevalence in the event of a major epidemic. Here $b_1 = 0.15$, $b_2 = 0.05$, $b_3 = b_4 = [0.03 - 0.17]$ corresponding to colored values, $d_{1,2,3,4} = 0.1$, $\mu_{s \to r} = 0.04$, $\mu_{r \to s} = 0.02$, $\rho = 1.0$ (fixed), σ varying for x-axis values. For top row of figure, $c = 1$, $p = 0$; for bottom row of figure, $c = 0.7, p = 0.3$.

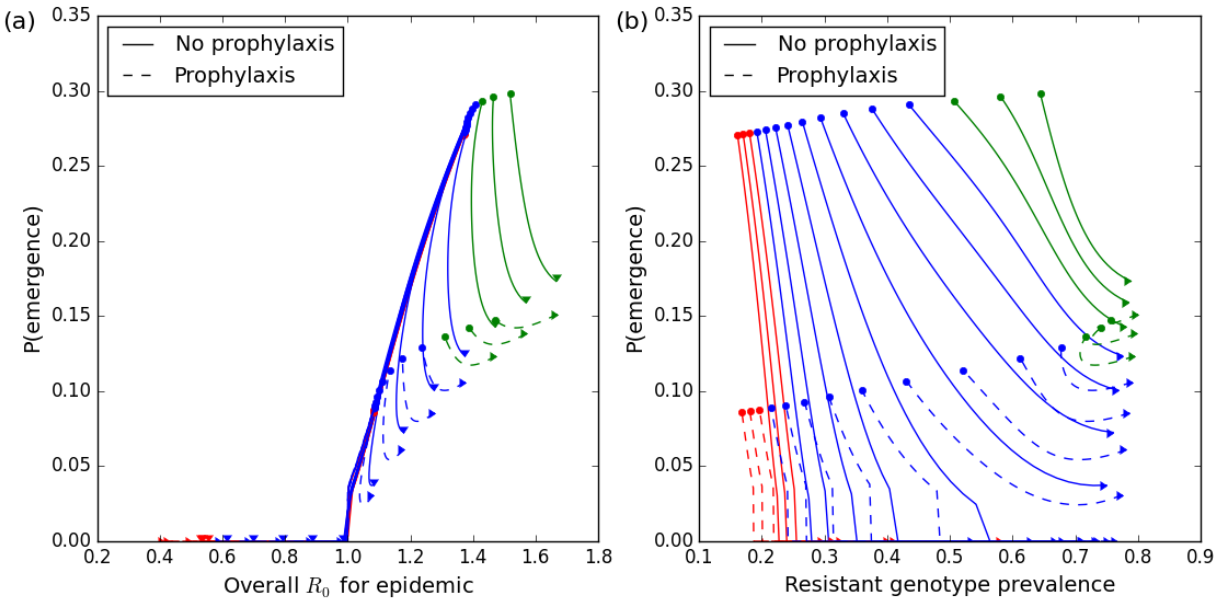

Figure 2.3: *Trade-offs between shorter-term and longer-term epidemic outcomes and drug resistance.* Circle indicates no time spent on treatment, with increasing time spent on treatment over the range of the trajectory towards the triangle symbol, corresponding to increasing x-axis values in Figure 2. Parameters and color values are as in Figure 2. Solid lines indicate scenarios with no prophylaxis (corresponding to Figure 2(abc)), dotted lines indicate scenarios with prophylaxis (corresponding to Figure 2(def)). $P(emergence)$ values are the same in both figures, but some values of the resistant genotype fitness trajectories where the resistant genotype fitnesses are lower (red) are obscured in panel (a) by the density of higher resistant genotype fitness trajectories (blue).

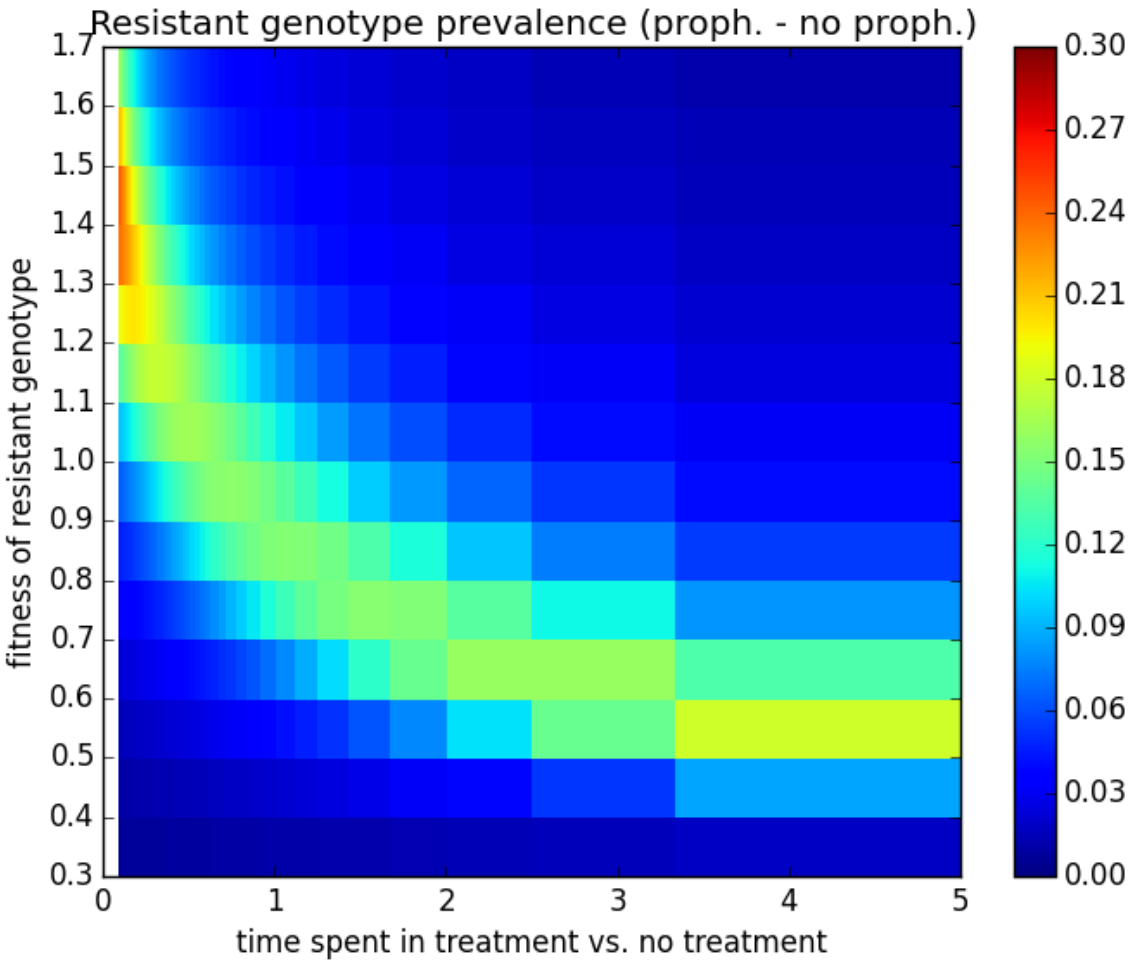

Figure 2.4: *Difference of resistant genotype prevalence with and without prophylaxis.* The x-axis represents time in treatment vs. time spend not in treatment. The y-axis represents the fitness of the resistant genotype. Color values represent the difference in resistant genotype prevalence for a system with prophylaxis and a system without prophylaxis, corresponding to parameter values in Figure 2.

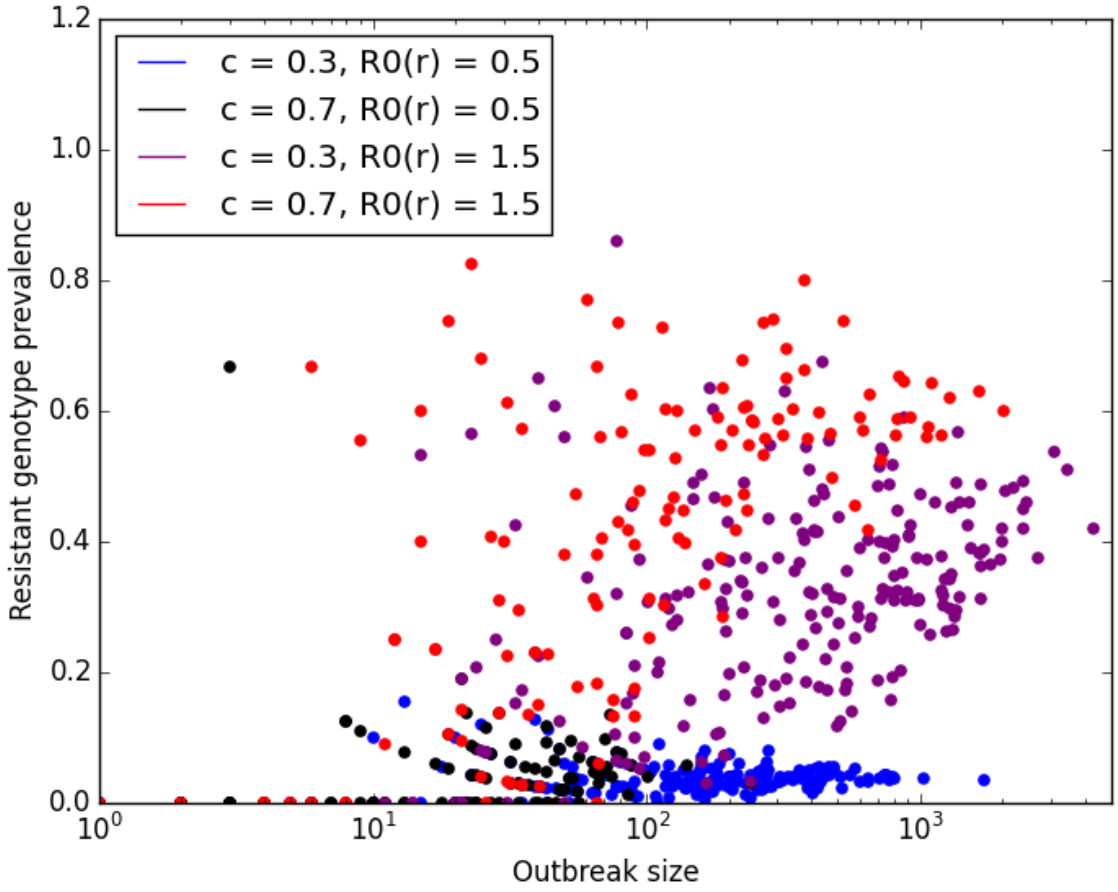

Figure 2.5: *Outbreak size and resistant genotype prevalence.* The x-axis represents outbreak size. The y-axis represents prevalence of the resistant genotype. Colors correspond to legend values as shown, $\sigma = 10.0$. 1000 epidemics are simulated for each parameter set and run for 150 time units to ensure sufficient establishment of successful epidemics.

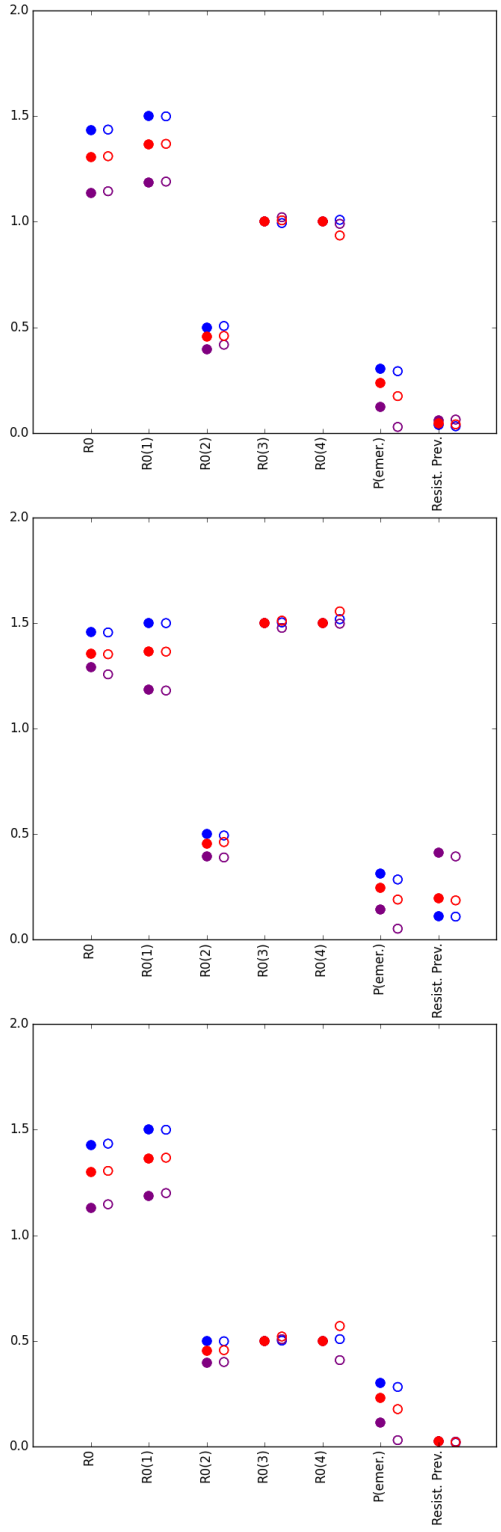
2.0
1.5
1.0
0.5
0.0
R0
R0(1)
R0(2)
R0(3)
R0(4)
P(emer.)
Resist. Prev.

Figure 2.S1: *Validation of theoretical results by simulation.* The x-axis shows each parameter and the y-axis shows parameter values. Solid points are theoretical calculated results, hollow points are results from simulating epidemics starting with one infected individual of the sensitive untreated type. 1000 epidemics are simulated for each parameter set and run for 150 time units to ensure sufficient establishment of successful epidemics, for each parameter set, as in Figure 5. Figure S1(a) infection parameters are $b_i = [0.15, 0.05, 0.15, 0.15]$, Figure S1(b) $b_i = [0.15, 0.05, 0.1, 0.1]$, Figure S1(c) $b_i = [0.15, 0.05, 0.05, 0.05]$, with all other parameters indicated by colors in respective legend captions and otherwise fixed as used and described in main analysis.

2.7 References

Bibliography

[1] M. E. Alexander, C. S. Bowman, Z. Feng, M. Gardam, S. M. Moghadas, G. Röst, J. Wu, and P. Yan. Emergence of drug resistance: implications for antiviral control of pandemic influenza. *Proceedings of the Royal Society of London B: Biological Sciences*, 274(1619):1675–1684, 2007.

[2] J.-B. André and T. Day. The effect of disease life history on the evolutionary emergence of novel pathogens. *Proceedings of the Royal Society of London B: Biological Sciences*, 272(1575):1949–1956, 2005.

[3] R. Antia, R. Regoes, J. Koella, and C. Bergstrom. The role of evolution in the emergence of infectious diseases. *Nature*, 426(6967):658, 2003.

[4] M. Baz, Y. Abed, J. Papenburg, X. Bouhy, M.-È. Hamelin, and G. Boivin. Emergence of oseltamivir-resistant pandemic H1N1 virus during prophylaxis. *New England Journal of Medicine*, 361(23):2296–2297, 2009.

[5] J. D. Bloom, L. I. Gong, and D. Baltimore. Permissive secondary mutations enable the evolution of influenza oseltamivir resistance. *Science*, 328(5983):1272–1275, 2010.

[6] D. L. Chao. Modeling the global transmission of antiviral-resistant influenza viruses. *Influenza and other Respiratory Viruses*, 7(s1):58–62, 2013.

[7] A. Cingolani, A. Antinori, M. G. Rizzo, R. Murri, A. Ammassari, F. Baldini, S. Di Giambenedetto, R. Cauda, and A. De Luca. Usefulness of monitoring hiv drug resistance and adherence in individuals failing highly active antiretroviral therapy: a randomized study (argenta). *AIDS*, 16(3):369–379, 2002.

[8] I. Comas, S. Borrell, A. Roetzer, G. Rose, B. Malla, M. Kato-Maeda, J. Galagan, S. Niemann, and S. Gagneux. Whole-genome sequencing of rifampicin-resistant my-

cobacterium tuberculosis strains identifies compensatory mutations in rna polymerase genes. *Nature Genetics*, 44(1):106–110, 2012.

[9] C. Costelloe, C. Metcalfe, A. Lovering, D. Mant, and A. D. Hay. Effect of antibiotic prescribing in primary care on antimicrobial resistance in individual patients: systematic review and meta-analysis. *BMJ*, 340:c2096, 2010.

[10] J. N. Darroch and E. Seneta. On quasi-stationary distributions in absorbing discrete-time finite markov chains. *Journal of Applied Probability*, 2(1):88–100, 1965.

[11] F. Débarre, S. Bonhoeffer, and R. R. Regoes. The effect of population structure on the emergence of drug resistance during influenza pandemics. *Journal of the Royal Society Interface*, 4(16):893–906, 2007.

[12] M. Eichner, M. Schwehm, H.-P. Duerr, M. Witschi, D. Koch, S. O. Brockmann, and B. Vidondo. Antiviral prophylaxis during pandemic influenza may increase drug resistance. *BMC Infectious Diseases*, 9(1):4, 2009.

[13] N. M. Ferguson, S. Mallett, H. Jackson, N. Roberts, and P. Ward. A population-dynamic model for evaluating the potential spread of drug-resistant influenza virus infections during community-based use of antivirals. *Journal of Antimicrobial Chemotherapy*, 51(4):977–990, 2003.

[14] C. for Disease Control, P. (CDC, et al. Oseltamivir-resistant 2009 pandemic influenza a (H1N1) virus infection in two summer campers receiving prophylaxis–north carolina, 2009. *MMWR. Morbidity and mortality weekly report*, 58(35):969, 2009.

[15] C. for Disease Control and Prevention. *Antibiotic resistance threats in the United States, 2013*. Centers for Disease Control and Prevention, 2013.

[16] L. B. Gasink, D. R. Linkin, N. O. Fishman, W. B. Bilker, M. G. Weiner, and E. Lautenbach. Stockpiling drugs for an avian influenza outbreak: examining the surge in oseltamivir prescriptions during heightened media coverage of the potential for a worldwide pandemic. *Infection Control & Hospital Epidemiology*, 30(4):370–376, 2009.

[17] D. T. Gillespie. Exact stochastic simulation of coupled chemical reactions. *The Journal of Physical Chemistry*, 81(25):2340–2361, 1977.

[18] J. H. Gillespie. A simple stochastic gene substitution model. *Theoretical Population Biology*, 23(2):202–215, 1983.

[19] J. R. Gog, L. Pellis, J. L. Wood, A. R. McLean, N. Arinaminpathy, and J. O. Lloyd-Smith. Seven challenges in modeling pathogen dynamics within-host and across scales. *Epidemics*, 10:45–48, 2015.

[20] C. D. Goodman, J. E. Siregar, V. Mollard, J. Vega-Rodríguez, D. Syafruddin, H. Matsuoka, M. Matsuzaki, T. Toyama, A. Sturm, A. Cozijnsen, et al. Parasites resistant to the antimalarial atovaquone fail to transmit by mosquitoes. *Science*, 352(6283):349–353, 2016.

[21] A. Handel, I. M. Longini, and R. Antia. Antiviral resistance and the control of pandemic influenza: the roles of stochasticity, evolution and model details. *Journal of Theoretical Biology*, 256(1):117–125, 2009.

[22] A. Handel, E. Margolis, and B. R. Levin. Exploring the role of the immune response in preventing antibiotic resistance. *Journal of Theoretical Biology*, 256(4):655–662, 2009.

[23] S. Harbarth, M. H. Samore, D. Lichtenberg, and Y. Carmeli. Prolonged antibiotic prophylaxis after cardiovascular surgery and its effect on surgical site infections and antimicrobial resistance. *Circulation*, 101(25):2916–2921, 2000.

[24] T. E. Harris. *The theory of branching processes*. Berlin:Springer, 1963.

[25] F. G. Hayden, R. Belshe, C. Villanueva, R. Lanno, C. Hughes, I. Small, R. Dutkowski, P. Ward, and J. Carr. Management of influenza in households: a prospective, randomized comparison of oseltamivir treatment with or without postexposure prophylaxis. *The Journal of Infectious Diseases*, 189(3):440–449, 2004.

[26] C. H. Hinkin, T. R. Barclay, S. A. Castellon, A. J. Levine, R. S. Durvasula, S. D. Marion, H. F. Myers, and D. Longshore. Drug use and medication adherence among hiv-1 infected individuals. *AIDS and Behavior*, 11(2):185–194, 2007.

[27] A. C. Hurt, S. S. Nor'e, J. M. McCaw, H. R. Fryer, J. Mosse, A. R. McLean, and I. G. Barr. Assessing the viral fitness of oseltamivir-resistant influenza viruses in ferrets, using a competitive-mixtures model. *Journal of Virology*, 84(18):9427–9438, 2010.

[28] R. Ke, S. R. Lewin, J. H. Elliott, and A. S. Perelson. Modeling the effects of vorinostat in vivo reveals both transient and delayed hiv transcriptional activation and minimal killing of latently infected cells. *PLoS Pathogens*, 11(10):e1005237, 2015.

[29] J. G. Kemeny and J. L. Snell. Finite continuous time markov chains. *Theory of Probability & Its Applications*, 6(1):101–105, 1961.

[30] K. Lange. *Applied probability*. Springer Science & Business Media, 2010.

[31] D. A. Lehman, J. M. Baeten, C. O. McCoy, J. F. Weis, D. Peterson, G. Mbara, D. Donnell, K. K. Thomas, C. W. Hendrix, M. A. Marzinke, et al. Risk of drug resistance among persons acquiring hiv within a randomized clinical trial of single-or dual-agent preexposure prophylaxis. *The Journal of Infectious Diseases*, 211(8):1211–1218, 2015.

[32] M. Lipsitch, T. Cohen, M. Murray, and B. R. Levin. Antiviral resistance and the control of pandemic influenza. *PLoS Medicine*, 4(1):e15, 2007.

[33] F. Luciani and S. Alizon. The evolutionary dynamics of a rapidly mutating virus within and between hosts: the case of hepatitis c virus. *PLoS Computational Biology*, 5(11):e1000565, 2009.

[34] M. Madamet, T. Gaillard, G. Velut, C. Ficko, P. Houzé, C. Bylicki, S. Mérat, S. Houzé, N. Taudon, R. Michel, et al. Malaria prophylaxis failure with doxycycline, central african republic, 2014. *Emerging Infectious Diseases*, 21(8):1485, 2015.

[35] S. M. Moghadas. Management of drug resistance in the population: influenza as a case study. *Proceedings of the Royal Society of London B: Biological Sciences*, 275(1639):1163–1169, 2008.

[36] D. M. Morens and A. S. Fauci. Emerging infectious diseases: threats to human health and global stability. *PLoS Pathogens*, 9(7):e1003467, 2013.

[37] A. Moscona. Oseltamivir resistance-disabling our influenza defenses. *New England Journal of Medicine*, 353(25):2633–2636, 2005.

[38] M. K. Oli, M. Venkataraman, P. A. Klein, L. D. Wendland, and M. B. Brown. Population dynamics of infectious diseases: a discrete time model. *Ecological Modelling*, 198(1):183–194, 2006.

[39] W. H. Organization et al. Update on oseltamivir-resistant pandemic a (H1N1) 2009 influenza virus: January 2010. *Weekly Epidemiological Record*, 85(6):37–40, 2010.

[40] W. H. Organization et al. *Antimicrobial resistance: global report on surveillance*. World Health Organization, 2014.

[41] J. R. Ortiz, L. Kamimoto, R. E. Aubert, J. Yao, D. K. Shay, J. S. Bresee, and R. S. Epstein. Oseltamivir prescribing in pharmacy-benefits database, united states, 2004–2005. *Emerging Infectious diseases*, 14(8):1280, 2008.

[42] R. J. Orton, C. F. Wright, M. J. Morelli, N. Juleff, G. Thébaud, N. J. Knowles, B. Valdazo-González, D. J. Paton, D. P. King, and D. T. Haydon. Observing micro-evolutionary processes of viral populations at multiple scales. *Phil. Trans. R. Soc. B*, 368(1614):20120203, 2013.

[43] M. Park, C. Loverdo, S. J. Schreiber, and J. O. Lloyd-Smith. Multiple scales of selection influence the evolutionary emergence of novel pathogens. *Philosophical Transactions of the Royal Society of London B: Biological Sciences*, 368(1614):20120333, 2013.

[44] H. Qi, C. A. Olson, N. C. Wu, R. Ke, C. Loverdo, V. Chu, S. Truong, R. Remenyi, Z. Chen, Y. Du, et al. A quantitative high-resolution genetic profile rapidly identifies

sequence determinants of hepatitis c viral fitness and drug sensitivity. *PLoS Pathogens*, 10(4):e1004064, 2014.

[45] R. R. Regoes and S. Bonhoeffer. Emergence of drug-resistant influenza virus: population dynamical considerations. *Science*, 312(5772):389–391, 2006.

[46] D. I. Rosenbloom, A. L. Hill, S. A. Rabi, R. F. Siliciano, and M. A. Nowak. Antiretroviral dynamics determines hiv evolution and predicts therapy outcome. *Nature Medicine*, 18(9):1378–1385, 2012.

[47] S. J. Schreiber, R. Ke, C. Loverdo, M. Park, P. Ahsan, and J. O. Lloyd-Smith. Cross-scale dynamics and the evolutionary emergence of infectious diseases. *bioRxiv*, page 066688, 2016.

[48] S. J. Schreiber and J. O. Lloyd-Smith. Invasion dynamics in spatially heterogeneous environments. *The American Naturalist*, 174(4):490–505, 2009.

[49] A. K. Sethi, D. D. Celentano, S. J. Gange, R. D. Moore, and J. E. Gallant. Association between adherence to antiretroviral therapy and human immunodeficiency virus drug resistance. *Clinical Infectious Diseases*, 37(8):1112–1118, 2003.

[50] J. Soto, J. Toledo, M. Luzz, P. Gutierrez, J. Berman, and S. Duparc. Randomized, double-blind, placebo-controlled study of malarone for malaria prophylaxis in non-immune colombian soldiers. *The American Journal of Tropical Medicine and Hygiene*, 75(3):430–433, 2006.

[51] I. H. Spicknall, B. Foxman, C. F. Marrs, and J. N. Eisenberg. A modeling framework for the evolution and spread of antibiotic resistance: literature review and model categorization. *American Journal of Epidemiology*, 178(4):508–520, 2013.

[52] N. I. Stilianakis, A. S. Perelson, and F. G. Hayden. Emergence of drug resistance during an influenza epidemic: insights from a mathematical model. *Journal of Infectious Diseases*, 177(4):863–873, 1998.

[53] P. Van den Driessche and J. Watmough. Reproduction numbers and sub-threshold endemic equilibria for compartmental models of disease transmission. *Mathematical Biosciences*, 180(1):29–48, 2002.

[54] R. A. Weinstein, M. J. Bonten, D. J. Austin, and M. Lipsitch. Understanding the spread of antibiotic resistant pathogens in hospitals: mathematical models as tools for control. *Clinical Infectious Diseases*, 33(10):1739–1746, 2001.

[55] N. Wu, L. Dai, C. A. Olson, J. O. Lloyd-Smith, and R. Sun. Adaptation in protein fitness landscapes is facilitated by indirect paths. *eLife*, 5:e16965, 2016.

[56] Y. Xu, L. J. Allen, and A. S. Perelson. Stochastic model of an influenza epidemic with drug resistance. *Journal of Theoretical Biology*, 248(1):179–193, 2007.

[57] P. A. zur Wiesch, R. Kouyos, J. Engelstädter, R. R. Regoes, and S. Bonhoeffer. Population biological principles of drug-resistance evolution in infectious diseases. *The Lancet Infectious Diseases*, 11(3):236–247, 2011.

CHAPTER 3

Joint estimation of within-host and transmission fitness of a virus from experimental data: influenza in ferrets as a case study

Miran Park, Jessica, A. Belser, James O. Lloyd-Smith

3.1 Abstract

Pathogen evolutionary dynamics play out at multiple spatial scales, with pathogen population dynamics and selection occurring both within individual hosts and across host populations. Pathogen fitness has distinct consequences at different scales, corresponding to pathogen replication rate at the within-host scale and to transmissibility at the between-host scale. These two scales of fitness, and how they covary across pathogen strains, have been shown theoretically to have major influence on evolutionary outcomes. Yet there are remarkably few studies that estimate pathogen fitness at both scales for a given pathogen strain and host type. Indeed, there are few frameworks to analyzing pathogen data at multiple scales simultaneously, presumably due to the complexity of modeling multi-scale evolution and the limited availability of suitable data spanning within-host and between-host scales. Here we present a model-based method for estimating both within-host viral fitness and between-host transmission fitness from commonly available data from animal transmission experiments, using influenza in ferrets as a case study. Our model integrates data routinely measured in ferret transmission experiments, using a Bayesian data augmentation approach

to jointly estimate within-host and between-host fitness. We demonstrate the validity and sample size requirements of our framework using simulated data, showing that experiments as small as 3 transmission pairs can yield robust estimates of fitness values. We then estimate fitness values for 7 subtypes of influenza A virus, and for two modes of transmission. We identify an apparent negative correlation between within-host and between-host fitness in ferrets, implying a possible trade-off. Finally we find significant overlap in qualitative characteristics of influenza subtypes in their ability to transmit in ferrets and humans at the between-host scale, corroborating and extending earlier findings.. Overall, this work provides a mechanistic framework to jointly estimate within-host and between-host fitness from experimental data, opening the door to extract greater insights from animal transmission experiments for many pathogens.

3.2 Introduction

Selection acting at multiple scales have been shown to have important influence on pathogen evolution [15, 29, 19, 30]. Recent theoretical work has started to address the challenges and opportunities arising from modeling evolution at multiple scales, as it pertains to emergence of novel pathogen strains, immune escape, fitness landscapes, and genetic diversity [34, 14, 37, 3, 42, 33]. However, research that explicitly addresses cross-scale pathogen evolution remains largely theoretical, raising challenges in connecting its findings to real-world problems. In particular, efforts to estimate crucial parameters such as pathogen fitness have largely focused on a single pathogen scale [15]. This is in part due to the fact that is inherently difficult to measure fitness across scales. Recent empirical studies have increasingly presented correlates of fitness at both within-host and between-host scales [16, 41, 1, 20, 21], but measures at the two scales are typically presented as raw data (e.g. time course of viral titers within hosts, and raw success rates of transmission experiments). Thus, despite this growing body of theoretical and empirical work, there is a lack of methodology for systematic and quantitative comparison of fitness values derived simultaneously from within-host

and between-host data. We introduce a mechanistically-based approach for joint estimation of within-host and between-host fitness, and demonstrate its application to influenza A virus.

Influenza is a rapidly evolving virus with significant epidemic and pandemic potential. Epidemics consisting of novel strains or subtypes are largely a product of emergence from zoonotic reservoirs, and although potentially hazardous strains have been increasingly identified from animal populations, it is difficult to characterize the epidemic potential of these viruses in human populations [25]. Estimating the human-to-human transmissibility of these zoonotic strains is a particular challenge. Increased epidemiological surveillance efforts have captured outbreaks of emerging strains in humans, small case numbers and imperfect observation present challenges in inferring transmission rates [26]. Household outbreak data has been used to estimate transmissibility of emerging strains [43, 38], but it is unclear how well transmissibility parameters at the household level translate to larger human populations.

Ferrets are widely used as an animal model for studying the transmissibility of emerging subtypes of influenza [7, 32]. Ferret transmission experiments are generally conducted in one of two experimental setups: 1) where ferrets are co-housed in the same enclosure and able to interact freely (which we call direct contact, DC) and 2) where ferrets are contained in separate enclosures but aerosol particles can travel through connected airways to the enclosures (which we call respiratory droplet, RD). Physiological factors of ferrets lead to parallels in influenza pathology and transmission to influenza in humans [7], but few studies have considered the translatability of transmission experiments in ferrets to transmissibility in humans [32]. Controversy surrounding 'gain-of-function' experiments on influenza in ferrets [20, 21], which have discovered small numbers of mutations that allow avian strains to gain airborne transmissibility in mammals, has highlighted the importance of understanding whether ferret transmission experiments reflect potential for human pandemics in emerging strains of influenza. Ferret transmission studies typically collect data at both within-host and between-host scales, and given their relative abundance and consistent experimental design, ferret transmission studies make an excellent case study to develop empirical approaches to

studying pathogen dynamics across scales [7, 12].

In a recent study we demonstrated a strong quantitative connection between influenza transmissibility in ferret experiments and in human households and populations [12]. The previous analysis quantified transmission fitness using the secondary attack rate (SAR), defined as the probability of infection for a susceptible individual following known contact with an infectious individual [17]. SAR is calculated as the ratio of successful transmission to potential transmission in number of contacts; for ferret experiments, this was simply the fraction of ferret pairs where transmission occurred.

Transmissibility among humans was captured quantitatively as the SAR, calculated from household exposure data in the literature, and qualitatively as supercritical or subcritical, from the epidemiological behavior of each subtype. Supercritical strains exhibit sustained human-to-human transmission, i.e. influenza subtypes such as H3N2 and H1N1 that cause seasonal or pandemic flu. Subcritical strains do not transmit from human to human, or transmit so weakly that they cannot cause major outbreaks, i.e. influenza subtypes such as H7N9 or H9N2 that cause only zoonotic infections and self-limiting clusters.

Our previous study identified statistical relationships between the SAR in ferret transmission experiments and the different measures of human-to-human transmission. In particular, a strong positive correlation was found between the human SAR and the ferret SAR in respiratory droplet (RD) experiments, and the ferret RD SAR was shown to be a surprisingly good predictor of subcritical versus supercritical transmission among humans [12]. However, the results highlighted significant challenges arising from small sample sizes. Using SAR as a measure of between-host fitness in ferrets is especially limiting: because of the small sample size of ferret experiments (often on the scale of 3 pairs of ferrets), SAR estimates were very discrete and often saturated (100% successful transmission) for the more transmissible strains.The study emphasized the need for further research, including approaches to addressing this sample size challenge and opportunities for further insights from incorporating the within-host scale

Here we refine these estimates of transmission potential and incorporate within-host dynamics, by developing a Bayesian statistical modeling framework for simultaneously estimating within-host fitness and between-host fitness from transmission experiment data. At the within-host scale, we use viral titer dynamics to estimate the viral population growth rate, a measure of within-host fitness. Despite the focus on the between-host scale in transmission experiments, viral titers are commonly measured in ferret influenza transmission studies [7, 12]. At the between-host scale, we extract greater information from transmission data by using the time of infection, imputed through a data augmentation scheme, to estimate the force of infection (FOI) as a measure of between-host fitness. The FOI is defined as the per capita hazard rate of becoming infected for any given susceptible, and as a continuous quantity it allows better resolution of fitness differences than the discretized SAR. The method presented gives mechanistic underpinnings to the estimation of within-host fitness of viral populations, and addresses previous limitations in the estimation of between-host transmission fitness of SAR by allowing a continuous measure of the force of infection. We show that our analyses corroborate and expand upon previous results, and we call for further applications to broader cross-scale data.

3.3 Materials and methods

3.3.1 Ferret experiments and data

To estimate parameters of within-host and between-host viral fitness, we utilized data from 9 groups of ferret transmission experiments, each of which consisted of multiple transmission experiments [10, 4, 28, 8, 6, 9, 5, 27, 22]. To maximize consistency in the data, we used experiments from a single laboratory, and only paired designs with one donor ferret and one contact ferret were used. In these experiments, a naive ferret (donor ferret) is intranasally inoculated with a specific dose of the virus that has been grown from egg or cell culture. If the donor ferret is infected successfully, there is a delay period of 24 hours before a virus-naive contact ferret is exposed. Both direct contact (DC) and respiratory droplet

(RD) transmission experiments were included, but considered separately, as we have previously demonstrated that there is a significant difference between these experimental setups [12].

The viral titer data are taken from individual contact ferrets during the course of an infection via nasal wash, titrated by standard plaque assay, and taken at discrete time points (typically every 2 days). Viral titer data in our sources was presented as plaque forming units (PFU) or egg infectious dose (EID). Despite these differing units, we found these quantities comparable in magnitude and generally grouped subtype data was in one or another unit, and use these as a measurement of viral titer throughout our analysis. The threshold for detection of viral titers across studies was generally 1 $log_{10}(PFU, EID)$. Infection of contact ferrets (i.e. successful transmission events) were confirmed by detectable viral titers in the a 12 day window of exposure and observation. (Some studies consider transmission to have occurred if a ferret underwent seroconversion despite having no detectable titers. For our study, in order to be able to model viral growth, we considered this a negative transmission result). In total, 106 ferret pairs and 9 influenza A subtypes (H1N1, H3N2, pH1N1, H7N9, H7N3, H7N2, H7N7, trsH1N1, H5N1) were considered. However subtype trsH1N1 ended up being excluded from later analyses due to lack of comparison data for human SAR (6 ferret pairs), and H5N1 was excluded due to no successful DC or RD transmission in this set of data (9 ferret pairs) (Table 1). In order to have enough data per analysis to estimate viral fitness across scales, following previous analysis [12] we pooled data at the level of subtype rather than at the level of strain, and assumed that characteristics of viral fitness were sufficiently consistent across subtype-level data.

3.3.2 Likelihood model

At the between host-scale, for $N = n + m$ pairs of ferrets for a given subtype and transmission type (DC or RD), we denote n as the number of successful transmissions, and m as

the number of unsuccessful transmissions. We assume transmission to be stochastic, modeled as a Poisson process with rate parameter λ_y, where λ_y is the between-host transmission rate (force of infection or FOI) and $y = DC$ or RD. λ_{DC} estimates are fixed to be above λ_{RD}, as literature suggests the force of infection to be comparatively larger for DC than RD transmission [12]. For the n successful transmissions, each has a time of infection which we denote as τ_i for each individual i ferret out of n ferret pairs. For the m unsuccessful transmissions, we assume that they are exposed to the same force of infection λ_y for the subtype and transmission type for the duration of the total exposure time during the experiment, denoted as T. Because the outcomes in each ferret pair are independent, the probability of observing a particular transmission outcome is:

$$\prod_{i=1}^{n} \lambda_y e^{-\lambda_y \tau_i} \prod_{i=n+1}^{n+m} e^{-\lambda_y T} \tag{3.1}$$

for each type of transmission ($y = DC, RD$).

At the within-host scale, after a successful transmission event occurs, we assume the viral population initially grows exponentially with growth rate r. We assume this growth process is deterministic, and consider only this exponential growth phase for estimates in our model in order to avoid potential complications arising from innate immunity, cell resource availability, and other complexities. To be conservative, we base our estimation on only the first detectable titer in the contact ferret, to minimize contributions from these non-exponential processes that arise later in infection. We assume that across a subtype there exists one characteristic growth rate, which is not affected by transmission type (DC or RD). Following recent empirical studies, we assume that each transmission type inoculates the contact ferret with a fixed number of viral particles, which we refer to as the bottleneck width. In considering the viral titer data, we account for measurement error by imposing a normally distributed error. The probability of observing a given set of initial titer values, across all

successful transmission events, can then be written as:

$$\prod_{i=1}^{n} \frac{1}{\sqrt{2\pi\sigma^2}} e^{\frac{-(x_i-\mu_i)^2}{2\sigma^2}} \tag{3.2}$$

where

$$\mu_i = x_y e^{r(t_i-\tau_i)}. \tag{3.3}$$

where x_y is the initial viral population size after transmission bottleneck (DC or RD), x_i is the first detectable viral titer in contact ferret i, t_i is the time of that titer (in days from initial contact), and τ_i is the time of infection, as above.

Bringing together the between-host and within-host factors, we can write the likelihood function for all data from each subtype as :

$$\mathcal{L}(\lambda_y, r, \tau_1, ..., \tau_n) = \prod_{y=DC,RD} \left(\prod_{i=1}^{n} \lambda_y e^{-\lambda_y \tau_i} \frac{1}{\sqrt{2\pi\sigma^2}} e^{\frac{-(x_i-\mu_i)^2}{2\sigma^2}} \prod_{j=1}^{m} e^{-\lambda_y T} \right) \tag{3.4}$$

As is typical for infectious disease studies, the times of infection τ_i were not observed directly, so we took a data augmentation approach and imputed their values using MCMC.

The estimate we used for overall variance in viral titer measurement is $\sigma = 1 log_{10}(PFU, EID)$ unit, in line with standard deviations of source data as determined in analyses of individual datasets [10, 4, 28, 8, 6, 9, 5, 27, 22]. Values used for initial viral population size after

transmission bottleneck, $x_{DC} = 16$ and $x_{RD} = 4$ viruses [39]. For each subtype of influenza, we jointly estimated λ_{DC}, λ_{RD}, r, and all τ_i for a particular subtype.

3.3.3 Bayesian inference

We used Bayesian MCMC methods for our likelihood as described (package 'MHadaptive' in R) to obtain parameter estimation results for λ_{DC}, λ_{RD}, r, and the nuisance parameters τ_i for each successfully infected contact ferret. Prior distributions for λ_y and r were gamma distributions, with shape $k = 2$ and scale $\theta = 1$. Priors for the infection times τ_i were triangle distributions bounded by 0 and the first viral titer time for contact ferret i, such that the lower limit $a = 0$, upper limit $b = x_i$, and mode $c = x_i - 1$ unless the $x_i = 1$, in which case $c = x_i - 0.5$. Because DC transmission is known to be more rapid and efficient than RD transmission [7], we rejected any proposed set of parameters that had $\lambda_R D > \lambda_D C$. A 10000 iteration burn-in period was used with a total of 150000 iterations per set of parameter estimations. Convergence was assessed visually.

3.3.4 Simulated data for power analysis

For valid reasons, samples sizes in ferret experiments tend to be small, which has the potential to compromise statistical power [11, 31]. To explore the statistical power of our method, we conducted simulation analyses at sample sizes of $N = 3$, 6, and 12 ferret pairs (6, 12, and 24 total ferrets). Biologically reasonable values of λ_{DC}, λ_{RD}, and r were chosen based on preliminary analyses of our data. Infection events within ferret pairs were simulated as a Poisson process, so the time of transmission τ_i was drawn from the exponential distribution with rate parameter equal to the appropriate λ_y value. Viral populations were then modeled by exponential growth starting at x_y (with values as described previously) according to growth rate r, and viral titers calculated at the same time points as viral titer measurements in our data sources ($t = [2, 4, 6, 8, 10, 12]$ days). The first viral titer above the threshold for detection ($1\ log_{10}(PFU, EID)$) was taken as the simulated data point, x_i,

along with the corresponding time point. A normal error was then added to the viral titer measurement with $\sigma^2 = 1$ as described previously. If the random value drawn for τ_i was above the 12 day time period of exposure, we considered this an unsuccessful transmission event, and $x_i = 0$ and $T = 12$ accordingly.

3.3.5 Human data and SAR calculation

Human SAR estimates were obtained from Buhnerkempe et al 2015 [12]. To parallel the contact structure of ferret experimental data, human SAR values were calculated from household contact data. Both ad hoc SAR estimates, where estimates are simply the ratio of successful infections to household contacts, and SAR estimates from more sophisticated maximum likelihood approaches were considered in these estimates. Following the availability of data, and to match the ferret analyses, influenza strains were grouped at the subtype level for all analyses of human-to-human transmission.

3.4 Results

3.4.1 Validation of model inference with simulated data

Our model for joint parameter estimation for simulated parameters shows high accuracy for key model parameters chosen over a range of values, for realistic sample sizes of 3, 6, and 12 ferret pairs, which are comparable to sample sizes in our data (Figure 1). Estimates consist of posterior means and Bayesian credible intervals resulting from likelihood-based estimation by MCMC. Both accuracy (i.e. proximity of the posterior mean to the true parameter value) and precision (i.e. width of 95% credible interval) improve with larger sample sizes for both λ_y and r values. Importantly, though, 95% Bayesian credible intervals captured the true parameter values of λ_y and r in all sample size cases. Higher λ_y values tend to have wider credible intervals, as saturation of successful transmission in smaller sample sizes allows more possible values for λ_y. Posterior mean estimates for λ_{RD} are below those for

λ_{DC}, which are according to our assumption; the 95% credible intervals overlaps for sample sizes of 3 and 6 ferret pairs, but results are significantly different for 12 ferret pairs. Estimated τ_i values were also well captured by joint parameter estimation (results not shown). The sample sizes evaluated here are comparable to sample sizes in our ferret experimental data (Table 1), thus simulation results lend confidence to our effort to estimate parameters from the real data despite the small sample sizes.

3.4.2 Estimates of within-host and between-host fitness in ferret transmission experiments

Plotting the time-course of viral titer values in all contact ferrets illustrates the general pattern of infection (Figure 2), but it is difficult to elucidate any clear patterns across subtypes from these raw data. Figure 2(a) shows the individual variation arising for all contact ferrets infected by a single influenza subtype (pH1N1), along with the mean viral titer trajectory. Figure 2(b) shows a superposition of individual and mean trajectories for all contact ferrets infected by all subtypes. As a general pattern, viral titer trajectories initially follow an exponential growth pattern (note that y-axis is on a logarithmic scale), then plateau for a period of 2-4 days, subsequently decrease toward zero on roughly the same time scale as initial growth. Note that some infections do not initiate until several days after contact is initiated on day 1, highlighting the opportunity to use mechanistic models to understand more about between-host viral fitness than the more simplistic binary outcome of SAR.

Using our model-based inference framework, we estimated the fitness parameters of between-host transmissibility (for each transmission type) and within-host growth rate (Figure 3). Results are shown for for λ_{DC}, λ_{RD}, and r (the nuisance parameters τ_i were estimated but are not shown). In Figure 3, subtypes are plotted in order of increasing human SAR estimates from Buhnerkempe et al 2015 [12], from top to bottom of the figure (i.e. human SAR estimates in order of increasing transmissibility are ranked as H7N7 $<$ H7N2 $<$ H7N3

$<$ H7N9 $<$ pH1N1 $<$ H3N2 $<$ H1N1). Notably, the force of infection for ferret transmission in respiratory droplet experiments, λ_{RD}, increases monotonically with human SAR. The force of infection in direct contact experiments, λ_{DC}, shows some signs of fluctuation, but is consistent with the same monotonic trend. To quantify this relationship, we conducted Spearman rank correlation calculations between parameter sets. There is a fairly significant positive correlation between λ_{DC} and human SAR (Spearman rank correlation coefficient $\rho = 0.750$, $p = 0.066$) and a strong, significant positive correlation between λ_{RD} and human SAR ($\rho = 0.96$, $p = 0.0005$, however, p-value could not be computed exactly due to multiple zeroes in the data set). r shows a weak negative correlation with human SAR ($\rho = -0.43$). Parameter estimates for H7N9, while considered subcritical, are fairly similar in value to estimates for pH1N1, a known supercritical subtype. Importantly, our estimates provide a more continuous estimation of between-host fitness, as previous estimates of ferret SAR were limited to discrete ratios due to small groups of ferrets (often out of 2 or 3 pairs per experiment). Regarding within-host growth rate, r, viral growth rates for less transmissible subtypes are not compromised, although limited data leads to broader confidence intervals on estimates. This highlights the fact that within-host and between-host fitness are separate quantities, and can vary independently from one another.

To explore the relationship between within-host and between-host fitness, we plot the force of infection estimates, λ_y, versus the within-host growth rate, r, categorized by transmission type and transmission ability in human populations (Figure 4). Results show a potential negative correlation between between-host fitness and within-host growth rate, at the subtype level. A Spearman rank correlation calculation on these parameters shows a negative correlation between λ_{RD} and r ($\rho = -0.55$, $p = 0.195$, however, p-value could not be computed exactly due to multiple zeroes in the data set) and a nonsignificant negative correlation between λ_{DC} and r ($\rho = -0.32$, $p = 0.498$). This pattern holds for both transmission types, but is more evident in direct contact transmission since only a few subtypes successfully transmit by respiratory droplet. Supercritical subtypes occupy a notably higher parameter space for between-host fitness for both λ_{DC} and λ_{RD}, with some interesting excep-

tions. λ_{RD} is conspicuously lower for subtype pH1N1 than for other supercritical subtypes. Meanwhile H7N9 has a λ_{DC} value in a similar parameter space to supercritical subtypes, but a λ_{RD} value similar to other subcritical subtypes in our estimates.

3.4.3 Comparison of estimates to existing data on influenza transmission in humans

To support previous analyses and further confirm estimates, we compare current model results to previous human SAR estimates collected in Buhnerkempe et al 2015[12]. Generally, between-host transmission estimates exhibit positive correlations with human SAR estimates in both DC and RD experiments (Figure 5). Subcritical and supercritical subtypes occupy distinctly lower and higher parameter spaces, respectively, for both λ_y and SAR. Again Subtype H7N9 is an outlier: its human SAR estimate positions it at the high end of transmissibility in the subcritical grouping. Combined with its λ_{DC} estimate, this causes H7N9 to occupy a region of parameter space closest to supercritical subtypes, while its λ_{RD} estimate again groups it with subcritical subtypes. Our estimation of between-host fitness using FOI offers considerable advantages over previous analyses using ferret SAR, in which supercritical estimates of ferret SAR were saturated at 1 or very close to 1 for both DC and RD transmission (Supplemental Figure 1).

When comparing r and human SAR, there is no evident correlation within the subcritical or supercritical groups of subtypes (Figure 6). Combining all estimates, again it appears that subcritical subtypes occupy a distinct parameter space from supercritical subtypes. Interestingly, when distinguished by criticality, there is a clear signal of higher within-host growth rates in the subtypes with lower human SAR, echoing the patterns shown in Figure 4 for ferret between-host fitness, and implying a possible trade-off between transmissibility and within-host viral fitness in both ferrets and humans. More data are needed to further clarify these relationships, both from ferret and human data sources, since with few estimates for

supercritical subtypes it is difficult to currently ascertain the strength of the distinction of clustering. In any case, it is clear that within-host fitness in the ferret is not compromised for the subtypes that are less transmissible among humans or ferrets.

3.5 Discussion

We have introduced and demonstrated a statistical inference framework, based on a mechanistic model, that uses data routinely collected in animal transmission experiments to simultaneously (and accurately) estimate within-host viral fitness and between-host transmission potential. The unique aspect of jointly estimating fitness across within-host and between-host scales introduces a methodology for analyzing any transmission experiments where data are collected at the two scales of within-host pathogen titer data and between-host transmission outcomes. Analysis of simulated data showed that pathogen fitness parameters can be reliably estimated from the small sample sizes that are typical of experimental studies of transmission or household contact studies. With more data, the relationship between within-host and between-host fitness can be better characterized for particular pathogens, and by understanding these trends, it is possible that between-host fitness could be predicted (cautiously) from within-host data alone. The apparent negative correlation we found in our case study of influenza transmission in ferrets highlights the distinction between within-host and between-host fitness, and may point to trade-offs in maximizing fitness at these two scales, as has been found empirically in some systems [16, 21]. Previous theoretical work has shown that correlations between within-host fitness and between-host fitness can have dramatic impacts on pathogen adaptation [33], so it will be important to revisit these trends with more data and with in-depth study of particular systems.

While our approach could be applied directly to any host-pathogen combination where transmission experiments are conducted, we have focused on influenza transmission in ferrets as a case study with relatively ample data and clear scientific impact. Our results support previous analyses which demonstrated quantitative links between ferret and human trans-

mission, with key improvements arising from incorporating within-host fitness estimates and an using a higher-resolution measure of between-host fitness. Our framework creates a context to analyze existing and future data from transmission experiments, and supports and extends the scientific value of such laboratory-based transmission studies. The parameters we estimated for H7N9 varied in closeness to those of subcritical and supercritical subtypes, and the fact that H7N9 has had significantly high numbers of human cases [36, 40, 24] may point to why our results show increased transmissibility. H5N1 was excluded from our analysis due to no successful transmission, however, would be valuable to reassess with further data.

Small sample size is always a limiting factor in animal transmission experiments, and there are potential trade-offs to using data from multiple sources which may include inconsistencies in experimental protocols [7, 32]. Existing ferret transmission experiment data need to be considered carefully, due to possible differences in inoculation protocols, units of measurement, or criteria defining successful transmission. For example, different studies use different units of measurement for estimating viral titers (e.g. EID, PFU), and although we found units to be comparable, measurement methods can vary across experimental designs. For all source data used in our analysis, any quantities in different units were comparable and units were generally consistent within subtype estimations, but a careful approach is necessary whenever dealing with multiple measurement approaches. Similarly, in some ferret transmission experiments, transmission is considered successful as long as seroconversion occurred even if a viral titer was never detected; we did not consider these successful transmissions in our model because there was no signal to estimate within-host fitness. We restricted our analysis to studies from a single laboratory, as standardized experimental protocols ensured consistency within the data, however our analysis could easily be extended to the literature of existing and future ferret transmission experimental data.

A promising avenue for future work is to revisit the logistic regression analysis described in Buhnerkempe et al 2015 [12], which revealed that the SAR from ferret respiratory droplet

experiments is an effective predictor of subcritical versus supercritical transmission in humans. The greater resolution achieved by estimating between-host fitness using a continuous quantity (force of infection) rather than the cruder discretized SAR may give more power to this statistical analysis. Additionally, it will be interesting to see whether within-host fitness (as estimated in the ferret) adds any predictive value to the model, though surprisingly our results point towards that the relationship might be a negative correlation.

There are numerous ways in which our analysis could be extended or improved. Data on ferret body temperature and body weight over time are often collected in these experiments, and could potentially aid in prediction of epidemic or pathogenic potential. Increasing amounts of data are becoming available using genomic diversity studies to more accurately estimate viral bottlenecks in influenza transmission [39, 13, 23], and it would be possible to incorporate more subtype specific estimates for transmission bottleneck size and other parameters of interest. Bottleneck size has been shown theoretically to have an important influence on adaptive evolution of pathogens [37], so it is important to consider how variation in bottleneck size may affect results. Our work focused on ferret transmission studies, both to study the relation of fitness values across scales within ferrets and to improve understanding of the relevance of ferret experiments to studying transmissibility in humans. If suitable data on influenza viral titers in humans soon after infection were available, it would be interesting to pursue similar analyses to study the multiple scales of viral fitness in humans, and their relationship to criticality across subtypes.

Due to the complexity of jointly estimating parameters at the within-host and between-host scales, we chose to use an exponential growth model at the within-host scale, coupled with the choice to use only the first viral titer value. Our methodology could be extended to incorporate more of the viral titer trajectory beyond the first detectable time-point, though this risks incorporating other processes such as immune response, and thus may call for a more complex within-host model along with a more complex within-host model. Many more mechanistic within-host models that incorporate immune response or target cell resource

availability [35, 18, 2] could be substituted for the mechanism of within-host parameter estimation. Estimates of the time of infection can allow for further exploration of transmission dynamics, e.g. in the case of ferret transmission experiments, is there a pattern to the viral titer of the donor ferret once it is successfully infected by inoculation, and could this trajectory be analyzed in conjunction with infection times to clarify the drivers of transmission potential? (The data we used shows a relatively reliable pattern to viral titers after donor ferrets have been successfully inoculated [results not shown]).

We have presented a novel model-based approach to estimating pathogen fitness at within-host and between-host scales simultaneously, and applied this method to present the first systematic analysis of cross-scale fitness values for a set of influenza subtypes. This work constitutes a substantial contribution to the literature on empirical approaches to cross-scale evolutionary dynamics of pathogens, a field that has been dominated by theoretical work. As a case study, our results support the translation of influenza transmissibility from the ferret animal model to human populations, and corroborate our previous findings that showed that ferret data can be used to predict transmissibility among humans. We have verified our results by simulation for small sample sizes, such that despite limited data, we are able to estimate fitness values across scales and transmission types with relative confidence, and to understand where these estimations are limited. Our results confirm and further increase the scientific value gained from ferret transmission experimental studies. Both the results and model we have presented highlight directions for further statistical and experimental research, and open opportunities for analyzing empirical within-host and between-host pathogen data more broadly.

Subtype	**Transmission type**	**Successful transmissions** n	**Total contact ferrets** $(n+m)$
H7N7	DC	4	9
H7N7	RD	0	9
H7N2	DC	4	9
H7N2	RD	0	6
H7N3	DC	5	6
H7N3	RD	0	3
H7N9	DC	14	17
H7N9	RD	5	21
pH1N1	DC	9	9
pH1N1	RD	6	9
H3N2	DC	3	3
H3N2	RD	11	11
H1N1	DC	3	3
H1N1	RD	3	3

Table 3.1: *Transmission data by subtype.* Data sources described in detail in text [10, 4, 28, 8, 6, 9, 5, 27, 22], numbers are totaled over all available data per subtype. For transmission type, DC indicates direct contact, RD indicates respiratory droplet.

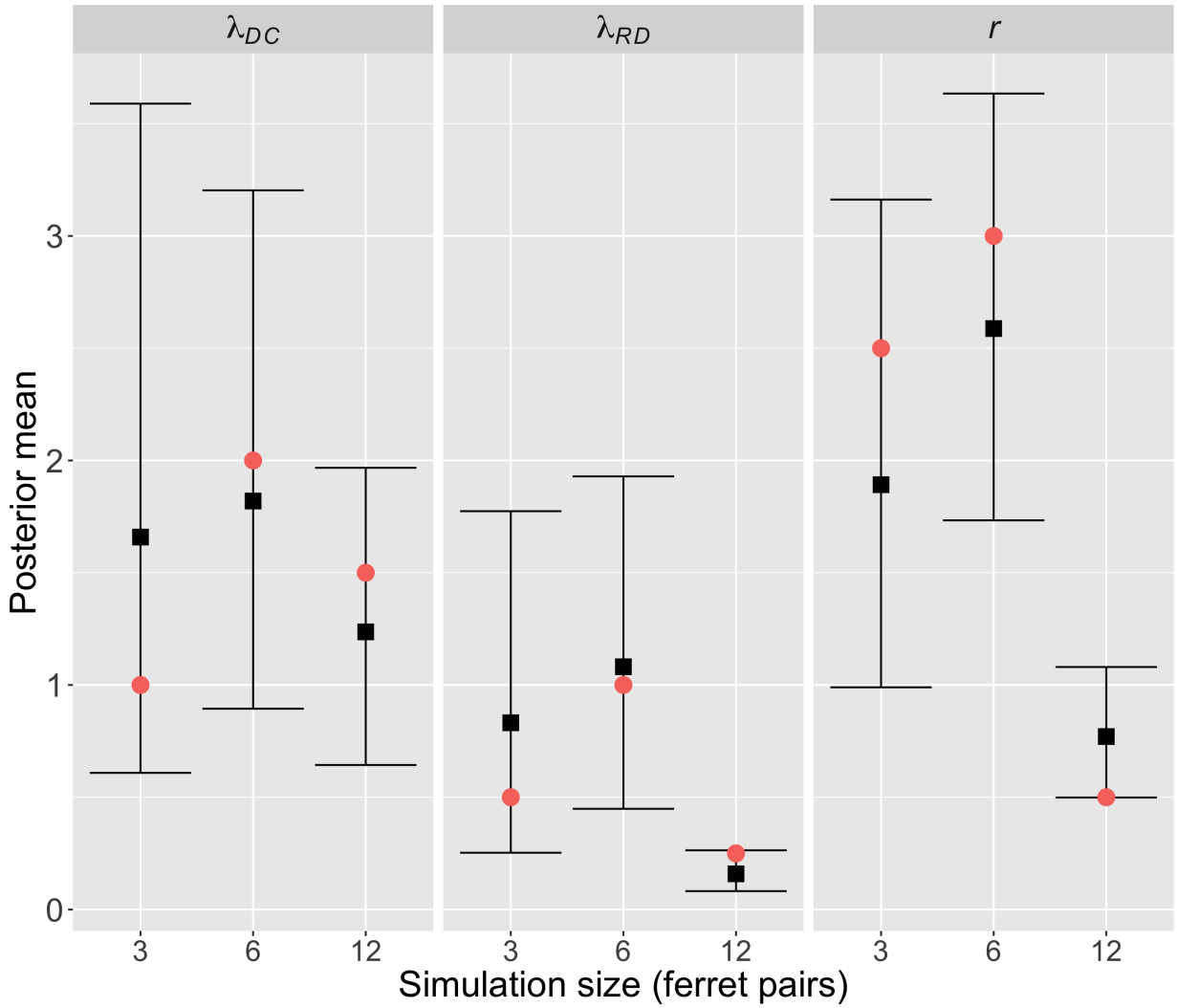

Figure 3.1: *Simulation parameters and model results.* Results from simulations of 3, 6, and 12 ferret pairs (6, 12, and 24 total ferrets). True parameter values are $[\lambda_{DC}, \lambda_{RD}, r] = [2.5, 0.5, 2.5]$ for 3 ferret pairs, $[\lambda_{DC}, \lambda_{RD}, r] = [2.0, 1.0, 3.0]$ for 6 ferret pairs, $[\lambda_{DC}, \lambda_{RD}, r] = [1.5, 0.5, 0.5]$ for 9 ferret pairs. x-axis shows these respective parameters, Circles on y-axis show chosen parameter values, with black line indicating mean posterior values, red line indicating upper bound of 95% Bayesian credible interval, blue line indicating lower bound of 95% Bayesian credible interval.

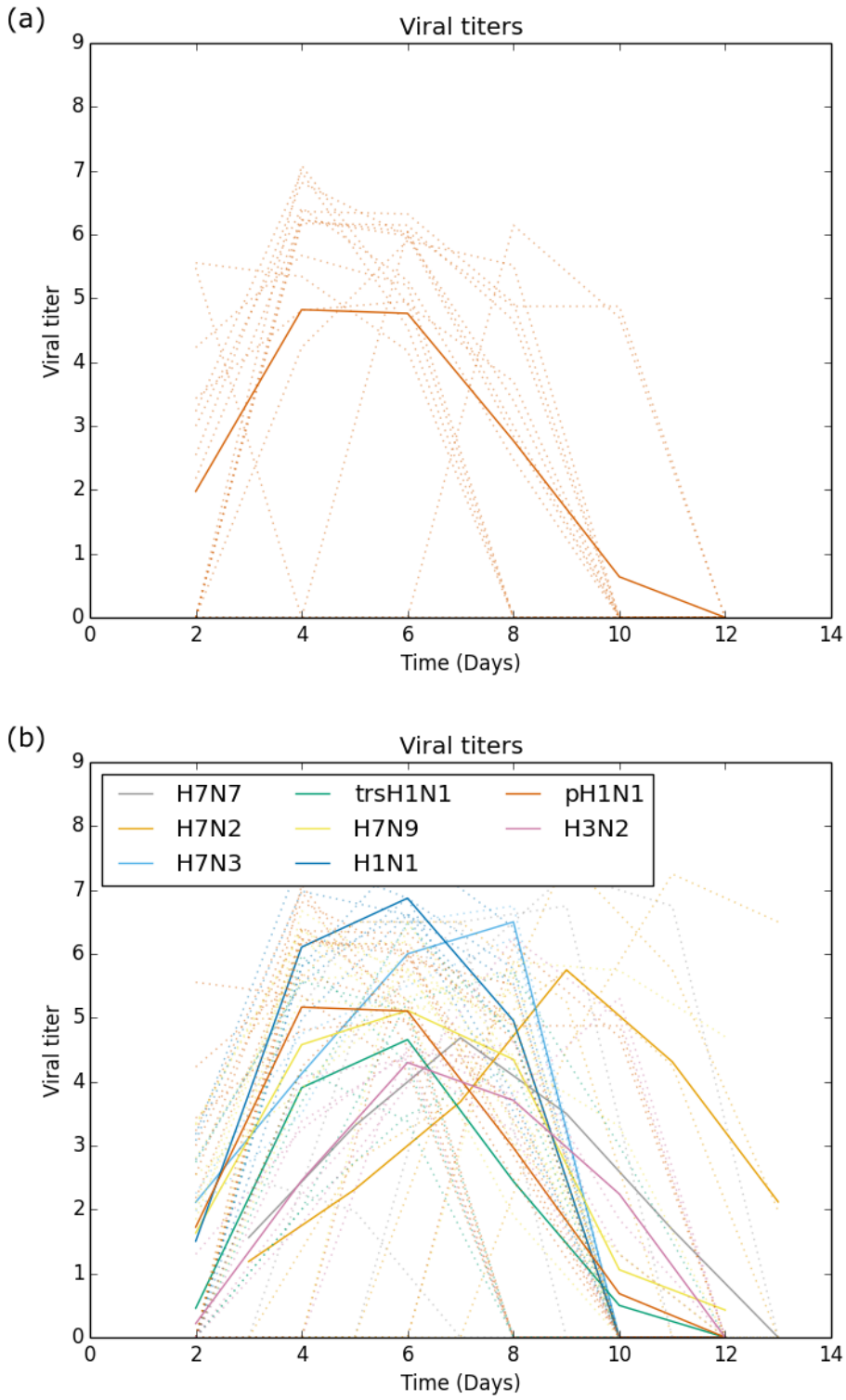

Figure 3.2: *Contact ferret viral titers.* Viral titers in $log_{10}(\text{EID}) or log_{10}(\text{PFU})$ versus time in days, separated by subtype. Solid lines indicate mean by subtype, dotted lines indicate individual ferret viral titer trajectories. Panel (a) shows contact ferret viral titer data for pH1N1 only, panel (b) shows contact ferret viral titer data for all subtypes.

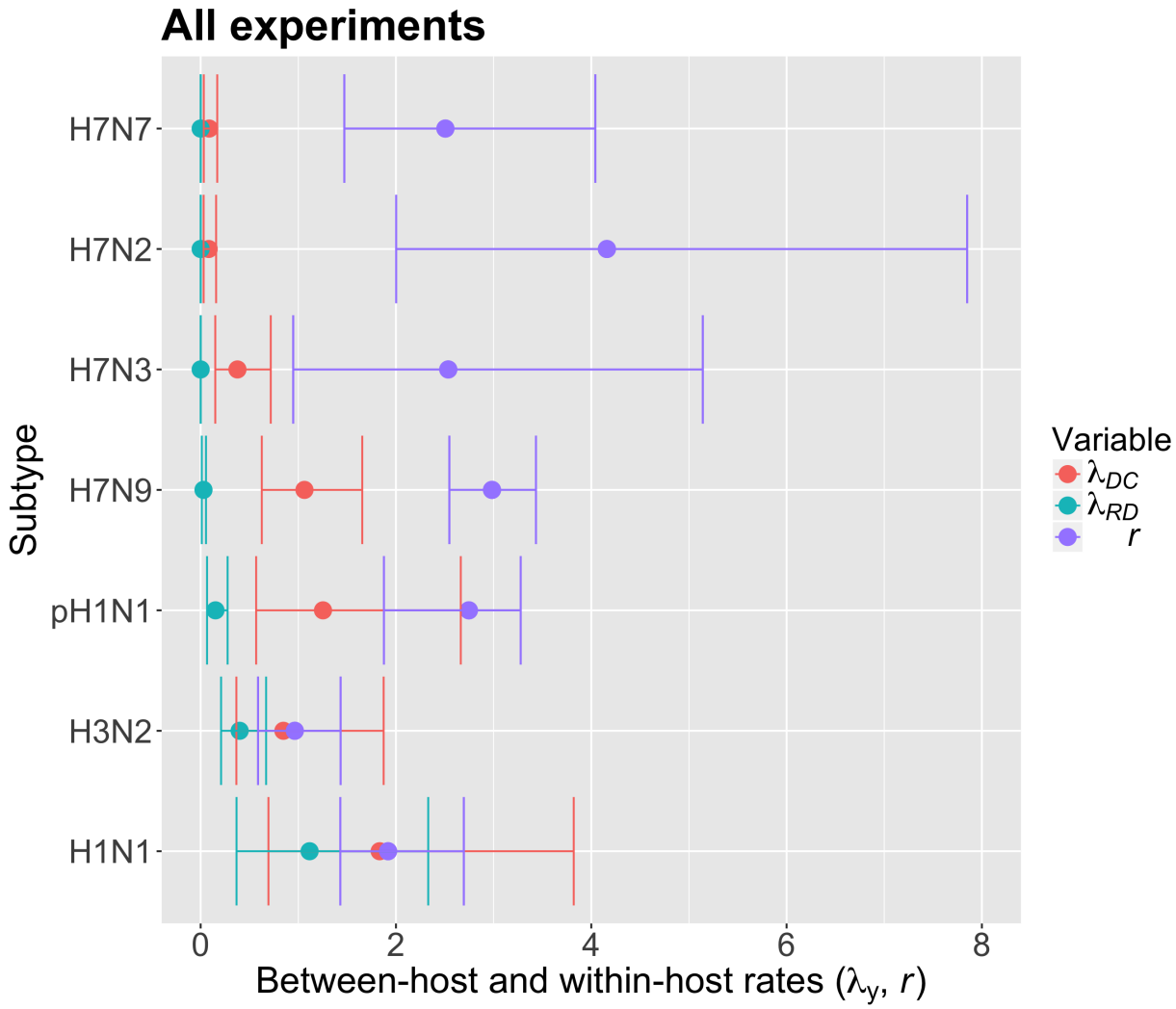

Figure 3.3: *Estimates of within-host and between-host fitness.* Points represent mean posterior values from MCMC analysis, bars indicate 95% Bayesian credible intervals. Estimates are grouped by influenza subtype. Between-host transmission fitnesses, λ_{DC} and λ_{RD}, are represented by red and blue colors, respectively, where DC is direct contact transmission and RD is respiratory droplet transmission. Within-host growth rate fitness, r, is represented by purple color. Subtypes are plotted in order of increasing human SAR estimates (from Buhnerkempe et al 2015) from top to bottom of figure.

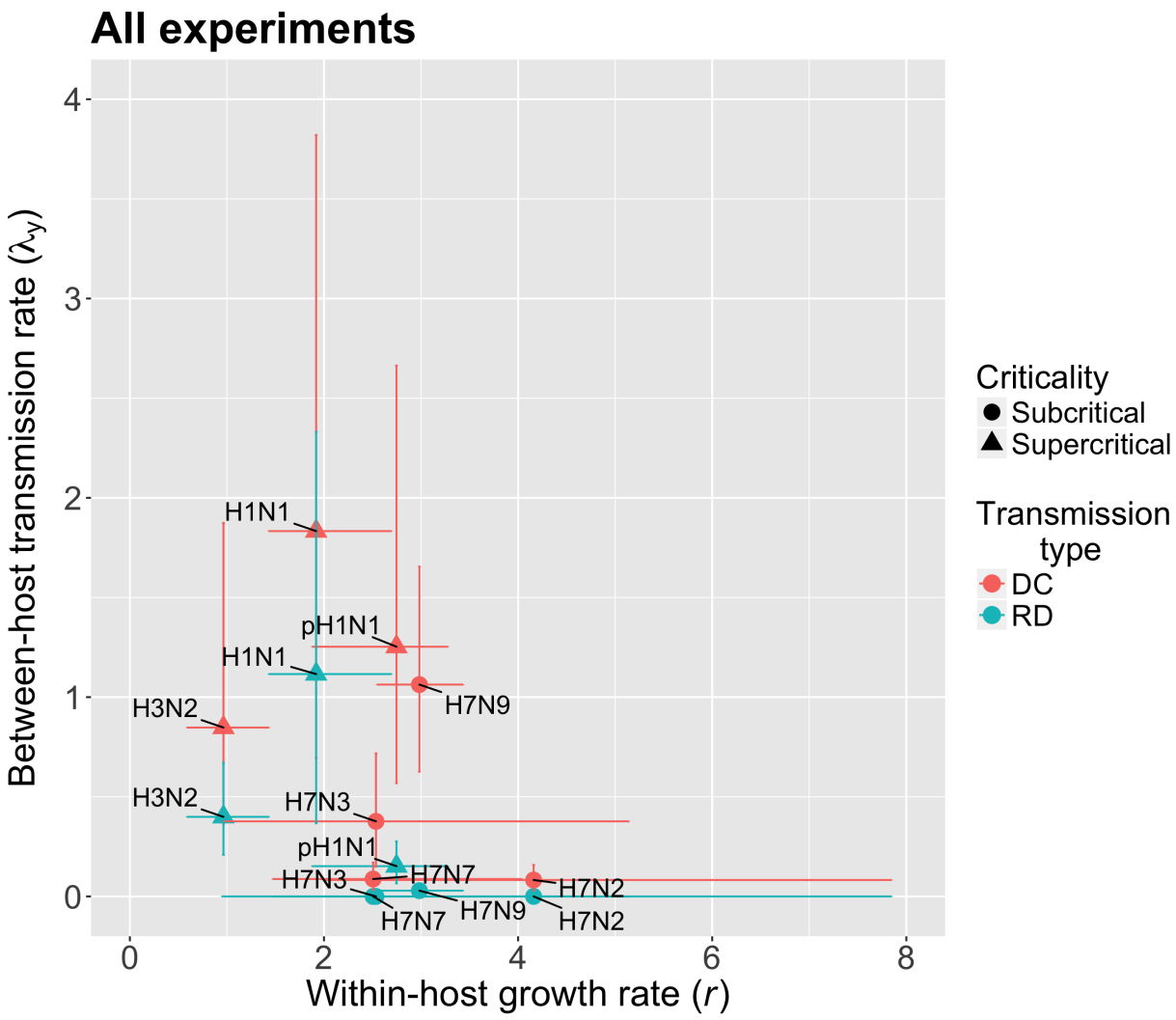

Figure 3.4: *Patterns of within-host and between-host fitness by transmission type and criticality.* Circles indicate estimates for subcritical subtypes, triangles indicate estimates for supercritical subtypes, with text labels indicating individual subtypes. Bars represent 95% Bayesian credible intervals. Direct contact transmission (DC) and respiratory droplet transmission (RD) are indicated by red and blue colors, respectively.

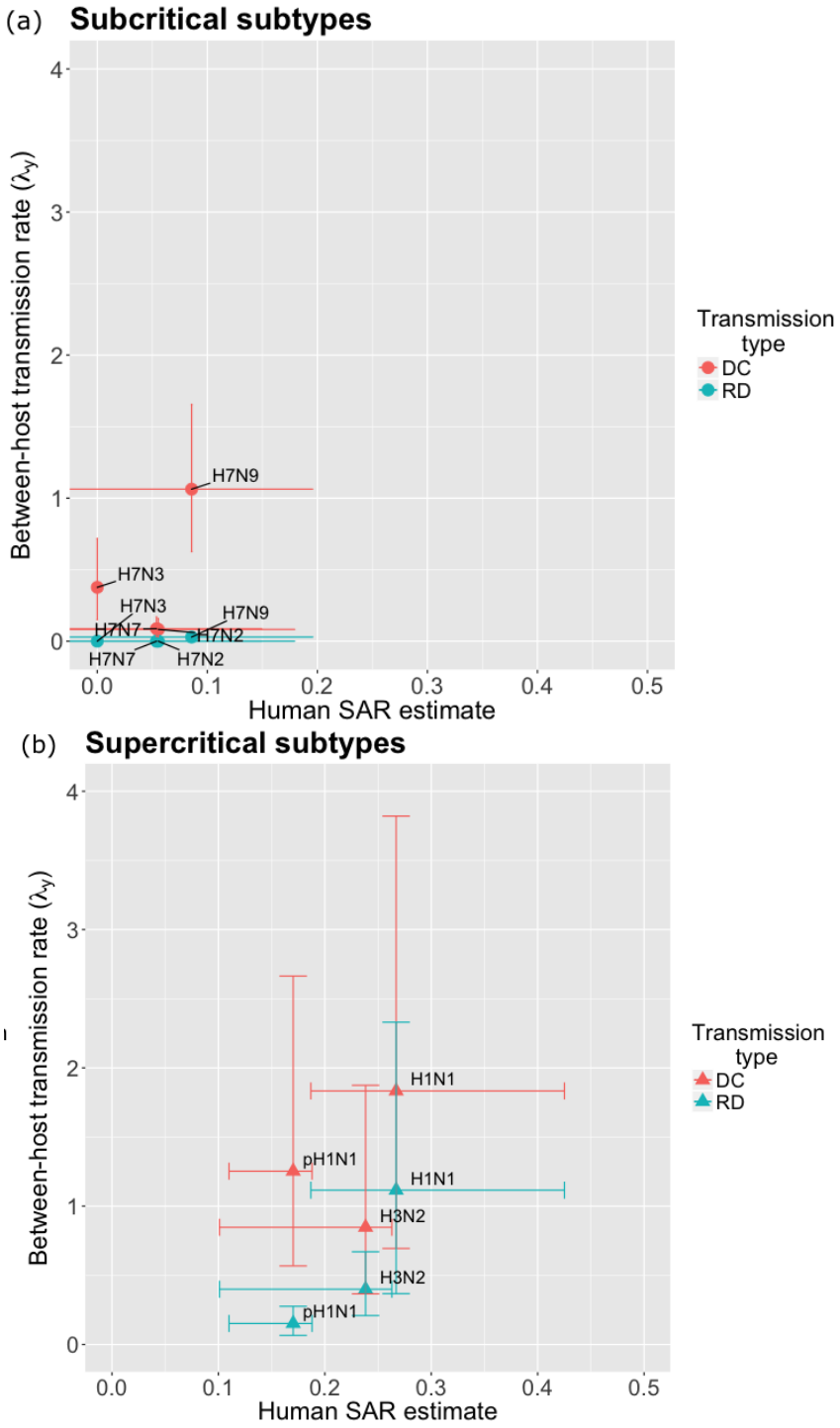

Figure 3.5: *Comparison of between-host fitness estimates to human SAR data.* Circles indicate estimates for subcritical subtypes, triangles indicate estimates for supercritical subtypes, with text labels indicating individual subtypes. Bars represent 95% confidence intervals for the x-axis, 95% Bayesian credible intervals for the y-axis. Direct contact transmission (DC) and respiratory droplet transmission (RD) are indicated by red and blue colors, respectively. Human SAR values (and data sources used to calculate these values) are taken from Buhnerkempe et al 2015 [12].

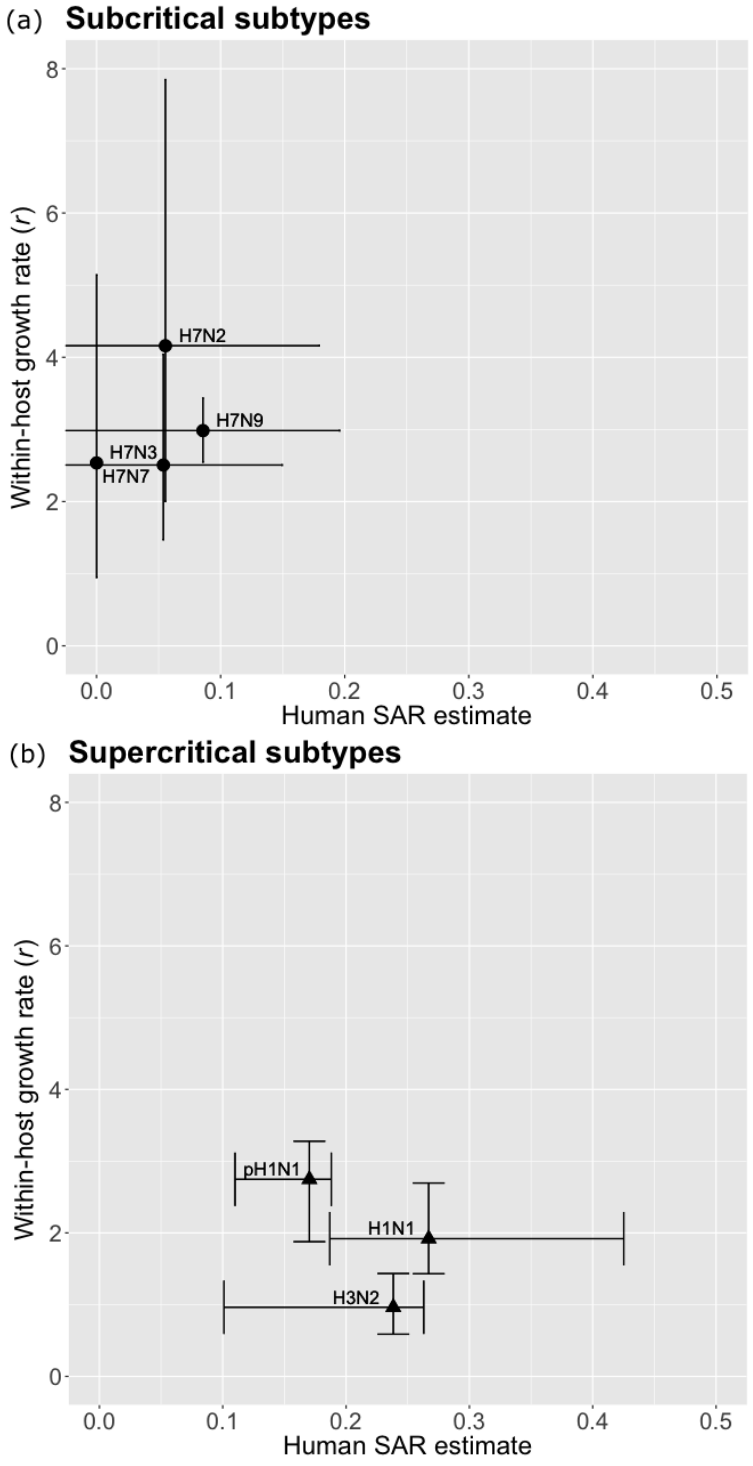

Figure 3.6: *Comparison of within-host fitness estimates to human SAR data.* Circles indicate estimates for subcritical subtypes, triangles indicate estimates for supercritical subtypes, with text labels indicating individual subtypes. Bars represent 95% confidence intervals for the x-axis, 95% Bayesian credible intervals for the y-axis. Human SAR values (and data sources used to calculate these values) are taken from Buhnerkempe et al 2015 [12].

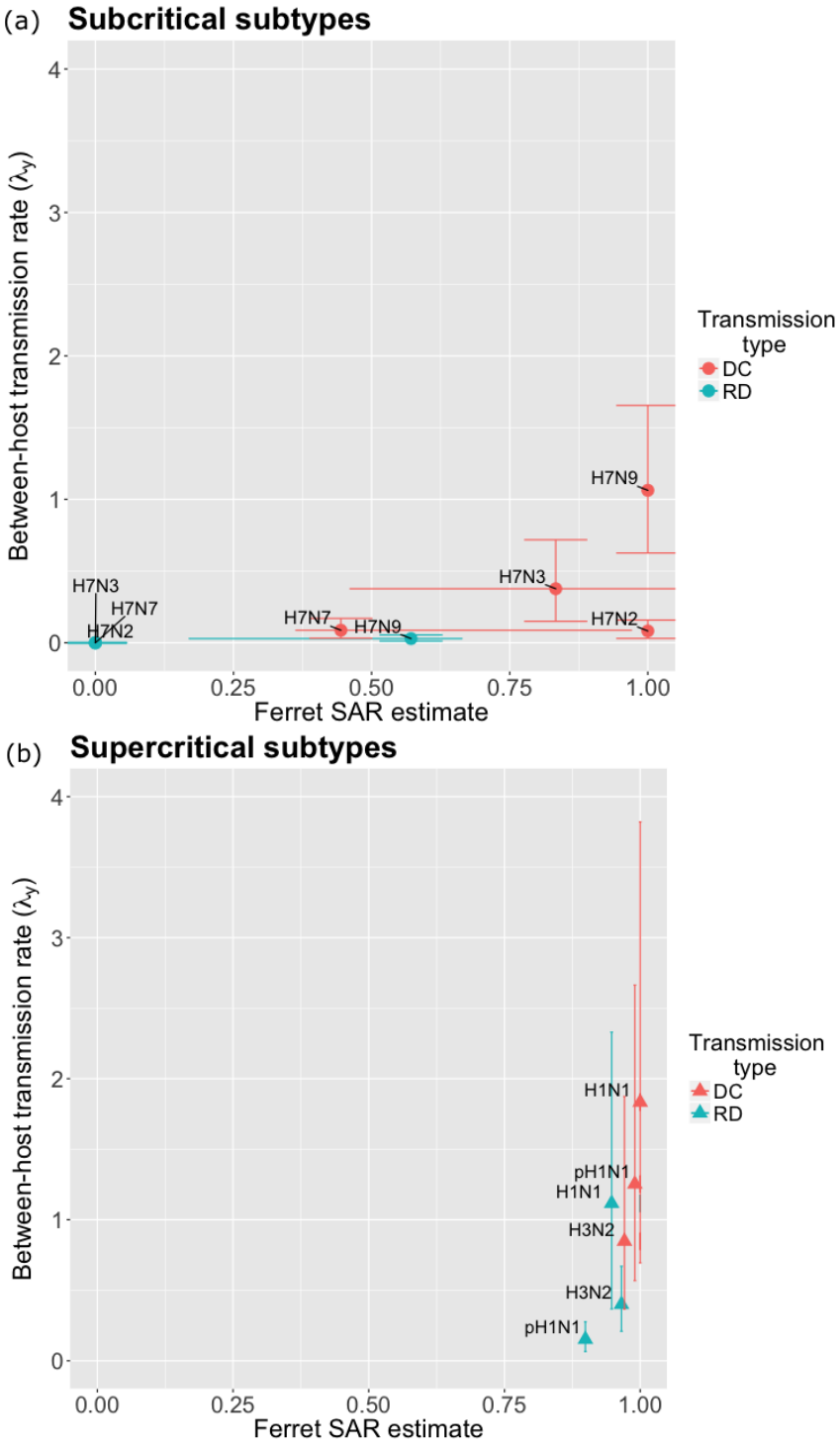

Figure 3.S1: *Comparison of between-host fitness estimates to ferret SAR data.* Circles indicate estimates for subcritical subtypes, triangles indicate estimates for supercritical subtypes, with text labels indicating individual subtypes. Bars represent 95% confidence intervals for the x-axis, 95% Bayesian credible intervals for the y-axis. Direct contact transmission (DC) and respiratory droplet transmission (RD) are indicated by red and blue colors, respectively. Ferret SAR values (and data sources used to calculate these values) are taken from Buhnerkempe et al 2015 [12].

3.6 References

Bibliography

[1] S. Alizon and C. Fraser. Within-host and between-host evolutionary rates across the hiv-1 genome. *Retrovirology*, 10(1):49, 2013.

[2] P. Baccam, C. Beauchemin, C. A. Macken, F. G. Hayden, and A. S. Perelson. Kinetics of influenza a virus infection in humans. *Journal of Virology*, 80(15):7590–7599, 2006.

[3] M. Barfield, M. E. Orive, and R. D. Holt. The role of pathogen shedding in linking within-and between-host pathogen dynamics. *Mathematical Biosciences*, 270:249–262, 2015.

[4] J. A. Belser, O. Blixt, L.-M. Chen, C. Pappas, T. R. Maines, N. Van Hoeven, R. Donis, J. Busch, R. McBride, J. C. Paulson, et al. Contemporary north american influenza H7 viruses possess human receptor specificity: Implications for virus transmissibility. *Proceedings of the National Academy of Sciences*, 105(21):7558–7563, 2008.

[5] J. A. Belser, H. M. Creager, X. Sun, K. M. Gustin, T. Jones, W.-J. Shieh, T. R. Maines, and T. M. Tumpey. Mammalian pathogenesis and transmission of H7N9 influenza viruses from three waves, 2013-2015. *Journal of Virology*, 90(9):4647–4657, 2016.

[6] J. A. Belser, C. T. Davis, A. Balish, L. E. Edwards, H. Zeng, T. R. Maines, K. M. Gustin, I. L. Martínez, R. Fasce, N. J. Cox, et al. Pathogenesis, transmissibility, and ocular tropism of a highly pathogenic avian influenza a (H7N3) virus associated with human conjunctivitis. *Journal of Virology*, 87(10):5746–5754, 2013.

[7] J. A. Belser, A. M. Eckert, T. M. Tumpey, and T. R. Maines. Complexities in ferret influenza virus pathogenesis and transmission models. *Microbiology and Molecular Biology Reviews*, 80(3):733–744, 2016.

[8] J. A. Belser, K. M. Gustin, T. R. Maines, D. M. Blau, S. R. Zaki, J. M. Katz, and T. M. Tumpey. Pathogenesis and transmission of triple-reassortant swine h1n1 influenza

viruses isolated before the 2009 H1N1 pandemic. *Journal of Virology*, 85(4):1563–1572, 2011.

[9] J. A. Belser, K. M. Gustin, M. B. Pearce, T. R. Maines, H. Zeng, C. Pappas, X. Sun, P. J. Carney, J. M. Villanueva, J. Stevens, et al. Pathogenesis and transmission of avian influenza a (H7N9) virus in ferrets and mice. *Nature*, 501(7468):556, 2013.

[10] J. A. Belser, X. Lu, T. R. Maines, C. Smith, Y. Li, R. O. Donis, J. M. Katz, and T. M. Tumpey. Pathogenesis of avian influenza (H7) virus infection in mice and ferrets: enhanced virulence of eurasian H7N7 viruses isolated from humans. *Journal of Virology*, 81(20):11139–11147, 2007.

[11] J. A. Belser, T. R. Maines, J. M. Katz, and T. M. Tumpey. Considerations regarding appropriate sample size for conducting ferret transmission experiments. *Future Microbiology*, 8(8):961–965, 2013.

[12] M. G. Buhnerkempe, K. Gostic, M. Park, P. Ahsan, J. A. Belser, and J. O. Lloyd-Smith. Mapping influenza transmission in the ferret model to transmission in humans. *eLife*, 4(September 2015), 2015.

[13] R. Frise, K. Bradley, N. Van Doremalen, M. Galiano, R. A. Elderfield, P. Stilwell, J. W. Ashcroft, M. Fernandez-Alonso, S. Miah, A. Lackenby, et al. Contact transmission of influenza virus between ferrets imposes a looser bottleneck than respiratory droplet transmission allowing propagation of antiviral resistance. *Scientific Reports*, 6, 2016.

[14] J. L. Geoghegan, A. M. Senior, and E. C. Holmes. Pathogen population bottlenecks and adaptive landscapes: overcoming the barriers to disease emergence. In *Proc. R. Soc. B*, volume 283(1837), page 20160727. The Royal Society, 2016.

[15] J. R. Gog, L. Pellis, J. L. Wood, A. R. McLean, N. Arinaminpathy, and J. O. Lloyd-Smith. Seven challenges in modeling pathogen dynamics within-host and across scales. *Epidemics*, 10:45–48, 2015.

[16] C. D. Goodman, J. E. Siregar, V. Mollard, J. Vega-Rodríguez, D. Syafruddin, H. Matsuoka, M. Matsuzaki, T. Toyama, A. Sturm, A. Cozijnsen, et al. Parasites resistant to the antimalarial atovaquone fail to transmit by mosquitoes. *Science*, 352(6283):349–353, 2016.

[17] M. E. Halloran. Secondary attack rate. *Encyclopedia of Biostatistics*, 2005.

[18] A. Handel, I. M. Longini, and R. Antia. Towards a quantitative understanding of the within-host dynamics of influenza a infections. *Journal of the Royal Society Interface*, 7(42):35–47, 2010.

[19] H. Heesterbeek, R. M. Anderson, V. Andreasen, S. Bansal, D. De Angelis, C. Dye, K. T. Eames, W. J. Edmunds, S. D. Frost, S. Funk, et al. Modeling infectious disease dynamics in the complex landscape of global health. *Science*, 347(6227):aaa4339, 2015.

[20] S. Herfst, E. J. Schrauwen, M. Linster, S. Chutinimitkul, E. de Wit, V. J. Munster, E. M. Sorrell, T. M. Bestebroer, D. F. Burke, D. J. Smith, et al. Airborne transmission of influenza a/H5N1 virus between ferrets. *Science*, 336(6088):1534–1541, 2012.

[21] M. Imai, T. Watanabe, M. Hatta, S. C. Das, M. Ozawa, K. Shinya, G. Zhong, A. Hanson, H. Katsura, S. Watanabe, et al. Experimental adaptation of an influenza H5 haemagglutinin (HA) confers respiratory droplet transmission to a reassortant H5 HA/H1N1 virus in ferrets. *Nature*, 486(7403):420, 2012.

[22] S. Jackson, N. Van Hoeven, L.-M. Chen, T. R. Maines, N. J. Cox, J. M. Katz, and R. O. Donis. Reassortment between avian H5N1 and human H3N2 influenza viruses in ferrets: a public health risk assessment. *Journal of Virology*, 83(16):8131–8140, 2009.

[23] A. S. Leonard, D. Weissman, B. Greenbaum, E. Ghedin, and K. Koelle. Transmission bottleneck size estimation from pathogen deep-sequencing data, with an application to human influenza a virus. *Journal of Virology*, pages JVI–00171, 2017.

[24] Q. Li, L. Zhou, M. Zhou, Z. Chen, F. Li, H. Wu, N. Xiang, E. Chen, F. Tang, D. Wang,

et al. Epidemiology of human infections with avian influenza a (H7N9) virus in china. *New England Journal of Medicine*, 370(6):520–532, 2014.

[25] M. Lipsitch, W. Barclay, R. Raman, C. J. Russell, J. A. Belser, S. Cobey, P. M. Kasson, J. O. Lloyd-Smith, S. Maurer-Stroh, S. Riley, et al. Science forum: Viral factors in influenza pandemic risk assessment. *eLife*, 5:e18491, 2016.

[26] J. O. Lloyd-Smith, S. Funk, A. R. McLean, S. Riley, and J. L. Wood. Nine challenges in modelling the emergence of novel pathogens. *Epidemics*, 10:35–39, 2015.

[27] T. R. Maines, L.-M. Chen, Y. Matsuoka, H. Chen, T. Rowe, J. Ortin, A. Falcón, N. T. Hien, E. R. Sedyaningsih, S. Harun, et al. Lack of transmission of H5N1 avian–human reassortant influenza viruses in a ferret model. *Proceedings of the National Academy of Sciences*, 103(32):12121–12126, 2006.

[28] T. R. Maines, A. Jayaraman, J. A. Belser, D. A. Wadford, C. Pappas, H. Zeng, K. M. Gustin, M. B. Pearce, K. Viswanathan, Z. H. Shriver, et al. Transmission and pathogenesis of swine-origin 2009 a (H1N1) influenza viruses in ferrets and mice. *Science*, 325(5939):484–487, 2009.

[29] C. Metcalf, R. Birger, S. Funk, R. Kouyos, J. Lloyd-Smith, and V. Jansen. Five challenges in evolution and infectious diseases. *Epidemics*, 10:40–44, 2015.

[30] N. Mideo, S. Alizon, and T. Day. Linking within-and between-host dynamics in the evolutionary epidemiology of infectious diseases. *Trends in Ecology & Evolution*, 23(9):511–517, 2008.

[31] H. Nishiura, H.-L. Yen, and B. J. Cowling. Sample size considerations for one-to-one animal transmission studies of the influenza a viruses. *PLoS One*, 8(1):e55358, 2013.

[32] D. Y. Oh and A. C. Hurt. Using the ferret as an animal model for investigating influenza antiviral effectiveness. *Frontiers in Microbiology*, 7, 2016.

[33] M. Park, C. Loverdo, S. J. Schreiber, and J. O. Lloyd-Smith. Multiple scales of selection influence the evolutionary emergence of novel pathogens. *Philosophical Transactions of the Royal Society of London B: Biological Sciences*, 368(1614):20120333, 2013.

[34] K. M. Pepin, S. L. Kay, B. D. Golas, S. S. Shriner, A. T. Gilbert, R. S. Miller, A. L. Graham, S. Riley, P. C. Cross, M. D. Samuel, et al. Inferring infection hazard in wildlife populations by linking data across individual and population scales. *Ecology Letters*, 20(3):275–292, 2017.

[35] A. S. Perelson and R. M. Ribeiro. Modeling the within-host dynamics of hiv infection. *BMC Biology*, 11(1):96, 2013.

[36] Y. Qin, P. W. Horby, T. K. Tsang, E. Chen, L. Gao, J. Ou, T. H. Nguyen, T. N. Duong, V. Gasimov, L. Feng, et al. Differences in the epidemiology of human cases of avian influenza a (H7N9) and a (H5N1) viruses infection. *Clinical Infectious Diseases*, 61(4):563–571, 2015.

[37] S. J. Schreiber, R. Ke, C. Loverdo, M. Park, P. Ahsan, and J. O. Lloyd-Smith. Cross-scale dynamics and the evolutionary emergence of infectious diseases. *bioRxiv*, page 066688, 2016.

[38] M. Van Boven, M. Koopmans, M. D. R. van Beest Holle, A. Meijer, D. Klinkenberg, C. A. Donnelly, et al. Detecting emerging transmissibility of avian influenza virus in human households. *PLoS Computational Biology*, 3(7):e145, 2007.

[39] A. Varble, R. A. Albrecht, S. Backes, M. Crumiller, N. M. Bouvier, D. Sachs, A. García-Sastre, et al. Influenza a virus transmission bottlenecks are defined by infection route and recipient host. *Cell Host & Microbe*, 16(5):691–700, 2014.

[40] X. Wang, C. Chai, F. Li, F. He, Z. Yu, X. Wang, X. Shang, S. Liu, and J. Lin. Epidemiology of human infections with avian influenza a (H7N9) virus in the two waves before and after october 2013 in zhejiang province, china. *Epidemiology & Infection*, 143(9):1839–1845, 2015.

[41] B. R. Wasik, A. Bhushan, C. B. Ogbunugafor, and P. E. Turner. Delayed transmission selects for increased survival of vesicular stomatitis virus. *Evolution*, 69(1):117–125, 2015.

[42] R. Wood, J. Egan, and I. Hall. A dose and time response markov model for the in-host dynamics of infection with intracellular bacteria following inhalation: with application to francisella tularensis. *Journal of The Royal Society Interface*, 11(95):20140119, 2014.

[43] Y. Yang, Y. Zhang, L. Fang, M. Halloran, M. Ma, S. Liang, E. Kenah, T. Britton, E. Chen, J. Hu, et al. Household transmissibility of avian influenza a (H7N9) virus, china, february to may 2013 and october 2013 to march 2014. *Euro surveillance: bulletin Europeen sur les maladies transmissibles= European communicable disease bulletin*, 20(10), 2015.